The Role of Fanconi Anemia Proteins in DNA Repair, Replication Stress and Genome Stability

A DISSERTATION
SUBMITTED TO THE FACULTY OF THE GRADUATE SCHOOL OF
UNIVERSITY OF MINNESOTA
BY

ELIZABETH THOMPSON

IN PARTIAL FULFILLMENT OF THE REQUIREMENTS
FOR THE DEGREE OF
DOCTOR OF PHILOSOPHY

ADVISORS:
Jakub Tolar, MD, PhD and Eric A. Hendrickson, PhD

October 2017

ACKNOWLEDGEMENTS

First, I would like to acknowledge and express gratitude to my advisors, Dr. Eric Hendrickson and Dr. Jakub Tolar for their guidance and support. Each contributed in a unique and equally important way to my graduate experience. Eric provided me with countless hours of his time and taught me to always reach to for his expectations and scientific integrity. Jakub provided inspiration and encouragement when I encountered problems and taught me to broaden my vision. Both provided the challenges that I sought, and encouraged me to pursue my own scientific interests and curiosities.

I want to thank Jung Eun Yeo and Alexandra Sobeck for their help with the FANCI/D2 paper. In addition, I would like to thank the current and former members of the Hendrickson, Bielinsky, Sobeck and Tolar laboratories for providing advice, technical expertise and friendship. A special thanks goes to to Yinan Kan, Brian Ruis, Adam Harvey, James Piper, Avani Gosalia, Wendy Leung, Ryan Baxley, and Cat Lee for their help, guidance and support.

Finally, I would like to thank my husband, Dave, and my three children, Colleen, Christopher and Megan for their understanding and support of me in my pursuit of this dream. I would also like to thank all my family, but especially my parents and my sister for their encouragement and support.

DEDICATION

In Loving Memory of

Shannon Claire Noonan
&
Katherine Michelle Diedrichsen

ABSTRACT

Fanconi anemia (FA) is a genetic chromosomal instability disorder characterized by progressive bone marrow failure and a strong predisposition to cancer. The FA proteins work together in a cellular pathway for the repair of DNA interstrand crosslinks (ICLs). Currently 22 different FA genes are implicated in this disease and contribute to the heterogeneity in symptoms and severity. Using gene targeting techniques, we successfully created a set of isogenic knockout cell lines to represents all 3 groups of proteins within the FA pathway to characterize protein function and identify differences that help explain FA disease heterogeneity.

In Chapter 2 we investigate the FA group 2 proteins, FANCI and FANCD2 that that form a heterodimer called the ID complex. We characterized the FANCI, FANCD2 and FANCI/FANCD2 double knockout cell lines and identified non-overlapping functions in the replication stress response. In fact, we found that only FANCD2 is required for restart of stalled replication forks and FANCI may even inhibit restart when FANCD2 is absent. In addition, FANCD2 has a more vital role in homologous recombination, and FANCI promotes apoptosis in the absence of FANCD2 with replication stress.

In Chapter 3 we investigate FANCN, an FA group 3 protein that is associated with more severe FA disease. We used FANCN conditional knockout cells to determine that FANCN is essential for viability and genome stability. In addition, we evaluated FANCN FA-associated mutations and breast cancer-associated variants of unknown significance (VUS) mutations. We confirmed that the BRCA1/2 binding domains of

FANCN are not essential for viability and identified two VUS mutations as potentially pathogenic.

In conclusion, we have demonstrated alternative functions of FA proteins in response to replication stress as a potential source of FA disease heterogeneity. In addition, we have demonstrated that FANCN is essential for viability whereas FANCI and FANCD2 are not, providing insight into both the frequency of occurrence and severity of FA disease associated with these different genes. Finally, we created isogenic cell lines that are a valuable asset for the FA and breast cancer fields for further investigations into protein function, characterization of patient mutations, and screening novel therapeutics.

TABLE OF CONTENTS

LIST OF TABLES

CHAPTER 2: FANCI and FANCD2 have common as well as independent function during the cellular replication stress response

CHAPTER 3: PALB2 is an essential gene and protects the genome from catastrophic instability

LIST OF FIGURES

CHAPTER 1: Introduction

CHAPTER 2: FANCI and FANCD2 have common as well as independent function during the cellular replication stress response

CHAPTER 1

INTRODUCTION

Fanconi anemia

Fanconi anemia (FA) was first described in 1927 by a Swiss pediatrician, Guido Fanconi, who reported on three brothers who all died at a young age with a severe form of anemia along with what has subsequently been recognized as the other characteristic symptoms of FA(1). Most cases of FA are inherited as an autosomal recessive genetic disease, but X-linked and a rare autosomal-dominant form of inheritance have also been identified(2,3). FA is estimated to occur in approximately 1 in 360,000 live births and can be caused by mutation of any of 22 currently recognized FA genes (denoted sequentially as *FANCA to FANCW*)(2,4). Of these 22 genes, 6 have been discovered in just the past 2 years, and there are still FA patients with undetermined genetic causes(4-11). Therefore, it is highly likely that new FA genes still remain to be discovered.

FA clinical symptoms, diagnosis and treatment

Clinical symptoms: Due to the genetic heterogeneity of the disease and a varied penetrance, there are a wide range of clinical symptoms associated with FA (12). The two most common and lethal symptoms are bone marrow failure and a strong predisposition to cancer(13). The hematological symptoms associated with bone marrow failure typically begin prior to the age of 10 and include aplastic anemia, myelodysplastic syndrome (MDS), or acute myeloid leukemia (AML)(13). Aplastic anemia is when the body is not making enough of all three blood cell types, and is also called pancytopenia. The three blood cell types include white blood cells (leukocytes), red blood cells (erythrocytes) and platelets (thrombocytes)(14). Low white blood cells (leukopenia) can increase the risk of infection, and low red blood cells (anemia) results in fatigue,

headaches, dizziness and exercise intolerance. Furthermore, low platelets (thrombocytopenia) results in bleeding issues, such as nose bleeds, gastrointestinal (GI) bleeding and stroke risks(14). Another possible hematological symptom of FA, MDS, occurs when blood cells are dysmorphic and typically is also associated with the reduction in one or more type of blood cell (cytopenia)(14). The last hematological symptom of FA is a rapidly progressing form of leukemia, called AML, and FA patients are at a 800-fold higher risk for AML than the general population (13). FA patients are also prone to solid tumors, especially squamous cell carcinomas (SCC) of the head and neck, esophageal and gynecological tract (15). All cancers in FA are aggressive and typically difficult to treat due to the inability of FA patients to handle normal chemotherapy and radiation regimens.

Other common symptoms of FA are morphological defects that are found in about 60 to 75% of FA patients and often include anomalies of the thumb and forearm, kidney and urinary tract malformation, short stature and microcephaly(13,16,17). Furthermore, it is common for patients to have *café au lait* spots and other types of abnormal skin pigmentation(13,17). Indeed, patients with more severe malformation are often diagnosed with FA earlier and prior to marrow failure as compared to patients with mild to moderate aesthetic malformation who are often only diagnosed later when symptoms of bone marrow failure appear.

Diagnosis: It has been well established that FA cells derived from any of the 22 genetic subtypes are highly sensitive to DNA interstrand crosslinks (ICLs). These highly toxic DNA lesions result from the covalent crosslinking of the two strands of double-stranded

DNA, and can interfere with both replication and transcription(18). The frequent occurrence and inability to repair/resolve ICLs is used in the diagnosis of FA. Thus, a patient suspected of having FA can be confirmed (or eliminated) as having the disease by a chromosomal fragility assay in which the patient's peripheral blood lymphocytes are treated with a DNA cross-linking agent such as mitomycin C (MMC) or 1,2,3,4-diepoxybutane (DEB) and then scored for the characteristic chromosomal breakage and radial formations that occur when authentic FA cells are exposed to these drugs(19). While hypersensitivity to MMC or DEB is often sufficient to diagnose a patient in the clinic the converse (*i.e.*, a lack of sensitivity) is not always sufficient to rule a patient out. Thus, FA has a high rate of hematopoietic somatic mosaicism where a gene conversion or an additional mutation occurs, allowing for the functional correction of one allele and, consequently, a negative chromosomal breakage assay result(20-24). A strong selective advantage for this type of compensating mutation has been observed in some patients when a gene conversion event occurs in a hematopoietic progenitor cell, and can result in the repopulation of blood cells and hematological improvement(23,25). Therefore, if a chromosomal breakage assay using lymphocytes is negative, but FA is still suspected, fibroblasts from the patient would then next be tested for chromosomal breakage with an ICL inducing agent, where the occurrence of such rescuing mutations is much lower(26).

Treatment: Currently, the only effective curative treatment for the BMF associated with FA is a hematopoietic stem cell transplant (HSCT). Impressively, improvements in the management of patient symptoms and in HSCT technology have extended the life expectancy for FA patients and many now live into adulthood; something that occurred rarely even just a decade ago(5,13).

Fanconi anemia and the BRCA pathway in ICL repair

Unrepaired ICLs are highly toxic to cells, especially to rapidly dividing cells and that is why ICL-inducing agents are such effective chemotherapeutics (27). ICLs can be generated from both exogenous and endogenous sources. Exogenous sources include chemotherapeutics such as MMC and DEB and these are not typical exposure risks. However, endogenous ICLs can occur from the consumption of dietary lipids, alcohols, and the nitrates used in food preservation (27). ICLs can even be caused by the spontaneous hydrolysis of the glycosidic bonds in DNA abasic sites (28-30).

All of the current 22 FA genes are believed to function together in a DNA repair pathway called the FA/breast cancer allele (BRCA) pathway for ICL repair(5,31). Within this pathway, the genes are organized into 3 groups: 1) the upstream and core complex proteins, 2) the central ID complex, and 3) the downstream proteins. The FA/BRCA pathway is primarily only active in S-phase of the cell cycle and is activated by the convergence of two replication forks on the ICL lesion (Figure 1A-D) (32,33).

Upstream/core complex: In response to the ICL, **FANCM** is first phosphorylated by the checkpoint kinase, ataxia telangiectasia and RAD3-related (ATR), and then subsequently binds to the ICL (34,35). FANCM then recruits the FA core complex composed of eight FA proteins and five FA-associated proteins (**FANCA, FANCB, FANCC, FANCE, FANCF, FANCG, FANCL**, FANCM, FA core complex associated protein 100 (FAAP100), FANCM interacting histone-fold protein 1 (MHF1), MHF2, FAAP20 and FAAP24). The core complex is then responsible for the monoubiquitination of FANCI

and FANCD2 (hereafter the ID complex) through the FANCL E3 ubiquitin ligase subunit, along with **FANCT**/UBE2T, the E2 ubiquitin conjugating enzyme (Figure 1A) (11,36,37). Mutations in any of the upstream/core complex FA proteins results in no monoubiquitinated FANCD2 (FANCD2-Ub). This phenotype (*i.e.*, the presence or absence of FANCD2-Ub) can be used to determine if an undetermined mutated gene in a patient is an upstream or downstream FA/BRCA pathway gene.

ID complex: FANCI and **FANCD2** form a heterodimer termed the ID complex(38,39). Both FANCD2 and FANCI are phosphorylated by ATR in response to ICLs, and only if both proteins are present will either become monoubiquitinated by the core complex: FANCI is monubiquitinated at lysine 523, and FANCD2 at lysine 561 (40). The monoubiquitinated ID complex then localizes to chromatin and facilitates the unhooking of the ICL through the recruitment of downstream nucleases (Figure 1A-B) (41,42).

Downstream proteins: Once on chromatin, FANCD2-Ub recruits **FANCP**/SLX4, which is a nuclease scaffold protein(43-45). FANCP, in turn, then recruits several endonucleases including the **FANCQ**/XPF/ERCC4:excision repair cross complementing gene 1 (ERCC1) heterodimer (41,46,47). The FANCQ:ERCC1 heterodimer is involved in unhooking of the ICL by nucleolytic incision and creating a DNA double strand break (DSB) on one DNA duplex of the replication fork and a DNA lesion on the other (Figure 1B). Translesion DNA synthesis is used to replicate over the lesion on the latter DNA duplex. Specifically, **FANCV**/MAD2L2/REV7 is a component of DNA polymerase

ζ (polζ), a translesion polymerase that can insert nucleotides directly across from DNA lesions including DNA adducts, abasic sites and DNA crosslinks (Figure 1C) (2,48,49). Finally, **FANCS**/BRCA1, **FANCD1**/BRCA2, **FANCJ**/BRIP1, **FANCN**/PALB2, **FANCO**/RAD51C, **FANCR**/RAD51, **FANCU**/XRCC2 and **FANCW**/RFWD3 are all involved in homologous recombination (HR) to restore the chromosome on the second DNA duplex containing the DSB (Figure 1D) (50,51). Curiously, deactivation of the FA pathway by USP1, a deubiquitinating enzyme that removes the monoubiquitin from FANCD2 is important for ICL resistance as well. In fact, the knockout of USP1 in DT40 chicken cells and in the mouse leads to increased levels of monoubiquitinated FANCD2, but also to increased ICL sensitivity (52,53).

A defining factor of the downstream proteins is that the monoubiquitination of FANCD2 is not dependent on their function, consequently if a FA patient has a downstream protein mutation, FANCD2-Ub will not be affected. Therefore, whether or not FANCD2 can become monoubiquitinated in a new FA patient can be used to narrow down the search for the causative mutations and FA subtype determination.

FA proteins involved in alternative functions

While all FA patient cells are sensitive to ICL-inducing agents, not all the clinical symptoms and phenotypes of FA patients can be explained by cellular defects in ICL repair. In agreement with this, many FA proteins have been implicated in multiple alternative functions outside of the canonical FA/BRCA ICL repair pathway (54-56). These alternative functions include the involvement of FA proteins in the replication

stress response, R-loop resolution, and cell cycle progression and each of these may also help to maintain the genomic integrity of the cell.

Replication stress response: Replication stress can lead to genomic instability and be a driving factor in tumorigenesis (57,58). Replication stress can occur endogenously through the attempt to replicate through highly repetitive chromosomal regions including trinucleotide repeats (TNRs), telomeres, long interspersed nuclear elements (LINEs), short interspersed nuclear elements (SINEs), DNA transposons and ALU repeat elements (59-61). These repetitive elements can transiently form complex DNA structures such as hairpins, triplexes and quadraplexes that create obstacles for replication resulting in the stalling of replication forks (59,62). Additionally, common fragile sites (CFS) that are late replicating, AT-rich regions are often sites of DNA breakage when the cell is under replication stress (63,64). These difficult to replicate regions are sources of genomic instability to a cell that is under replicative stress.

Experimentally, replication stress can be induced by the addition of hydroxyurea (HU) or aphidicolin (APH)(65). HU depletes cellular levels of deoxyribonucleoside triphosphate (dNTPs) pools by inhibiting the enzyme ribonucleotide reductase, and APH induces replicative stress through the inhibition of DNA polymerases (65). The FA pathway is activated in response to replication stress as indicated by an increase in FANCD2-Ub levels after replication stress is induced by HU treatment (66). In addition, BRCA1, BRCA2 and FANCD2 have been implicated in stabilizing stalled replication forks from meiotic recombination 11 (MRE11) degradation (67,68). Furthermore, FANCD2 can restart replication forks in cooperation with Bloom syndrome helicase

(BLM) and independently of FANCI (69,70). Therefore, FA proteins are activated and play a critical role in stabilizing and restarting stalled replication forks to prevent replication stress induced genomic instability.

R-loop resolution: R-loops occur during transcription and are formed as a three-stranded nucleotide structure with a DNA:RNA hybrid leaving the displaced non-template strand of DNA single stranded. The formation of these R-loops can result in genomic instability in two ways (54). First, the generation of single-stranded DNA (ssDNA) can provide access to DNA modifying enzymes or repair factors that cause DNA damage or mutagenesis (71,72). Second, R-loops can result in the obstruction of the replication machinery leading to hyper-recombination and chromosome fragility (73-76). Both FANCA and FANCD2 have roles in resolving R-loops and cells deficient in FANCA and FANCD2 accumulate R-loop-induced DNA damage (74). Furthermore, the translocase activity of FANCM was found to prevent R-loop-mediated replication fork arrest (77). In conclusion, FA proteins have been linked to R-loop resolution and protection of genomic instability through this mechanism as well.

Cell cycle regulation: Cell cycle checkpoints control the timing and progression through the cell cycle. When a cell encounters DNA damage brought on by replication stress, the ATR kinase is activated as the master regulator of the DNA damage response (78-80). ATR is recruited along with its binding partner ATR interacting protein (ATRIP) to extended tracts of ssDNA that have been coated with replication protein A (RPA)(81). The activation of ATR in S-phase results in the restraint of DNA synthesis and

suppression of replication origin firing, thus allowing time for DNA repair. ATR is similarly activated in G2-phase in response to under-replicated or ssDNA. ATR signaling works through activation of checkpoint kinase 1 (CHK1) and results in the restraint of cell-cycle progression through the degradation of cell division cycle 25A (CDC25A) (80). CDC25A is a phosphatase that activates cyclin-dependent kinases (CDKs). Therefore, the inactivation of CDKs by CHK1 slows or even arrests the cell cycle progression to prevent premature entry into mitosis. Yet another type of cell cycle checkpoint in mitosis is called the spindle assembly checkpoint (SAC), and it is important for ensuring that all the chromosomes are attached properly to the mitotic spindle. If the SAC is weakened, it can lead to aneuploidy, cancer, and random chromosome segregation (82).

Importantly, ATR is activated in response to ICL-induced replication fork stalling, and subsequently phosphorylates several of the FA proteins including FANCA, FANCE, FANCM, FANCI and FANCD2 (34,35,83-87). In fact, the phosphorylation of FANCI and FANCD2 has been implicated as necessary for the subsequent monoubiquitination of the ID complex and full activation of the FA/BRCA repair pathway (87,88). Therefore, checkpoint activation and the follow-up repair by the FA pathway are tightly linked and an intact FA pathway is required for proper functioning of the checkpoint response to ATR. This was confirmed by several studies in which a FANCD2 deficiency resulted in a faulty S phase checkpoint (89-91). In addition, cells deficient in FANCD2, FANCC, and BRCA1 a have faulty G2 phase checkpoint (92,93). Lastly, several FA patient cell lines were tested for SAC defects and all were found to have defects (94). Therefore,

failure to maintain checkpoints can be a driver of cancer and genomic instability and it may well explain some of the cellular phenotype of FA.

The intersection of FA with other DNA repair pathways

In the canonical FA/BRCA pathway of ICL repair, there is an interplay of additional repair pathways that work together to resolve these toxic DNA lesions. For instance, a nuclease normally associated with nucleotide excision repair (NER), XPF/FANCQ, is involved in the incisions utilized to unhook the ICL(95). Similarly, a polymerase, polζ, required for translesion synthesis (TLS) is utilized for replication across the ICL adduct(8). Finally, several downstream FA proteins involved in HR are utilized to repair the DSB and restore the replication fork to complete the repair(50). This entwined and overlapping use of proteins is representative of the complexity of DNA repair pathways that cells have evolved for the repair of DSBs.

Classic non-homologous end joining (C-NHEJ): C-NHEJ repairs of the majority of cellular DBS in humans, and is the pathway of choice in G0 and G1 phases of the cell cycle when a sister chromatid is not available(96). C-NHEJ does not require a homologous template and can simply religate two ends of broken DNA back together with minimal end processing. The simplicity of this repair mechanism makes it efficient, but also error prone because the repair can often incorporate small insertions or deletions (indels). If the DSB occurs in a non-coding region, the resultant repair-mediated indel

damage is likely small or irrelevant, however, if an indel occurs in a gene coding region, it could have deleterious effects. C-NHEJ requires the Ku70/Ku80 heterodimer (Ku), which binds to DNA termini and then recruits the DNA-dependent protein kinase catalytic subunit (DNA-PKcs)(97). Ku translocates inward from the end, allowing DNA-PKcs to contact DNA. This, in turn, activates the DNA-PKcs kinase activity permitting via *trans* autophosphorylation a synapse to form between two bound DNA-PKcs proteins on each broken end of DNA(98). The nuclease, Artemis is then recruited to process the DNA ends for repair and a trimeric complex of DNA ligase IV (LIGIV), XRCC4 like factor (XLF) and X-ray cross complementing gene 4 (XRCC4) ligates the DNA ends together(99).

It has been proposed that the FA pathway may limit the use of C-NHEJ, and that C-NHEJ may be aberrantly upregulated in FA-deficient cells. For instance, ICL hypersensitivity is reduced in the FANCC knockout DT40 cell line and the chromosome breakage phenotype could be rescued by the additional knockout of Ku (100). Furthermore, in the *C. elegans fcd-2* (FANCD2) knockout model, ICL sensitivity was rescued when lig-4 (LIGIV) was additionally mutated (101). Moreover, inactivating C-NHEJ in BRCA1- or BRCA2-deficient cells reduced the frequency of abnormal chromosomes (102). Together these results implicate C-NHEJ as having detrimental effects when the FA pathway is deficient. However, knocking out DNA-PKcs or LIGIV in FANCC knockout DT40 cells did not rescue ICL sensitivity (100). Additionally, a knockout of Ku70 in FancA$^{-/-}$ mouse embryonic stem cells did not rescue ICL sensitivity. Therefore, there is conflicting evidence for the rescue, via knockout of C-NHEJ pathway, of the phenotypes of FA-deficient cells.

Alternative Non-homologous End Joining (A-NHEJ): A-NHEJ is a DNA repair process for DSBs that does not require a homologous template, but also does not use the C-NHEJ proteins such as Ku, XRCC4 or LIGIV. A-NHEJ, also called microhomology mediated end joining (MMEJ) anneals small tracts of microhomology (generally 2 to 20 bp) flanking the DSB to repair the break (103). Therefore, repair involves a deletion and contains short (micro) stretches of homology at the breakpoint (96,104). The MRE11:radiation sensitive 50 (RAD50):Nijmegen breakage syndrome gene 1 (NBS1) complex (MRN complex) DNA polymerase *theta*, CtBP-interacting protein (CtIP), poly (ADP-ribose) polymerase 1 (PARP1), ataxia telangiectasia mutated (ATM) and flap endonuclease 1 (FEN1) are all required for — or certainly implicated in— A-NHEJ repair (103,105-109). In the first step of DSB repair by A-NHEJ, PARP1 binds to the broken DNA ends and recruits CtIP and MRN complex to resect the DNA ends and expose the regions of microhomology (MH)(109,110). Next, the regions of MH anneal and the non-homologous flaps of DNA are cleaved by XPF/ERCC1(111). Finally, DNA polymerase *theta* fills in the gaps and LIGIII completes the repair (108,112). Of particular interest, A-NHEJ has been implicated in genetic rearrangements and chromosomal translocations associated with cancer, and even with reversions of BRCA2 mutations following PARP inhibitor treatment (113,114). Additionally, several of the FA proteins support A-NHEJ, since knockdown of FANCA, FANCC, FANCD2, FANCE, FANCF and FANCM all resulted in reduced A-NHEJ repair (115). However, knockdown of FANCI and FANCL did not reduce A-NHEJ repair, therefore indicating that not all FA proteins influence A-NHEJ.

HR: HR is considered an error free repair pathway for DSB repair and is typically restricted to S/G2 phase of the cell cycle when an intact sister chromatid is available as a repair template. The first step in committing repair to HR is resection of the DNA ends creating 3' ssDNA overhangs. CtIP phosphorylation by CDKs initiates a complex between CtIP, MRN and BRCA1/FANCS in S/G2 to promote resection (116). The ssDNA is then bound by RPA and subsequently displaced by nucleoprotein filaments of RAD51/FANCR(117). RAD51 filament formation and loading onto DNA is aided by BRCA2/FANCD1 in conjunction with PALB2/FANCN(118). Next, RAD51 performs 3' strand invasion, homology search, and D-loop formation with the help of RAD51 paralogs including RAD51C/FANCO and XRCC2/FANCU(10,119,120). The D-loop is extended by a polymerase and this recombination intermediate can be resolved by synthesis dependent strand annealing (SDSA) or through formation of a double Holliday junction (HJ) structure. RAD51C has also been implicated in resolution of recombination intermediates in favor of SDSA to prevent long-tract gene conversion(121). SDSA occurs through displacement of the nascent DNA strand followed by gap filling and ligation to complete the repair. However, if SDSA is not employed then the D-loop may capture the second end of the break to form a double HJ that can be resolved with either crossover or non-crossover products(96). At an end stage of HR, RFWD3/FANCW polyubiquitinates both RPA and RAD51 in DNA repair foci through its E3 ubiquitin ligase activity and targets them for removal and degradation(4,51,122). Disruption of any of these FA protein functions in HR results in FA.

FA and breast cancer susceptibility

With the importance of FA proteins in DNA repair and genome stability, it is not surprising that so many of them are tumor suppressors. In fact, five of the FA downstream proteins with direct roles in HR are hereditary breast and ovarian cancers (HBOC) genes including BRCA1, BRCA2, PALB2, BRCA1 interacting protein C-terminal helicase 1 (BRIP1), and RAD51C (123). In addition, FANCM has been implicated as a HBOC gene but seems to be mostly involved in ovarian cancer and head and neck SSC (124). Monoallelic mutation in any one of these six genes results in increased cancer risks, therefore HBOC is inherited in an autosomal dominant manner.

HBOC syndrome has historically been linked to pathogenic variants in BRCA1 and BRCA2 but this accounts for less than 10% of all breast cancer cases (125). However, the lifetime risk of breast cancer for a pathogenic variant in BRCA1/2 is between 41 to 90% emphasizing the importance of these two genes. The mutation of BRCA1 or BRCA2 results in a similar phenotype and they both function in HR. In proliferating cells, HR is the primary mechanism for protecting genomic integrity. Proteins that function at all three levels of the DNA damage response (DDR) to resolve DBS during replication by HR are all implicated in HBOC (123,126). The first level of DDR involves the recognition of DNA damage by ATM and ATR. The second level of DDR involves signal transduction by CHK2 and BRCA1, and the third level is initiation of repair and involves BRCA2, PALB2, BRIP1, and RAD51(126).

The main difference between breast cancers associated with BRCA1 and those associated with BRCA2 is that BRCA1 mutation carriers predominately develop estrogen

receptor (ER)-negative tumors and BRCA2 carriers do not have any tendencies either way (127). BRCA1 and BRCA2 do not physically interact with each other, but PALB2 bridges them into a common complex. The BRCA1 coiled-coil domain binds to PALB2's N-terminal coiled-coil domain and BRCA2 binds to PALB2's C-terminal WD40 domain (128-132). The interaction of PALB2 with BRCA1 is required for the recruitment of BRCA2 and RAD51 to DNA damage, and is promoted by BRCA1 phosphorylation by CHK2 (133). The BRCA2:PALB2 interaction is essential for the chromatin loading of RAD51 (117,134). Not surprising, PALB2 mutations increase the risk of breast cancer by 33% for someone without family history to almost 60% for someone with a family history of breast or ovarian cancer (135). However, PALB2 mutations occur less frequently than BRCA1 and BRCA2 mutations with an incidence of only 1 to 4% of all breast cancer patients having a pathogenic PALB2 mutation. Overall, this suggests that PALB2 plays an important role in tumor suppression by complexing with BRCA1 and BRCA2 and facilitating their function in HR.

Summary and project overview

FA is a complex genetic disease with at least 22 genes working together in the FA/BRCA pathway to resolve ICLs, which are highly toxic DNA lesions. However, the complex interactions of these proteins with each other and with other cellular pathways has made it difficult to find effective treatments for FA patients. We set out to generate a set of isogenic knockout cell lines in the HCT116 parental line representative of the 3 different groups of proteins of the FA pathway: the Upstream/core complex, the ID complex, and downstream proteins. We wanted to use these cell lines to investigate the function of the

different protein groups to gain insight into disease heterogeneity resulting from the different FA genes and mutations. I used both recombinant adeno-associated virus (rAAV) as well as clustered regularly interspaced palindromic repeat/CRISPR associated 9 (CRISPR/Cas9)-mediated gene targeting techniques to create isogenic cell lines to study the cellular defects of FA knockout cell lines. FANCA was selected from the upstream/core complex because it is the most commonly mutated gene in FA. Both FANCI and FANCD2 were selected from the ID complex, and a double ID2 knockout (DKO) cell line was made of the ID complex as well. Finally, a PALB2/FANCN conditional knockout was created to represent the downstream proteins.

The goal of the first project was to determine if there was a separation of function between FANCI and FANCD2 in the replication stress response. FANCI and FANCD2 were known to form a heterodimer, be dependent on each other for monoubiquitination, and they colocalized on chromatin (38). However, recent data from the Sobeck laboratory had revealed that FANCD2 had additional functions independent of FANCI in the restart of stalled replication forks and in interactions with the BLM helicase (69). Therefore, we used the newly generated FANCI, FANCD2, and ID2 DKO knockout cell lines to further characterize the co-dependent and independent functions of these two proteins.

The goal of the second project was to gain mechanistic insight into FANCN function and to characterize FA-associated patient mutations and breast cancer-associated single nucleotide polymorphisms (SNPs). FANCN/PALB2 is an important protein involved in HR and interacts closely with BRCA1 and BRCA2 (131). PALB2 is also a tumor suppressor that predisposes humans to breast and ovarian cancer (136,137). Most patient

mutations associated with FA are nonsense mutations creating, in some cases, severely truncated protein (138). However, several breast cancer studies involving next generation sequencing of patients have been uncovering variants of unknown significance (VUSs) in PALB2 (125,139). Comparing the function of the known pathogenic FA mutations to the VUS mutations could potential confirm if the VUS mutations were driver or passenger mutations in breast cancer.

FIGURE LEGEND

Figure 1. FA proteins in ICL repair. The 22 FA proteins (FANC**A-W**) are colored according to their group in the FA pathway. The upstream/core complex is blue, the ID complex is purple and the downstream proteins are green. (A) The FA pathway is activated in S-phase by the convergence of two replication forks on an ICL (red lesion). Subsequently, the FA core complex composed of FANC**A, B, C, E, F, G, L,** and **M** acts as an E3 ubiquitin ligase to monoubiquitinate the ID complex composed of FANC**I** and FANC**D2**. FANC**T** is the E2 ubiquitin ligase for the FA core complex. Once monoubiquitinated, the ID complex recruits downstream nucleases to perform the ICL unhooking. (B) Unhooking of the ICL by nucleolytic incision on either side of the ICL (orange arrows) is facilitated by FANC**P** and FANC**Q**. (C) Replication across the DNA lesion by translesion synthesis (blue arrow) is facilitated by FANC**V**. (D) Homologous recombination to repair the DNA DSB and complete the repair is performed by FANC**D1, J, N, O, R, S, U,** and **W.**

Figure 1 FA proteins and their role in ICL repair

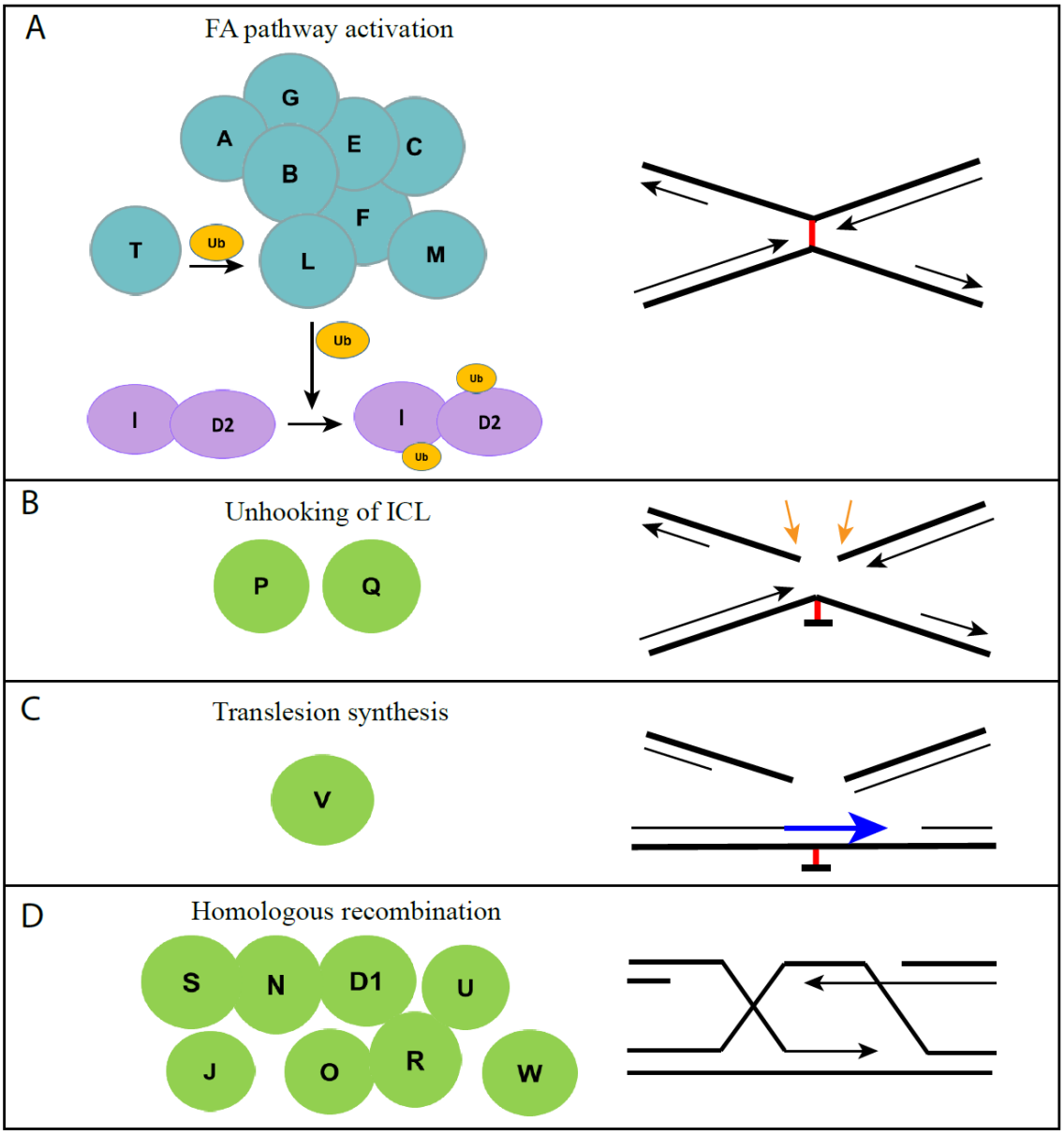

CHAPTER 2

FANCI AND FANCD2 HAVE COMMON AS WELL AS INDEPENDENT FUNCTIONS DURING THE CELLULAR REPLICATION STRESS RESPONSE

This chapter has been accepted for publication in *NAR* (September 2017) published by Oxford University Press.

Thompson EL, Yeo JE, Lee EA, Kan Y, Raghunandan M, Wiek C, Hanenberg H, Schärer OD, Hendrickson EA, and Sobeck A. FANCI and FANCD2 have common as well as independent functions during the cellular replication stress response.

SUMMARY

Fanconi Anemia (FA) is an inherited cancer predisposition syndrome characterized by cellular hypersensitivity to DNA interstrand crosslinks (ICLs). To repair these lesions, the FA proteins act in a linear hierarchy: following ICL detection on chromatin, the FA core complex monoubiquitinates and recruits the central FANCI and FANCD2 proteins that subsequently coordinate ICL removal and repair of the ensuing DNA double-stranded break by homology dependent repair (HDR). FANCD2 also functions during the replication stress response by mediating the restart of temporarily stalled replication forks thereby suppressing the firing of new replication origins. To address if FANCI is also involved in these FANCD2-dependent mechanisms, we generated isogenic *FANCI*-, *FANCD2*- and *FANCI:FANCD2* double-null cells. We show that FANCI and FANCD2 are partially independent regarding their protein stability, nuclear localization and chromatin recruitment and contribute independently to cellular proliferation. Simultaneously, FANCD2 – but not FANCI – plays a major role in HDR-mediated replication restart and in suppressing new origin firing. Consistent with this observation, deficiencies in HDR-mediated DNA DSB repair can be overcome by stabilizing RAD51 filament formation in cells lacking functional FANCD2. We propose that FANCI and FANCD2 have partially non-overlapping and possibly even opposing roles during the replication stress response.

INTRODUCTION

FA (Fanconi anemia) is an inherited genomic instability disorder that is characterized by bone marrow failure and a strong predisposition to cancer, predominantly leukemia and squamous cell carcinoma (13,140). A defining characteristic of FA patient cells is that they are highly sensitive to DNA ICL (interstrand crosslink)-inducing agents such as MMC (mitomycin C) and DEB (diepoxybutane). Moreover, FA cells exhibit spontaneous chromosomal aberrations that are further exacerbated upon treatment with replication inhibiting agents such as HU (hydroxyurea) or APH (aphidicolin) (13,68,141). Thus, the FA pathway constitutes an extremely important pathway for the maintenance of genome stability. Currently, 21 different FA genes have been identified and mutations in any one of them are sufficient to cause FA (5,8,10).

The canonical FA pathway of DNA ICL repair is thought to consist of three layers: an upstream FA core complex (8 proteins), a central protein heterodimer composed of FANCI and FANCD2 (the ID2 complex), and a growing number of downstream proteins including FANCD1/BRCA2 (breast cancer associated protein 2) and the FANCR/RAD51 (radiation sensitive 51) recombinase (5,31). Repair of the DNA ICLs occurs predominately in S-phase when they block the progression of replication forks (142,143). Following DNA ICL detection during S-phase, the FA core complex acts as an E3 ubiquitin ligase that monoubiquitinates FANCI and FANCD2, facilitating their recruitment to DNA ICLs on chromatin (144-147). Subsequently, the chromatin-bound ID2 complex coordinates downstream FA scaffolding proteins and nucleases like FANCP/SLX4 (synthetically lethal in the absence (X) of *Sgs1* 4) and FANCQ(XPF)/ERCC1 (*xeroderma pigmentosum* F/excision repair cross-complementing

1), respectively, along with BRCA2 and RAD51 to mediate incisions at the DNA ICL, followed by HDR (homology dependent repair) of the newly generated DNA DSBs (double-stranded breaks) (3,5,31,43-45,95,148).

Recent studies from our laboratory and others discovered novel roles for FANCD2 during the replication stress response (42,67-70,149,150). Upon replication fork stalling in the presence of HU or APH, FANCD2 is recruited to the stalled forks where it performs dual roles. First, it protects the stalled replication forks from nucleolytic degradation (68,149). FANCD2 fulfills this role in concert with the upstream FA core complex and several downstream FA proteins such as BRCA2 and RAD51 (67,68). Second, FANCD2 promotes restart of the stalled replication forks while blocking the firing of new replication origins (42,69,150). Interestingly, the fork restart function of FANCD2 does not depend on the FA core complex nor on FANCD2 monoubiquitination (150). Instead, the non-ubiquitinated FANCD2 isoform binds chromatin upon replication fork stalling and cooperates with downstream FA factors such as BRCA2 and FANCJ (150) as well as non-FA DNA repair proteins such as the BLM (Bloom syndrome) helicase complex (69), CtIP (C-terminal interacting protein) (42) and FAN1 (Fanconi-associated nuclease 1) (70) to promote fork restart. Intriguingly, previous findings from our laboratory suggested that FANCD2 may fulfill some of its roles during the cellular replication stress response independently of FANCI. Using the *Xenopus laevis* S-phase extract system, we showed that FANCD2 dissociates from FANCI upon replication stress and is recruited to chromatin prior to FANCI (151). Moreover, FANCD2 participates in the assembly of the BLM complex independently of FANCI (69). However, if and how FANCI contributes to mechanisms of replication stress recovery is not well understood.

To dissect the roles of FANCI and FANCD2 during the replication stress response, we generated human *FANCI*$^{-/-}$, *FANCD2*$^{-/-}$ and *FANCI*$^{-/-}$:*FANCD2*$^{-/-}$ knockout cells in an isogenic background (the HCT116 cell line). Analysis of these cells revealed that FANCI and FANCD2 act in concert to promote DNA ICL repair, but have partially independent roles during the HU- or APH-triggered replication stress response. Our findings indicate that FANCD2 fulfills crucial roles in mediating cellular resistance to HU or APH independent of FANCI. In fact, HU- or APH-triggered cell death in *FANCD2*-deficient cells was FANCI-dependent, suggesting opposing roles of FANCD2 and FANCI during cell survival. Moreover, FANCD2 played a significantly more important role during the HDR-mediated, RAD51-dependent mechanisms of replication fork restart and DNA DSB repair. Our results suggest that whereas FANCD2 supports cellular survival and fork recovery in the face of APH- or HU-triggered replication stress, FANCI may in fact oppose those functions.

MATERIALS AND METHODS

Generation of *FANCI*-null ($I^{-/-}$) and *FANCD2*-null ($D2^{-/-}$) cells using rAAV-mediated gene targeting

FANCI-null and *FANCD2*-null HCT116 cells were generated using rAAV (recombinant adeno-associated virus)-mediated gene targeting (152). Conditional and knock-out rAAV vectors targeting *FANCI* exon 10 and *FANCD2* exon 12 were constructed using Golden Gate cloning and designed as described (152-154). We targeted *FANCD2* exon 12 and *FANCI* exon 10 since these exons both lie within regions encoding conserved protein domains associated with heterodimer formation and putative DNA binding (39,155,156), and the deletion of these exons should result in frameshift mutations. The first round of targeting with a conditional vector replaced *FANCI* exon 10 and *FANCD2* exon 12 with their respective conditional, floxed (flanked by LoxP sites) alleles along with a *NEO* (neomycin) selection cassette, also flanked by LoxP sites. G418-resistant clones were screened by PCR to confirm correct targeting, and Cre (cyclization recombinase) transiently expressed from an adenoviral vector (hereafter AdCre) was then used to remove the *NEO* selection cassette as described (152-154). Retention of the *FANCI* floxed exon 10 and *FANCD2* floxed exon 12 in the conditional allele was confirmed by PCR. The second round of *FANCD2* gene targeting was performed in the $FANCD2^{flox/+}$ cells with a knock-out rAAV vector in which exon 12 was replaced with a *NEO* selection cassette. The second round of *FANCI* gene targeting was performed in the $FANCI^{flox/+}$ cells using the same conditional vector that had been used in the first round of targeting. G418-resistant clones were screened by PCR for correct targeting. Primer sequences for all PCR reactions are listed in Supplementary Table S1. AdCre recombinase was then

used to remove both the *NEO* selection cassette and the conditional allele(s) and resulted in viable $I^{-/-}$ and $D2^{-/-}$ clones. Two independent $I^{-/-}$ clones (labeled as clones #28 and #30) and a single $D2^{-/-}$ clone (labeled as clone #39) were generated. These three clones and the clones described below were used interchangeably for most of the subsequent experiments.

CRISPR/Cas9 generation *of FANCD2*$^{-/-}$ and *FANCI*$^{-/-}$*:FANCD2*$^{-/-}$ (ID2 DKO) cells

A guide RNA (gRNA) targeting *FANCD2* exon 11 was designed so that Cas9 (CRISPR associated 9) cleavage would disrupt an endogenous restriction enzyme recognition site for BpuEI. The gRNA was cloned into a CRISPR (clustered regularly interspersed short palindromic repeats) /Cas9 plasmid (hSpCas9-2A-Puro/px459) as described (157). WT (wild type) HCT116 cells were transfected with the CRISPR/Cas9 plasmid containing the gRNA targeting *FANCD2* exon 11 using Lipofectamine 3000 (Life Technologies). Two days after transfection, the cells were subcloned, and individual subclones were screened for targeting by PCR amplification of exon 11 and by subsequent digestion with the restriction enzyme BpuEI (New England BioLabs, Inc.). Clones that were resistant to digestion with BpuEI were TOPO TA cloned (Life Technologies). Sequencing of the TOPO TA clones confirmed targeted bi-allelic disruption that induced frameshifts in *FANCD2*, generating an independent *FANCD2*-null cell line, designated as clone #29 (Supplementary Figure S1A).

In a highly similar fashion *FANCI*-null cells were also transfected with the CRISPR/Cas9 plasmid containing the gRNA targeting *FANCD2* exon 11 using Lipofectamine 3000 (Life Technologies). Subsequent sequencing of the resulting TOPO TA clones confirmed targeted bi-allelic disruption that induced frameshifts in *FANCD2*, generating two

independent *ID2* DKO (double knockout) cell lines, which were arbitrarily designated as clone #1 and clone #2. Western blot analysis further confirmed that these clones were null for FANCD2 and FANCI expression. Primer sequences for all PCR reactions are listed in Supplementary Table S1.

To demonstrate unequivocally that the reagents (rAAV or CRISPR/Cas9) were irrelevant to the resulting phenotypes of the cell lines used in these experiments we also generated additional *ID2* DKO clones (arbitrarily designated as clones #3 and #4). These clones were created starting with $D2^{-/-}$ clone #29 (CRISPR/Cas9 generated) and $D2^{-/-}$ clone #39 (rAAV generated) cell lines, respectively. A gRNA targeting *FANCI* exon 9 was designed so that Cas9 cutting would disrupt an endogenous restriction enzyme recognition site for AcuI. The gRNA was cloned into a CRISPR/Cas9 plasmid (hSpCas9(BB)-2A-GFP/ PX458; Addgene plasmid #48138). This CRISPR/Cas9 plasmid co-expresses Cas9 and GFP, and therefore GFP-expressing cells were collected two days after transfection by flow cytometry and subcloned. Subclones were screened for correct targeting by PCR amplification of *FANCI* exon 9 and subsequent digestion with AcuI (New England BioLabs, Inc.). Clones that were resistant to digestion with AcuI were TOPO TA cloned and $ID2^{-/-}$ clones #3 and #4 were sequence confirmed for biallelic frameshift-inducing mutations (Supplementary Figures S1B, C). Additionally, western blot analyses confirmed that these cell lines did not express any WT FANCI or FANCD2 protein nor was there any evidence of expression of potential truncated protein products (Supplementary Figures S1D, E). *In toto*, these experiments demonstrated that the cells were functional DKOs. DKO clones #3 and #4 were used exclusively in the experiments in which growth of the cell lines was assessed (Fig. 4A).

Complementation of *D2*$^{-/-}$ and *I*$^{-/-}$ cells

For expression of *hFANCD2*, the human *FANCD2* transcript 1 cDNA (NM_001018115) was optimized by silent mutagenesis, thereby introducing unique restriction enzyme recognition sites and removing potential prokaryotic instability motifs, cryptic splice sites, RNA instability motifs and polyA sites (Hanenberg *et al.*, manuscript in preparation). The cDNA was purchased from GenScript (Piscataway, NJ). The *D2*$^{-/-}$ cells were complemented using the optimized human *FANCD2* expression cassette that was Gateway-cloned into a PiggyBac transposase vector containing a CAG (cytomegaloviral/*beta*-actin/*beta*-globin) promoter and a *NEO* selection cassette. G418-resistant clones were screened for FANCD2 expression by Western blot analyses.

The *I*$^{-/-}$ cells were complemented by performing a third round of gene targeting to "knock back in" a functional *FANCI* allele. This was accomplished using a CRISPR/Cas9 gRNA designed to target immediately 5' of the LoxP scar left when exon 10 was removed to create the *I*$^{-/-}$ cells. The *FANCI* conditional rAAV plasmid containing the *FANCI* exon 10 flanked by LoxP sites and a *NEO* selection cassette, also flanked by LoxP sites was used as the donor template. G418-resistant clones were screened for the knock-in of *FANCI* exon 10, and PCR was used to confirm heterozygous knock-in in two clones. The *NEO* selection cassette was subsequently removed by transient treatment with AdCre recombinase, and retention of *FANCI* exon 10 was confirmed by PCR and DNA sequencing. Restored FANCI expression from the knock-in floxed allele was confirmed by Western blot analyses. Throughout the manuscript, the complemented cell lines are designated as (*D2*$^{-/-:D2}$, *I*$^{-/-:I}$) for *D2*- and *I*-null, cells respectively.

Finally, $I^{-/-}$ cells overexpressing FANCD2 protein were established by introducing a PiggyBac transposon containing the *FANCD2* codon-optimized cDNA described above into $I^{-/-}$ cells (clone #28). Two FANCD2-overexpressing *FANCI*-null cell lines (named clones #2 and #12) were identified by Western blot analysis. These clones were designated as $I^{-/-:D2o/e}$.

Cell proliferation assay

WT cells, knockout cells and complemented cells were plated in 6-well tissue culture plates according to their plating efficiency: WT cells were plated at 2,500 cells/well, complemented cells ($D2^{-/-:D2}$, $I^{-/-:I}$) were plated at 5,000 cells/well, and the $D2^{-/-}$, $I^{-/-}$ and *ID2* DKO cells were plated at 6,000 cells/well. Cell counts were performed in triplicate 4, 6 or 8 days after seeding.

MMC sensitivity assay

Cells were plated in triplicate in 96-well plates according to their plating efficiency. WT cells were plated at 750 cells/well, complemented cells ($D2^{-/-:D2}$, $I^{-/-:I}$) were plated at 1,000 cells/well and the $D2^{-/-}$, $I^{-/-}$ and *ID2* DKO were plated at 1,200 cells/well. On the following day, the media was removed and replaced with media containing 0, 5, 10 or 15 nM MMC. Cells were allowed to grow for 5 days and cell viability was measured with CellTiter96 Aqueous (Promega) according to the manufacturer's instructions. The viability of MMC-treated cells was normalized to the average viability of the untreated control cells for each cell line.

Cell cycle analysis

WT cells, knockout cells and complemented cells were plated in 6-well plates according to their plating efficiency. WT cells were plated at 100,000 cells/well, singly-null and

complemented cells were plated at 200,000 cells/well and DKO cells were plated at 320,00 cells/well. After 24 hr, the media was removed and either untreated media, media containing 100 nM APH or media containing 10 nM MMC was added to the cells. After 24 hr the cells were harvested and fixed with 1% paraformaldehyde and subsequently with cold 70% ethanol. Fixed cells were washed with PBS (phosphate buffered saline), stained (with PBS containing 40 mg/mL propidium iodide; 100 mg/mL RNase A) and RNase treated (37° C for 30 min). Samples were then filtered through a cell strainer cap (Corning) and sorted on a BD Accuri C6 instrument and analyzed using FlowJo software (V10.1).

Colony forming assay

WT cells, null cells and complemented cells were plated in 6-well plates in triplicate according to their plating efficiency. WT cells were plated at 300 cells/well, complemented cells ($D2^{-/-:D2}$, $I^{-/-:I}$) were plated at 400 cells/well, $I^{-/-}$ cells were plated at 600 cells/well and $D2^{-/-}$ and *ID2* DKO cells were plated at 800 to 1,000 cells/well. After 24 hr, the media was removed and DMSO media or media containing 0, 50 100 or 150 μM HU, or media containing 0, 10, 25 or 50 nM APH was added in triplicate. Cells were incubated for 12 to 14 days, washed in PBS, fixed in 10% acetic acid/10% methanol and stained with Coomassie as described (158). Colonies reaching a minimum size of 50 cells were counted and normalized to the average colony number in untreated wells.

DNA repair assays

The HDR reporter assay was performed with the DR-GFP plasmid as described (159). The DR-GFP reporter plasmid contains two mutated GFP genes in tandem, and one of the mutated GFP genes contains an I-SceI restriction enzyme recognition site. If

HDR/gene conversion between the two mutated GFP genes is used to repair the DSB induced by I-SceI digestion, then GFP expression is restored.

The A-NHEJ (alternative non-homologous end joining) reporter assay was performed with the pEJ2-GFP plasmid as described (104,154). The pEJ2-GFP reporter plasmid contains a GFP expression cassette interrupted by an I-SceI restriction enzyme site and three stop codons flanked by 8 bp of microhomology. If microhomology-mediated repair (*i.e.*, A-NHEJ) is used to repair the DSB induced by I-SceI restriction enzyme digestion, then GFP expression is restored. For both DNA repair assays, three plasmids including the reporter plasmid (DR-GFP or pEJ2-GFP), an I-SceI expression plasmid, and a mCherry expression plasmid (which was used as a transfection control) were co-transfected into the cells using Lipofectamine 3000 (Life Technologies). 72 hr after transfection, the cells were fixed with 4% paraformaldehyde and sorted by FACS (fluorescence-activated cell sorting). The DNA repair efficiencies were determined as the number of dual GFP-positive and mCherry-positive cells divided by the number of mCherry-positive cells. The values were normalized to the repair efficiency observed in WT cells. For the RS-1 treatment during the HDR assay, 7.5 nM RS-1 was added to the media 2 hr prior to plasmid transfection. Fresh media containing 7.5 nM RS-1 was added again 24 hr after transfection.

Preparation of whole cell extracts (WCE), as well as nuclear, and chromatin fractions

For WCE (whole cell extract) preparation, cells were washed in PBS, resuspended in lysis buffer (10 mM Tris pH 7.4, 150 mM NaCl, 1% NP-40, 0.5% sodium deoxycholate, 1 mM EDTA, 1 mM DTT, 0.5 mg/ml pefabloc protease inhibitor) and incubated on ice

for 20 min. Cell extracts were centrifuged for 5 min at 10,000 rpm, and the supernatant was used for further analysis. Nuclear and chromatin fractions were prepared using a Subcellular Protein Fractionation Kit (Thermo Scientific).

Antibodies

The following antibodies were used for Western blotting and immunofluorescence assays: anti-FANCD2 (Santa Cruz, sc-20022 and Abcam, ab2187), anti-FANCI (Bethyl Laboratories, A300-212), anti-FANCI (160), anti-Ku86 (Santa-Cruz, sc-5280), anti-CtIP (161), anti-RAD51 (Santa Cruz sc-8349), anti-GAPDH (Genetex, GTX627408), anti-tubulin (Abcam, ab7291), anti-g-H2AX (Bethyl Laboratories, A300-081), anti-phospho-p53 (Ser15) (Santa Cruz, sc-11764-R), anti-p21 (Santa Cruz, sc-397) and anti-PCNA (Calbiochem, PC10).

Immunoblotting

Protein samples were separated on gradient gels and transferred to Immobilon P membranes (Millipore). After blocking in 5% milk, the membranes were incubated with the following primary antibodies: FANCD2 (1:1,000), FANCI (1:2,000), Ku86 (1:5,000), GAPDH (1:5,000), CtIP (1:400), PCNA (1:5000), g-H2AX (1:10,000), phospho-p53 (1:1,000), and p21 (1:400). A horseradish peroxidase-conjugated rabbit secondary antibody (Jackson Laboratories) or a mouse secondary antibody (Biorad) were used at dilutions of 1:10,000 and 1:3,000, respectively. Protein bands were visualized using an EL Plus system (Amersham).

Immunofluorescence analysis of DNA repair foci

Indirect immunofluorescence was carried out essentially as described (162). The primary antibodies used were: FANCD2 (Abcam, ab2187, 1:4,000), CtIP (mouse monoclonal,

1:400), and RAD51 (Calbiochem, PC130, 1:1000). The secondary antibodies used were: Alexa Fluor 594-conjugated goat anti-rabbit (1:1,000) and Alexa Fluor 488-conjugated goat anti-mouse (1:1000; Molecular Probes). For statistical analysis of nuclear foci formation, images were taken using a Leica DM LB2 microscope with a Hamamatsu Orca-ER camera. Quantification of CtIP and RAD51 foci was carried out using ImageJ.

DNA fiber assay

We used a vetted DNA fiber protocol (163). Moving replication forks were labeled with DigU (digoxigenin-dUTPs) for 25 min and then with BioU (biotin-dUTPs) for 40 min. To allow efficient incorporation of the dUTPs, a hypotonic buffer treatment (10 mM HEPES, 30 mM KCl, pH 7.4) preceded each dUTP-labeling step. To visualize labeled fibers, cells were mixed with a 10-fold excess of unlabeled cells, fixed and dropped onto slides. After cell lysis, DNA fibers were released and extended by tilting the slides. Incorporated dUTPs were visualized by immunofluorescence detection using anti-digoxigenin-Rhodamine (Roche) and streptavidin-Alexa-Fluor-488 (Invitrogen). Images were captured using a Deltavision microscope (Applied Precision) and analyzed using Deltavision softWoRx 5.5 software. All DNA fiber results shown are the means of two or three independent experiments (using 300 DNA fibers/experiment). Error bars represent the standard error of the mean (SEMS) and the significance was determined by t-test and Mann-Whitney tests. Statistical significance at $P < 0.05$, $P < 0.01$, and $P < 0.001$ are indicated as *, **, ***, respectively.

Molecular DNA combing assay

We carried out DNA combing assays (164) as described in the manufacturer's protocol (Genomic Vision), with some modifications as described below. Briefly, moving

replication forks were labeled with 5-chloro-20-deoxyuridine (CldU, Sigma-Aldrich) for 20 min and then with 5-iodo-20-deoxyuridine (IdU, Sigma-Aldrich) for 40 min. To achieve lysis, the cells were embedded in low-melting agarose (Bio-Rad) followed by incubation in DNA extraction buffer (0.5M MES buffer, pH 5.5, Millipore). To stretch the DNA fibers, silanized coverslips (22 mm X 22 mm, Genomic Vision) were dipped into the extracted DNA buffer for 13 min and then pulled out a constant speed at 300 um/s. The coverslips were then baked at 60□ for 4 hr and incubated with 2.5 M HCl for denaturation. Incorporated CldU and IdU were visualized using a rat anti-BrdU antibody (dilution 1:50 ~ 1:100 for CldU, Abcam) or a mouse anti-BrdU antibody (1:10 ~ 1:50 for IdU, Becton Dickinson). Slides were fixed with 4% paraformaldehyde in PBS and incubated with Alexa Fluor 488-conjugated goat anti-rat antibody (dilution 1:100 ~ 1:200, Molecular Probes/Thermo Fisher) or Alexa Fluor 568-conjugated goat anti-mouse antibody (dilution 1:100 to 1:200, Molecular Probes/Thermo Fisher) for 1 hr. Finally, coverslips were mounted with ProLong Gold Antifade Reagent (Molecular Probes) and stored at -20□. DNA fiber images were captured using LSM880 microscope (Carl Zeiss).

All DNA combing results shown are the means of two or three independent experiments (using 300 DNA fibers/experiment). Error bars represent the standard error of the mean (SEMS) and the significance was determined by a t-test. Statistical significance at $P < 0.05$, $P < 0.01$, and $P < 0.001$ are indicated as *, **, ***, respectively.

Statistical analysis

Error bars represent the standard deviation of the mean and p-values were determined using a Student's t-test. Statistical significances at $P < 0.05$, $P < 0.01$, and $P < 0.001$

were indicated as *, ** and ***, respectively. A summary of all P-values for results shown in Figures 3 to 6 is provided in Supplementary Table S2.

RESULTS

Generation and complementation of human *FANCI*, *FANCD2* and *FANCI:FANCD2* DKO knockout cell lines

To knock out the *FANCD2* and *FANCI* genes in the parental HCT116 cell line, a conditional knockout approach was used. We chose this approach since all patient-derived cells from complementation groups FA-D2 and FA-I described to date exhibit residual expression of FANCD2 (165) or FANCI (145,166,167), respectively, which raised the possibility that *FANCD*2 and/or *FANCI* might be essential in human somatic cells. The conditionally null cell lines were created using recombinant adeno-associated virus (rAAV) gene targeting techniques, as described (Figure 1)(152-154,168). Thus, the *FANCD2*$^{-/-}$ cell line (*D2*$^{-/-}$ clone #39) was generated using two rounds of rAAV gene targeting, first with the conditional vector (Figure 1A) and second with the knockout vector (Figure 1B). To unequivocally demonstrate that the technology utilized to generate the knockout cell lines was irrelevant to the cell's subsequent phenotypes we also generated (described in the Materials and Methods) a second *FANCD2* knockout clone (*D2*$^{-/-}$ clone #29) utilizing CRISPR/Cas9 technology.

Similarly, the *FANCI*$^{-/-}$ cell lines (*I*$^{-/-}$) were generated using two rounds of targeting with a conditional rAAV vector (Figure 1A). In this fashion, two independent *FANCI*-null clones were obtained and designated as clone #28 and clone #30, respectively. These experiments demonstrated that our original concern about the possibility of these genes being essential was unwarranted as null cell lines corresponding to both genes were readily isolated.

Deletion of the targeted exons was confirmed by PCR amplification across the deleted exon region resulting in significantly smaller PCR products for the null alleles (Figure 2A). Since the *FANCD2* exon 12 was targeted with two different rAAV vectors that were designed to generate different-sized deletions the $D2^{-/-}$ genotype could consequently be confirmed by the appearance of the two differently-sized PCR products ("Null" bands of 365 and 151 bp; Figure 2A). Confirmation of the $I^{-/-}$ genotype was achieved by PCR amplification across *FANCI* exon 10 resulting in a single PCR band representing deletion of exon 10 on both alleles ("Null" band of 252 bp; Figure 2A).

To generate the $FANCD2^{-/-}$:$FANCI^{-/-}$ doubly-null cell line (*ID2* DKO), we utilized CRISPR/Cas9 gene targeting to knock out *FANCD2* in the $I^{-/-}$ cell line (Figure 2 B-D). A guide RNA was designed to target the Cas9 endonuclease to cleave within an endogenous restriction enzyme recognition site (BpuEI) in *FANCD2* exon 11. Subsequently, mutagenic insertion or deletions (indels) created by end joining repair of the CRISPR/Cas9-mediated DSB in *FANCD2* were detected by disruption of the BpuEI restriction enzyme site (Figure 2B). Screening of targeted clones revealed two independent clones with complete resistance to digestion with BpuEI, indicating bi-allelic disruption of *FANCD2* in the $I^{-/-}$ cells (Figure 2C). Sequence analysis of the targeted region was used to confirm that both clones had CRISPR/Cas9-induced bi-allelic frameshift mutations in *FANCD2*, resulting in two independent viable *ID2* DKO cell lines (Figure 2D; arbitrarily designated as clones #1 and #2, respectively). To once again demonstrate that the knockout technology used to construct the cell lines was irrelevant to their biological phenotypes, we also generated (described in the Materials and Methods) two additional *ID2* DKO clones in a converse fashion to that described above,

thus inactivating *FANCI* in a *FANCD2*-null cell line. These clones were arbitrarily designated as *ID2* DKO clones #3 and #4, respectively.

Western blot analysis of WCE prepared from WT, $D2^{-/-}$, $I^{-/-}$, and *ID2* DKO cells confirmed that the genetically-null cells lacked expression of FANCD2, FANCI or both proteins, respectively, compared to the WT cells (Figure 3A, B and Supplementary Figures S1D, S1E). Complementation of the $D2^{-/-}$ cell line ($D2^{-/-:D2}$) was accomplished by stable genome integration of a constitutively expressed, sequence-optimized *FANCD2* cDNA via a PiggyBac transposon vector. Interestingly, we were unable to follow this complementation strategy in $I^{-/-}$ cells, since these cells did not maintain stable FANCI protein expression of a constitutively expressed *FANCI* cDNA (regardless of whether the expression vector was a transposon, retrovirus or plasmid; data not shown), similar to previous reports (167,169). Instead, complementation of the $I^{-/-}$ cell line was accomplished by a third round of CRISPR/Cas9-mediated knock-in of the conditional exon 10 allele, resulting in reversion of the $FANCI^{-/-}$ genotype to a $FANCI^{flox/-}$ genotype (designated as $I^{-/-:I}$). Western blot analysis of the complemented cell lines showed that the $D2^{-/-:D2}$ and $I^{-/-:I}$ cells exhibited WT-like protein expression of FANCD2 and FANCI, respectively (Figure 3A, B). In agreement with previous reports that FANCD2 and FANCI are interdependent for their DNA damage-inducible monoubiquitination (87,145,151,166), HU treatment triggered $FANCD2^{Ub}$ and $FANCI^{Ub}$ formation in WT cells, but not in $I^{-/-}$ or $D2^{-/-}$ cells, respectively (Figure 3A, B). Importantly, $FANCD2^{Ub}$ and $FANCI^{Ub}$ formation was fully restored in $D2^{-/-:D2}$ and $I^{-/-:I}$ cells (Figure 3A, B), demonstrating a functional restoration of the key monoubiquitination step in both complemented cell lines.

FANCD2 and FANCI are partially independent for their protein stability, nuclear import and chromatin recruitment and contribute separately to normal cell proliferation

Several previous studies suggested that the FANCD2 and FANCI proteins stabilize one another, while other reports did not (87,145,151,166). To address this question, we compared the expression levels of FANCD2 and FANCI in WT, $I^{-/-}$ or $D2^{-/-}$ cells that were untreated or treated with 2 mM HU. FANCD2 protein levels in WCEs were reduced by approximately 50% in $I^{-/-}$ cells compared to WT cells regardless of the absence or presence of HU-induced DNA damage (Figure 3C). Similarly, FANCI protein levels were reduced by approximately 60% in untreated or HU-treated $D2^{-/-}$ cells compared to WT cells (Figure 3C). Thus, approximately half of the cellular FANCD2 and FANCI protein levels remain unaffected in the absence of the respective binding partner.

FANCD2 and FANCI each contain nuclear localization signals and can bind chromatin constitutively; moreover their chromatin binding increases after replication stress induction (66,145,151,170,171). To determine if FANCD2 and FANCI rely on each other for their nuclear import, we analyzed nuclear extracts from WT, $D2^{-/-}$ or $I^{-/-}$ cells that were untreated or HU-treated for 6 or 24 hr. In untreated conditions, $D2^{-/-}$ and $I^{-/-}$ cells contained nuclear protein levels of FANCI and FANCD2, respectively, that were comparable to those in WT cells (Figure 3D, compare lanes 1 to 3). In contrast, while HU treatment stimulated a strong increase in nuclear FANCD2 and FANCI protein levels in the WT cells (Figure 3D, lanes 1, 4 and 7), no such increase was observed in $I^{-/-}$ cells (Figure 3D, lanes 6 and 9) or $D2^{-/-}$ cells (Figure 3D, lanes 5 and 8). These results suggest

that nuclear accumulation of FANCD2 and FANCI occurs independently in unperturbed conditions, but becomes interdependent during replication stress.

To determine the extent to which FANCD2 and FANCI chromatin recruitment occurs interdependently, we prepared chromatin factions from WT, *D2*$^{-/-}$ or *I*$^{-/-}$ cells that were either untreated or HU-treated for 6 or 24 hr. In WT cells, FANCD2 and FANCI were robustly bound to chromatin and accumulated further during the course of HU treatment (Figure 3E, lanes 1, 4, and 7). In contrast, no chromatin-bound FANCI was detectable in the *D2*$^{-/-}$ cells regardless of the presence or absence of HU (Figure 3E, lanes 2, 5 and 8). Interestingly, a small amount of residual chromatin-associated FANCD2 was detected reproducibly in untreated or HU-treated *I*$^{-/-}$ cells (Figure 3E, lanes 3, 6, and 9, red arrows). Since FANCD2 cannot become monoubiquitinated in *I*$^{-/-}$ cells (Figure 3B, C), this finding demonstrates that the non-ubiquitinated FANCD2 isoform retains chromatin binding ability in the absence of FANCI. Thus, although FANCD2 and FANCI are monoubiquitinated in a strictly interdependent manner, they are partially independent of one another regarding their protein stability, nuclear accumulation and chromatin recruitment, hinting at separate cellular functions of the two factors . To further test this, we compared cellular growth between the WT or WT-like *D2*$^{-/-:D2}$ and *I*$^{-/-:I}$ cell lines and the *I*$^{-/-}$, *D2*$^{-/-}$ and *ID2* DKO knockout cells in a cell proliferation assay. The three knockout cell lines exhibited significantly reduced cellular growth rates compared to the WT, *D2*$^{-/-:D2}$ and *I*$^{-/-:I}$ cells, indicating that FANCD2 and FANCI both contribute to cellular proliferation (Figure 4A). Strikingly, the cellular growth rates of the three knockout cell lines were also significantly different from one another, with decreasing colony formation abilities in the following order: *I*$^{-/-}$ > *D2*$^{-/-}$ > *ID2* DKO cells. These

results indicate that FANCD2 and FANCI have partially non-overlapping roles to promote cellular proliferation in otherwise unperturbed conditions.

FANCD2 and FANCI act in concert during ICL repair

A hallmark of FA is the cellular hypersensitivity to ICL-inducing agents such as MMC (172), accompanied by a persistent G2/M cell cycle arrest due to a failure to arrest (and repair) cells at the intra-S-phase checkpoint (13,91,145,173). To test if FANCD2 and FANCI cooperate to promote cellular resistance to DNA ICLs, we performed a survival assay. The cells were plated with increasing concentrations of MMC and the cell viability was measured after 5 days. *D2*$^{-/-}$, *I*$^{-/-}$ and *ID2* DKO cells were highly and equally sensitive to even the lowest MMC concentration (5 nM) when compared to the WT cells; moreover the complemented *D2*$^{-/-:D2}$ and *I*$^{-/-:I}$ cells exhibited WT-like MMC resistance, further indicating full functional complementation of these cells (Figure 4B). To analyze the cell cycle profiles of *FANCD2*- and/or *FANCI*-deficient cells in unperturbed and ICL-treated conditions, asynchronous cell populations were either untreated or treated with 10 nM MMC for 24 hr, followed by staining with propidium iodide and FACS analysis. In untreated conditions, the *D2*$^{-/-}$, *I*$^{-/-}$ and *ID2* DKO cells exhibited unaltered cell cycle profiles compared to the WT cells or their complemented counterparts (Figure 4C). In contrast, MMC treatment triggered a robust and comparable G2/M arrest in *D2*$^{-/-}$, *I*$^{-/-}$ and *ID2* DKO cells compared to WT, *D2*$^{-/-:D2}$ or *I*$^{-/-:I}$ cells (Figure 4C, D and Supplementary Figure S2). Thus, FANCD2 and FANCI act in concert to promote cellular resistance to DNA ICLs.

FANCD2 negatively regulates FANCI to promote cellular resistance to APH or HU

FANCD2 and FANCI accumulate on S-phase chromatin in response to the replication inhibitors APH or HU (66,151,170,174). Moreover, the Kupfer laboratory recently demonstrated that *FANCD2*-deficient patient cells are sensitive to HU treatment (174). To investigate if FANCD2 and FANCI both contribute to cellular APH or HU resistance, WT, *D2*$^{-/-}$, *D2*$^{-/-:D2}$, *I*$^{-/-}$, *I*$^{-/-:I}$ and *ID2* DKO cells were plated and either left untreated or treated with increasing doses of HU (50, 100 or 150 μM) or APH (10, 25 or 50 nM). Colony formation of each cell line was determined after 12 to 14 days. The *D2*$^{-/-}$ cells exhibited a strikingly increased, dose-dependent hypersensitivity to both HU and APH compared to WT cells (Figure 5A, B and Supplementary Figures S3A, B). In contrast, the *I*$^{-/-}$cells did not exhibit any HU or APH hypersensitivity compared to WT cells, indicating that FANCI is dispensable for the cellular resistance to HU or APH. Strikingly, the *ID2* DKO cells did not exhibit HU or APH sensitivity either, demonstrating that the depletion of FANCI restores the cellular resistance to these replication stressors in the absence of FANCD2 (Figure 5A, B and Supplementary Figures S3A, B). To further investigate this, we set out to analyze the cellular replication stress response in WT, *D2*$^{-/-}$, *I*$^{-/-}$ or *ID2* DKO cells in more detail. Since FANCD2 is predicted to protect stalled replication forks from collapsing into DNA DSBs (68-70), we asked if spontaneous or HU-triggered DNA DSB levels differed between *D2*$^{-/-}$ cells and the WT, *I*$^{-/-}$ or *ID2* DKO cells. Cells were untreated or treated with doses of low HU (500 μM) or high HU (2 mM) for 24 hr and WCEs were analyzed for the DNA DSB markers γ-H2AX and phospho-RPA2 (replication protein A; phosphorylated at serines 4 and 8). We did not observe any differences in the spontaneous or HU-triggered γ-H2AX or

phospho-RPA2 levels between the four cell lines, indicating that the DNA DSB burden *per se* is not elevated in cells lacking FANCD2 and/or FANCI (Figure 5C, D). Next, we asked if the chromatin recruitment of HDR repair proteins during replication stress was differently affected in $D2^{-/-}$ cells compared to WT, $I^{-/-}$ or ID2 DKO cells. CtIP, a key HDR factor required for replication restart and DNA DSB repair, relies on FANCD2 for its own chromatin recruitment (42,175,176). To analyze CtIP chromatin binding and CtIP relocalization into nuclear DNA repair foci, cells were left untreated or treated with 2 mM HU for 20 hr, followed by chromatin blotting or immunofluorescence analyses. In support of our previous findings, CtIP recruitment to chromatin and into DNA repair foci was severely reduced in untreated and HU-treated $D2^{-/-}$ cells compared to the WT cells (Figure 5E, F and Supplementary Figure S4). However, the $I^{-/-}$ and *ID2* DKO cells exhibited CtIP recruitment defects comparable to those observed in the $D2^{-/-}$ cells, suggesting that CtIP recruitment to stalled or collapsed replication forks relies on both FANCD2 and FANCI. We next analyzed the HU-triggered foci recruitment of RAD51, a second key HDR protein that forms protein-DNA filaments and is required for replication fork recovery and HDR repair of DNA DSBs. As expected, WT cells showed spontaneous RAD51 foci formation (10% cells), which increased significantly following 2 mM HU treatment for 20 hr (65% cells). Somewhat unexpectedly, the $D2^{-/-}$, $I^{-/-}$ and *ID2* DKO cells were fully competent for RAD51 foci formation before and after HU treatment (Figure 5G and Supplementary Figure S5), indicating that neither FANCD2 nor FANCI are crucial for the relocalization of RAD51 to HU-induced DNA repair foci. Supportive of this idea, we observed no difference in RAD51 foci formation in the

untreated or HU-treated *FA-D2* patient cell line, PD20, compared to its complemented counterpart, the PD20+D2 cell line (Supplementary Figure S6).

In addition to its role in DNA repair, FANCD2 has also been implicated in the so-called DNA damage tolerance (DDT) pathway that allows for cellular survival in the face of persistent DNA damage and replication stress (177,178). A key activation step of this pathway is the monoubiquitination of PCNA (proliferating cell nuclear antigen), which in turn recruits DNA TLS (translesion synthesis) polymerases to promote continuous, albeit mutagenic, replicative DNA synthesis. Recent studies showed that HU-induced PCNA monoubiquitination ($PCNA^{Ub}$) occurs in a FANCD2-supported manner to promote cellular HU resistance (174,179). To test if $PCNA^{Ub}$ formation is affected differently in $D2^{-/-}$ cells compared to WT, $I^{-/-}$ or *ID2* DKO cells, cells were left untreated or treated with 2 mM HU for 20 hr, followed by a chromatin blotting analysis. As expected, $D2^{-/-}$ cells exhibited a decreased spontaneous and HU-induced $PCNA^{Ub}$ formation; however, we observed similarly reduced $PCNA^{Ub}$ levels in the $I^{-/-}$ or *ID2* DKO cells (Figure 5H), suggesting that HU-induced PCNA monoubiquitination relies on both FANCD2 and FANCI.

Since none of these analyses adequately explained the unique hypersensitivity of $D2^{-/-}$ cells to HU and APH we next assessed the status of activated p53 in all of the cell lines. WT and all three knockout cell lines were untreated or treated with APH for 20 hr, followed by analysis of phospho-p53 (S15) and — as a relevant downstream p53 target — cellular p21 protein levels. Strikingly, phospho-p53 and p21 levels were highly elevated in untreated and APH-treated $D2^{-/-}$ cells, but not in the WT, $I^{-/-}$ or *ID2* DKO cells

(Figure 5I). These findings suggest that FANCD2 may protect cells from FANCI-mediated, replication stress-induced cell death.

FANCD2 promotes the restart of stalled replication forks independently of FANCI

FANCD2 functions to restart HU or APH-stalled replication forks, while simultaneously suppressing the firing of new replication origins (42,69,70,150). To test if FANCI shares these functions, we monitored replication events in WT, *D2*$^{-/-}$, *I*$^{-/-}$ and *ID2* DKO cells with a dual-labeling DNA fiber assay (69,163). Replication tracts were first labeled with DigU (red label) for 25 min, then left untreated or treated with 30 μM APH for 6 hr to cause replication fork arrest, followed by a second labeling with BioU (green label) for 40 min (Figure 6A). Different from the efficient fork restart in WT cells, the proportion of replication forks competent for restart after APH treatment was severely reduced in *D2*$^{-/-}$ cells (45% vs 85%, $p < 0.01$) (Figure 6B). In parallel, the proportion of newly originated replication tracts (BioU label only) increased significantly (two-fold; $p < 0.01$) in *D2*$^{-/-}$ cells compared to WT cells (Figure 6C). In contrast, we observed much milder replication restart defects in the *I*$^{-/-}$ cells (63%; $p < 0.05$) and the *ID2* DKO cells (54%; $p < 0.01$), accompanied by a lower number of newly fired replication origins (*I*$^{-/-}$ cells: 1.4-fold, $p < 0.05$; *ID2* DKO cells: 1.6-fold, $p < 0.01$) compared to the *D2*$^{-/-}$ cells (Figure 6B, C). Importantly, the replication restart efficiencies were significantly different between the three knockout cell lines, with an increase in restart efficiency in the order: *D2*$^{-/-}$ < *ID2* DKO < *I*$^{-/-}$ cells (Figure 6B). To further validate these findings in the presence of a second replication fork stalling agent, HU, we performed a technically improved DNA replication fork restart analysis using DNA combing (164). Moving replication forks were labeled with CldU (green label) for 20 min, then left untreated or treated with 4 mM

HU for 4 hr to cause replication fork arrest, followed by a second labeling with IdU (red label) for 40 min (Figure 6D). Comparable to what we observed following APH-mediated fork stalling, WT cells exhibited efficient fork restart following HU treatment, whereas the proportion of restarted replication forks after HU treatment was significantly reduced in $D2^{-/-}$ cells (68%, $p < 0.01$) (Figure 6E). Moreover, we observed milder replication restart defects in the $I^{-/-}$ cells (81%; $p < 0.05$) and in the *ID2* DKO cells (71%; $p < 0.01$).

These findings indicate that FANCD2 plays a more crucial role than FANCI during replication fork restart and the inhibition of new origin firing. Moreover, the fact that FANCI depletion in $D2^{-/-}$ cells improved these cells' ability to restart replication forks and suppress new origin firing, particularly after APH treatment, provocatively suggests that FANCI may have an inhibitory effect on both mechanisms in the absence of FANCD2.

Considering that non-ubiquitinated FANCD2 retains weak chromatin binding activity in $I^{-/-}$ cells (see Figure 3E), we then hypothesized that the few remaining chromatin-bound FANCD2 molecules may still be functional and capable of promoting replication fork restart in the absence of FANCI. If this were indeed the case, it should be possible to completely alleviate the replication fork restart defect in $I^{-/-}$ cells by increasing the amount of chromatin-bound FANCD2. To test this, we overexpressed FANCD2 in $I^{-/-}$ cells ($I^{-/-:D2o/e}$, Figure 7A), resulting in chromatin-bound, non-ubiquitinated FANCD2 levels comparable to those observed for chromatin-bound, monoubiquitinated FANCD2 in WT cells, before and after HU treatment (Figure 7B). WT, $D2^{-/-}$ and $I^{-/-}$ cells, as well as two different $I^{-/-:D2o/e}$ cell clones, were then analyzed for their replication fork restart

efficiencies following HU treatment using the DNA combing assay. Strikingly, unlike the $I^{-/-}$ cells that were moderately defective for replication fork restart (81%, $p < 0.05$), both $I^{-/-:D2o/e}$ cell clones were completely proficient in restarting HU-stalled replication forks, comparable to the WT cells (Figure 7C). These results indicate that non-ubiquitinated, chromatin-bound FANCD2 is fully competent to promote replication fork restart in the absence of FANCI.

Stabilizing RAD51 nucleoprotein filaments restores HDR-mediated DNA DSB repair in cells lacking functional FANCD2

Cells can utilize HDR to repair DNA DSBs (5,50), including those created by the unhooking of a DNA ICL lesion (142,143). In addition, a growing number of HDR factors have been implicated in promoting replication fork recovery in concert with FANCD2 (42,67-70,83,150), suggesting that the restart machinery utilizes HDR-related mechanisms to restart DNA synthesis at a stalled fork. To investigate the roles of FANCD2 and FANCI in HR-mediated DNA DSB repair we utilized a well-established reporter plasmid DNA repair assay (159). In this assay, a plasmid containing two non-functioning *GFP* genes in tandem is transfected into the cells. One non-functioning *GFP* gene contains an I-SceI restriction enzyme recognition site and the other is truncated at both the 5'- and 3'-ends. Digestion of the plasmid with I-SceI creates a DNA DSB in the non-functional *GFP* gene that can subsequently use the truncated *GFP* gene as template to restore GFP expression by homology-directed gene conversion repair. As a control for this assay, we included the $RAD54B^{-/-/-}$ HCT116 cell line that has an established HDR defect (180,181). The $D2^{-/-}$ cells were severely deficient in HDR-mediated DNA DSB repair (34% of WT), a level that was comparable to the $RAD54B^{-/-/-}$ cells (Figure 8A). In

contrast, the *I*$^{-/-}$ and *ID2* DKO cells exhibited much milder HDR repair defects (62% and 56% of WT, respectively (Figure 8A)). These results indicate that (i) FANCD2 has a more important role than FANCI in HDR-mediated DNA DSB repair and — surprisingly that — (ii) FANCI opposes HDR-mediated DNA DSB repair in the absence of FANCD2.

FANCD2 was proposed to recruit the HDR factor RAD51 to chromatin during replication stress and to stabilize RAD51 nucleoprotein filaments that are crucial to promote HDR mechanisms of replication fork recovery and DSB repair (68,182). Thus, we wanted to ask if the HDR repair deficiency observed in cells lacking functional FANCD2 can be overcome by stabilizing RAD51 filament formation. To this end, we repeated the GFP HDR assay described above in WT, *D2*$^{-/-}$ *I*$^{-/-}$ and *ID2* DKO cells in the absence or presence of a RAD51 filament stabilizing agent, RS-1 (183). In the presence of RS-1, all three knockout cell lines restored their HDR repair efficiency to a level comparable to the untreated WT cells (Figure 8B). Taken together, these findings support a current model (68,182) in which chromatin-bound FANCD2 plays a crucial role in stabilizing RAD51 filament formation during HDR-mediated DNA repair and, consequently, replication fork recovery.

DISCUSSION

In this study, we analyzed the functions of FANCD2 and FANCI during DNA replication, using isogenic knockout cell lines. Our results suggest that FANCD2 and FANCI fulfill partially independent and at times opposing roles in the cellular replication stress response (Figure 9).

A novel cell model to study common and independent roles of FANCD2 and FANCI

Our model system provides unique advantages compared to the use of FA patient cells or siRNA knockdown approaches. First, patient-derived *FA-D2* and *FA-I* cell lines are derived from different genetic backgrounds and exhibit residual FANCD2 and FANCI protein expression (145,165,166); second, siRNA-mediated knockdown approaches cannot completely or permanently eliminate protein expression (42,145,150,166). In contrast, our system allowed for a functional dissection of the roles of FANCD2 and FANCI in identical genetic background settings and in the complete absence of any FANCD2 and/or FANCI protein expression. On a technical note, but similar to previous reports (167,169), our attempts to complement $I^{-/-}$ cells with a stably integrated FANCI cDNA were unsuccessful due to the rapid loss of FANCI expression, strongly suggesting that cells may not tolerate FANCI expression from a random genomic locus or, more likely, that FANCI overexpression is toxic (see also below).

Based on the fact that all known *FA-D2* or *FA-I* patient cell lines have residual FANCD2 and FANCI (respective) expression (145,165,166), we predicted that the complete loss of one or both proteins may be lethal. However, the $D2^{-/-}$, $I^{-/-}$ and *ID2* DKO cell lines were viable, indicating that neither *FANCD2* nor *FANCI* are essential in human somatic cells; needless to say, however, these experiments do not rule out important developmental

roles for either of these genes, a likelihood that is consistent with the developmental abnormalities often observed in FA patients. While not formally essential, both proteins contribute to cellular proliferation. Importantly, the fact that *ID2* DKO cells proliferated significantly slower than either of the singly-null cells demonstrates that FANCD2 and FANCI have (at least) partially non-overlapping roles during normal cellular proliferation. Consistent with this idea, in the *Xenopus* system the ID2 dimer dissociates upon activation in S-phase, followed by consecutive recruitment of FANCD2 and FANCI to S-phase chromatin (151). Furthermore, FANCD2 acts independently of FANCI to assemble and recruit the BLM helicase complex to replicating chromatin (69).

A separation-of-function between FANCD2 and FANCI is further supported by our finding that approximately 40 to 50% of either protein is stably expressed in absence of the respective other partner, in agreement with some previous studies (87,145,166). Interestingly, nuclear accumulation of FANCD2 and FANCI occurred independently of one another in unperturbed conditions. This suggests that FANCD2 and FANCI are not interdependent for their nuclear localization *per se*: in unperturbed conditions, cells simply upregulate the nuclear import of residual FANCI in absence of FANCD2 and *vice versa*, possibly in an attempt to partially compensate for one another. During replication stress however, the reduced FANCI and FANCD2 protein levels in $I^{-/-}$ and $D2^{-/-}$ cells, respectively, become limiting and block sufficient nuclear FANCD2 and FANCI accumulation. Inconsistent with this interpretation, it has been reported that the *FA-D2* patient cell line, PD20, lacks any nuclear FANCI protein compared to the complemented PD20+D2 cells (171). We suggest that this discrepancy may be because the difference in

FANCI protein expression appears to be greater between the PD20 cells and the highly FANCD2-overexpressing PD20+D2 cells (145) than between our $D2^{-/-}$ and $D2^{-/-:D2}$ cells.

Different roles for chromatin-bound and non-chromatin-bound FANCD2 and FANCI?

Importantly, the independent nuclear accumulation of FANCD2 and FANCI was not mirrored by their chromatin binding behavior, since both proteins appeared to be strongly interdependent for chromatin recruitment even in unperturbed conditions. Considering that the three knockout cell lines have significantly different growth rates, the chromatin binding ability of FANCD2 and FANCI is not indicative of a cell's proliferation ability. This in turn suggests that FANCD2 and FANCI have functions that do not require a direct association with chromatin and supports accumulating evidence that FANCD2 and FANCI have independent roles, such as the (only FANCI-mediated) stabilization of the FA core complex on chromatin or the (only FANCD2-mediated) support of alternative non-homologous end joining (A-NHEJ) DNA repair mechanisms (see also Supplementary Figure S7) (69,83,150,151,169,174,184). Our observation that non-ubiquitinated FANCD2 is present on chromatin in the absence of FANCI is in agreement with our previous findings that non-ubiquitinated FANCD2 binds chromatin in FANCI-depleted *Xenopus* extracts (69,151) and supports a recent study that showed that FANCD2 binds DNA prior to being monoubiquitinated (185). Moreover, we have shown that low levels of non-ubiquitinated FANCD2 accumulate on chromatin in an APH-inducible manner to promote replication fork restart, regardless of the presence or absence of a functional FA core complex (150). Finally, this current study shows that $I^{-/-}$ cells that have residual levels of chromatin-bound, non-ubiquitinated FANCD2 are still

capable of partially supporting replication fork restart following APH or HU treatment; moreover, simply increasing the chromatin-bound FANCD2 levels via FANCD2 overexpression completely alleviated the replication restart defects in these cells. *In toto*, these observations argue strongly that the non-ubiquitinated FANCD2 isoform is functional in its chromatin-bound state.

Importantly, however, the residual FANCD2 chromatin binding in *FANCI*-deficient cells did not alleviate their ICL sensitivity, reinforcing the model of a linear FA ICL repair pathway, where the FANCI-dependent FANCD2 monoubiquitination is crucial for cellular ICL resistance (145,147,166,186) (Figure 8A). Thus, these experiments define a separation-of-function for FANCD2 monoubiquitination: it is required for ICL repair but dispensable for replication fork restart.

The striking finding that only *D2*$^{-/-}$ cells — but not *I*$^{-/-}$ or *ID2* DKO cells — were sensitive to HU or APH and exhibited elevated activation of phospho-p53 and p21 expression is supported by a recent report showing HU sensitivity in *FA-D2* patient cells (174). Together, these studies suggest that FANCD2 may prevent FANCI-mediated cell death following replication stress (Figure 9). Since *D2*$^{-/-}$ cells are indistinguishable from *I*$^{-/-}$ or *ID2* DKO cells regarding their spontaneous or stress-induced DNA DSB accumulation, and the recruitment of HDR repair factors or the activation of the DDT pathway, FANCD2's role in preventing APH- or HU-triggered cell death appears to be separate from its role in protecting chromosomal stability. Moreover, since *I*$^{-/-}$ and *ID2* DKO cells are equally resistant to HU or APH despite harboring different residual chromatin-bound FANCD2 levels, FANCD2's role in preventing APH/HU-induced cell death may in fact not depend on its own chromatin association. Consistent with our

findings and interpretation, a role for FANCD2 in preventing apoptosis and cell death was also suggested by several groups (187-189). Moreover, a recent study showed that siRNA-mediated knockdown of FANCI, but not FANCD2, substantially reduced cellular apoptosis after UV treatment (184). Clearly, in the future, the mechanistic basis of FANCD2's putative role in cell death induction will be a key question for the field to answer (Figure 9).

Opposing roles for FANCD2 and FANCI during HDR-mediated mechanisms of fork recovery and DNA DSB repair?

In agreement with our previous findings (42,69,70), FANCD2 promoted the restart of APH-stalled replication forks, a process that requires several members of the HDR repair machinery, including RAD51 (42,69,150,163,190). The fact that the HDR repair defect in *D2*$^{-/-}$ cells could be almost completely rescued by stabilizing RAD51 filaments via RS-1 supports a model in which FANCD2 functions to (i) promote replication fork restart and (ii) protect nascent DNA from nucleolytic degradation (42,68-70) by promoting RAD51 filament formation. In support of this model, a recent study showed that the FANCD2:FANCI heterodimer stabilizes RAD51 filament formation *in vitro* (182). It should be noted that wild type-like RAD51 foci formation was observed in all three knockout cell lines including the *D2*$^{-/-}$ cells (Figure 5G), seemingly contradicting the idea that FANCD2 is required for RAD51 filament formation. However, findings from our laboratory and others (42,190) indicate that foci formation of HDR repair factors, such as RAD51 or CtIP, does not occur at intact stalled replication forks, but instead occurs much later once the forks have collapsed. The question, therefore, of whether RAD51 foci can form in the absence of FANCD2 remains controversial (182,191-195).

I$^{-/-}$ cells exhibited milder defects in HDR-mediated replication restart and DSB repair than the *D2*$^{-/-}$ cells, initially suggesting separate roles for FANCD2 and FANCI during HDR as well. However, two additional findings suggest otherwise: First, overexpression of FANCD2 completely rescued HDR-mediated replication restart defects in *I*$^{-/-}$ cells. Second, *ID2* DKO cells exhibited a less pronounced HDR defect than the *D2*$^{-/-}$ cells. Thus, FANCI's role in HDR may be to simply stabilize FANCD2, which by itself is the actual recruiter of HDR factors. In this scenario, the residual chromatin-bound, non-ubiquitinated FANCD2 would allow *I*$^{-/-}$ cells to partially support HDR-mediated fork restart, similar to chromatin-bound FANCD2 in FA core complex-deficient cells (150). Importantly, *FANCD2*- and *FANCI*-deficient cells can compensate for their replication restart defects by the enhanced firing of new replication origins (69,163), which likely counteracts chromosomal instability in the presence of replication stress. Our finding that cells lacking FANCI modestly upregulate new origin firing during replication stress seemingly contradicts a recent study showing that FANCI is required for new origin firing during replication stress (83). However, these authors investigated the role of FANCI mostly under continuous low replication stress conditions (0.2 mM HU), whereas our study used transient, high replication stress conditions (30 μM APH for 6 hr), indicating, at the very least, that FANCI is not required for new origin firing when replication forks are stalled for several hours.

Perhaps the most unexpected finding was that cells lacking both FANCD2 and FANCI exhibited intermediate HDR repair and replication fork restart defects, more severe than *FANCI*-deficient cells, but less severe than *FANCD2*-deficient cells. We suggest at least two possible explanations: (A) FANCI actively opposes FANCD2 to negatively regulate

HDR or (B) FANCD2 and FANCI work in concert during HDR, but FANCI becomes inhibitory to HDR *in the absence of FANCD2* (Figure 9). FANCD2 and FANCI can form a protein complex with RAD51 and contribute to RAD51 recruitment to DNA (182). If FANCI is in fact the direct interactor with RAD51 *in vivo*, the nuclear (but not chromatin-bound) FANCI may actively sequester RAD51 away from the DNA in *FANCD2*-deficient cells, causing the particularly severe HDR phenotype observed in these cells. Importantly, in both of these scenarios it would be predicted that the overexpression of FANCI would be deleterious for HDR (and presumably, therefore, cell viability), which was indeed observed by us and others in our inability to establish FANCI-overexpressing complemented clones. Lastly, it may also be possible that only in the absence of both proteins is a compensatory/back-up pathway engaged that can facilitate RAD51 recruitment.

In summary, our findings suggest a model in which FANCD2 and FANCI have partially non-overlapping roles in promoting cell survival and HR-mediated fork recovery in the presence of APH or HU-induced replication stress.

ACKNOWLEDGMENTS

The authors would like to thank the FA patients and their families for their interest in our research over the years. We are especially grateful to the Fanconi Anemia Research Fund (FARF), Inc. and the German family organizations "Fanconi-Anämie-Stiftung e. V.", "Aktionskreis Fanconi-Anämie e.V." and "Deutsche Fanconi-Anämie-Hilfe e.V." for their support of our ideas and work. We would like to thank Dr. Sarah Riman for technical help in generating the *FANCD2*-null cell line and Jihyeon Yang for technical help with cell culture and western blots. We would also like to thank Dr. Anja-Katrin Bielinsky for her comments on the manuscript during its preparation.

FIGURE LEGENDS

Figure 1. rAAV-mediated generation of *FANCD2*$^{-/-}$ (*D2*$^{-/-}$), *FANCI*$^{-/-}$ (*I*$^{-/-}$) and *FANCI*$^{-/-}$:*FANCD2*$^{-/-}$ (*ID2* DKO) cell lines.

(A) Schematic of FANCD2 (left panel) and FANCI (right panel) targeting strategies in HCT116 cells. FANCD2 exon 12 and FANCI exon 10 were targeted for deletion by rAAV gene targeting. The first allele targeting was performed using conditional rAAV vectors for *FANCD2* and *FANCI*. The conditional vectors contain rAAV inverted terminal repeats (ITRs) (grey boxes), homology arms (white boxes), a NEO selection cassette (green boxes) and the targeted exon (blue boxes) flanked by LoxP sites (orange triangles). Targeted clones were treated with Cre recombinase to remove the *NEO* selection cassette. (B) The second allele targeting was performed in the *FANCD2*$^{flox/+}$ cell line (f/+) using a *FANCD2* knockout rAAV vector and in the *FANCI*$^{flox/+}$ cell line (f/+) with the same *FANCI* conditional rAAV vector utilized in the first round of targeting. Targeted clones were treated with Cre recombinase to remove both the *NEO* selection cassette and the conditionally floxed exons, resulting in the generation of *FANCD2*$^{-/-}$ (*D2*$^{-/-}$) and *FANCI*$^{-/-}$ (*I*$^{-/-}$) cell lines.

Figure 2. Confirmation of *D2*$^{-/-}$, *I*$^{-/-}$ and *ID2* DKO cell lines.

(A) PCR genotyping of *D2*$^{-/-}$ and *I*$^{-/-}$ cells and targeting intermediates. Left panel: analyses of DNA fragments for WT (lane 1), *D2*$^{flox/Neo}$ (lanes 2 and 3), and *D2*$^{-/-}$ (lanes 4 and 5) after PCR amplification with primers FANCD2_EX11SF and FANCD2_LoxPSR flanking the targeted exon. Right panel: analyses of DNA fragments after PCR amplification from WT (lane 1), *I*$^{flox/+}$ (lane 2), and *I*$^{-/-}$ (lanes 3 and 4) cells using primers FancIc_GG_LIF and FancIcond_GG_LoxR flanking the targeted exon. The PCR

amplification spanning the targeted exons (exon 12 in *FANCD2*; exon 10 in *FANCI*) was used to confirm the removal of the respective exon in the $D2^{-/-}$ and $I^{-/-}$ cell lines. M: 1 kb markers. (B) Schematic of the *FANCD2* targeting strategy in $I^{-/-}$ cells. CRISPR/Cas9-mediated gene targeting was used to functionally inactivate *FANCD2* in the $I^{-/-}$ cell line. A guide RNA (purple sequence) was designed targeting *FANCD2* exon 11 with the Cas9 cut site (red arrow) overlapping an endogenous BpuEI restriction enzyme recognition site (black bar). The PAM sequence of the sgRNA is shown in blue. Indels introduced at the Cas9 cut site should disrupt the BpuEI cleavage site. (C) Genotyping of *ID2* DKO cells. PCR amplification and BpuEI restriction enzyme digestion of *FANCD2* exon 11 in WT, $I^{-/-}$ and two $ID2^{-/-}$ clones (1 and 2). Analyses of DNA fragments after PCR amplification with primers FancD2_CC_ F2 and FancD2_CC_ R2 (blue arrows from panel B) from WT (lanes 1 and 2), $I^{-/-}$ (lanes 3 and 4), and *ID2* DKO cells (lanes 5, 6, 7 and 8) that had been untreated (lanes 1, 3, 5 and 7) or treated with BpuEI (lanes 2, 4, 6, and 8). Cleavage by BpuEI produces 2 faster migrating fragments (D, lanes 2 and 4). Resistance (R) to BpuEI digestion is seen in lanes 6 and 8 with the two *ID2* DKO clones. (D) Sequence confirmation of CRISPR/Cas9 induced bi-allelic frameshift mutations in *FANCD2* in the two *ID2* DKO clones #1 and #2.

Figure 3. Initial characterization of the $I^{-/-}$, $I^{-/-:I}$, $D2^{-/-}$, $D2^{-/-:D2}$ and *ID2* DKO cell lines.

FANCD2 and FANCI are completely interdependent for their replication stress-triggered monoubiquitination. (A) WCE was prepared from WT cells (lanes 1 and 2), $D2^{-/-}$ cells (lanes 3 and 4) or $D2^{-/-:D2}$ cells (lanes 5 and 6) that had been untreated (lanes 1, 3 and 5) or treated with 2 mM HU for 20 hr (lanes 2, 4 and 6) and analyzed for the presence of

FANCD2 and FANCI by western blot analysis. Ku86 was used as a loading control. (B) WCE were prepared from WT cells (lanes 1 and 2), $I^{-/-}$ cells (lanes 3 and 4), $I^{-/-:I}$ (clone 7) cells (lanes 5 and 6), $I^{-/-:I}$ (clone 11) cells (lanes 7 and 8), and *ID2* DKO cells (lanes 9 and 10) that were untreated (lanes 1, 3, 5, 7 and 9) or treated with 2 mM HU for 20 hr (lanes 2, 4, 6, 8 and 10) and analyzed for the presence of FANCD2 and FANCI by western blot analysis. Ku86 was used as a loading control. (C) FANCD2 and FANCI are partially stable in the absence of one another. Left panel: WCE were prepared from WT (lanes 1, 4 and 7), $D2^{-/-}$ (lanes 2, 5 and 8), and $I^{-/-}$ (lanes 3, 6 and 9) cells that were untreated (lanes 1 to 3) or treated with 2 mM HU for 6 hr (lanes 4 to 6) or for 20 hr (lanes 7 to 9) and analyzed for FANCD2 and FANCI expression by western blot analysis. Tubulin was used as a loading control. Right panel: Immunoblot signals shown in the left panel were analyzed by densitometry and normalized against the tubulin signals using ImageJ software. The graph shows the percentage of FANCD2 and FANCI protein levels in $I^{-/-}$ and $D2^{-/-}$ cells, respectively, compared to the WT cells. (D) Nuclear import of FANCD2 and FANCI becomes interdependent during replication stress. Nuclear fractions were isolated from WT, $D2^{-/-}$ and $I^{-/-}$ cells that were untreated (lanes 1 to 3) or HU-treated (lanes 4 to 9) for the indicated time points and analyzed for the presence of FANCD2 and FANCI. Ku86 was used as a loading control. (E) Non-ubiquitinated FANCD2 binds chromatin independently of FANCI during normal replication and following replication stress. Chromatin fractions were isolated from WT, $D2^{-/-}$ and $I^{-/-}$ cells that were untreated (lanes 1 to 3) or HU-treated (lanes 4 to 9) for the indicated time points and analyzed for the presence of FANCD2 and FANCI. Ku86 was used as a loading control.

Figure 4. FANCD2 and FANCI contribute differently to cell proliferation and the cellular response to replication stress.

(A) The absence of FANCD2 and FANCI affects cell proliferation synergistically. WT, *D2*$^{-/-}$(clones #29 and #39), *I*$^{-/-}$ (clones #28 and #30) and *ID2* DKO (clones #1 to #4) cells, as well as the complemented counterparts, were plated according to their plating efficiency and total cell counts were performed in triplicate at days 4, 6 and 8. Data points were averaged between clones of identical genetic backgrounds. Error bars represent the standard deviation. (B) FANCD2 and FANCI act in concert to promote MMC resistance. Cell viability was measured for WT, *D2*$^{-/-}$, *I*$^{-/-}$, *ID2* DKO and complemented cell lines using CellTiter96 Aqueous staining 5 days after the addition of 0, 5, 10 or 15 nM MMC. Results were averaged from a minimum of 3 replicates and normalized to the average viability of the respective untreated cells. Error bars represent the standard deviation. (C) FANCD2 and FANCI act in concert to activate the MMC-triggered intra-S phase checkpoint. WT, *D2*$^{-/-}$(clones #29 and #39), *I*$^{-/-}$ (clones #28 and #30) and *ID2* DKO (clones #1 and #2) cells, as well as the complemented counterparts, were untreated or treated with 10 nM MMC for 20 hr, followed by propidium iodide (PI) staining and FACS analysis. Representative histograms of the cell cycle profiles are shown for each cell line. Blue shading represents G1 phase cells, orange shading represents S phase cells and grey shading represents G2/M phase cells. (D) Graphic representation of the percentage of the indicated cell populations present in the G2/M phase of the cell cycle in the absence or presence of MMC. Data points were averaged between clones of identical genetic backgrounds. The average percentage of the G2/M

cell population was determined from a minimum of 3 replicates. Error bars represent the standard deviation and the significance was determined by t-test.

Figure 5. FANCI promotes replication stress-induced cellular apoptosis in the absence of FANCD2.

(A) FANCD2, but not FANCI, promotes cellular resistance to HU. WT, *D2*$^{-/-}$(clone #39), *I*$^{-/-}$ (clone #28) and *ID2* DKO (clone #1) cells, as well as the complemented cell lines were plated at low density and incubated with increasing doses of HU (0 to 150 μM) for 12 to 14 days to allow for single cell colony formation. Plates were fixed and stained with Coomassie, and colonies with a minimum of 50 cells were scored. Results were averaged from a minimum of 3 replicates and normalized to the respective untreated cells. Error bars represent the standard deviation and significance was determined by t-test. Statistical significance at $p < 0.05$, $p < 0.01$, and $p < 0.001$ are indicated as *, **, ***, respectively. (B) FANCD2, but not FANCI, promotes cellular resistance to APH. WT, *D2*$^{-/-}$(clone #39), *I*$^{-/-}$ (clone #28) and *ID2* DKO (clone #1) cells, as well as the complemented cell lines were plated at low density and incubated with increasing doses of APH (0 to 50 nM) for 12 to 14 days to allow for single cell colony formation. Plates were fixed and stained with Coomassie, and colonies with a minimum of 50 cells were scored. Results were averaged from a minimum of 3 replicates and normalized to the respective untreated cells. Error bars represent the standard deviation and significance was determined by t-test. Statistical significance at $p < 0.05$, $p < 0.01$, and $p < 0.001$ are indicated as *, **, ***, respectively. (C) FANCD2 and FANCI are dispensable for the prevention of spontaneous or replication stress-induced DNA DSBs. WCE were prepared from WT (lanes 1 and 5), *D2*$^{-/-}$ (lanes 2 and 6), *I*$^{-/-}$ (lanes 3 and 7), and *ID2* DKO

(lanes 4 and 8) cells that were untreated (lanes 1 to 4) or treated with 500 μM HU for 20 hr (lanes 5 to 8) and analyzed for the induction of pRPA32 (S4/8) and γ-H2AX expression by western blot analysis. GAPDH was used as a loading control. (D) WCE was prepared from WT (lanes 1 and 5), *D2*$^{-/-}$ (lanes 2 and 6), *I*$^{-/-}$ (lanes 3 and 7), and *ID2* DKO (lanes 4 and 8) cells that were untreated (lanes 1 to 4) or treated with 2 mM HU for 20 hr (lanes 5 to 8) and analyzed for DNA DSB markers, pRPA32 (S4/8) and γ-H2AX by western blot analysis. GAPDH was used as a loading control. (E) FANCD2 and FANCI cooperate to recruit CtIP to chromatin in the absence or presence of replication stress. Chromatin fractions were isolated from WT, *D2*$^{-/-}$ (clone #39) and *I*$^{-/-}$ (clone #28) cells that were untreated (lanes 1 to 3) or treated with 2 mM HU (lanes 4 to 9) for the indicated time points and analyzed for the presence of CtIP by western blot analysis. Ku86 was used as a loading control. (F) FANCD2 and FANCI cooperate to promote CtIP foci formation during replication stress. WT, *D2*$^{-/-}$ (clone #39), *I*$^{-/-}$ (clone #28) and *ID2* DKO (clone #1) cells were untreated or treated with 2 mM HU for 20 hr and cellular nuclei were analyzed for the presence of CtIP foci. Nuclei with >5 foci were considered positive for CtIP foci formation. (G) FANCD2 and FANCI are dispensable for RAD51 foci formation during replication stress. WT, *D2*$^{-/-}$ (clone #39) and *I*$^{-/-}$ (clone #28) and *ID2* DKO (clone #1) cells were untreated or treated with 2 mM HU for 20 hr and cellular nuclei were analyzed for the presence of RAD51 foci. Nuclei with >5 foci were considered positive for RAD51 foci formation. (H) FANCD2 and FANCI cooperate to promote the monoubiquitination of chromatin-bound PCNA in the absence or presence of HU-triggered replication stress. Chromatin fractions were isolated from WT, *D2*$^{-/-}$ (clone #39), *I*$^{-/-}$ (clone #28) and *ID2* DKO (clone #1) cells that were untreated (lanes 1, 3, 5, and

7) or treated with 2 mM HU (lanes 2, 4, 6, and 8) for 20 hr and analyzed for the presence of PCNA and $PCNA^{Ub}$ by western blot analysis. H2AX was used as a loading control. (I) FANCD2 prevents FANCI-dependent cellular apoptosis in unperturbed conditions and following replication stress. WCE were prepared from WT (lanes 1 and 5), $D2^{-/-}$ (lanes 2 and 6), $I^{-/-}$ (lanes 3 and 7), and ID2 DKO (lanes 4 and 8) cells that were untreated (lanes 1 to 4) or treated with 100 nM APH for 20 hr (lanes 5 to 8) and analyzed for phospho-p53 (S15) and p21 by western blot analysis. Ku86 was used as a loading control.

Figure 6. FANCD2 plays a more crucial role than FANCI to promote replication fork recovery.

(A) Schematic of the replication fork restart protocol with representative images of DNA fibers. Red tracks: DigU; green tracks: BioU. (B) FANCD2 plays a more crucial role than FANCI in promoting the restart of APH-stalled replication forks. The efficiency of replication restart in WT, $D2^{-/-}$ (clone #39), $I^{-/-}$ (clone #28) , and *ID2* DKO (clone #1), as well as in the complemented cells was measured as the number of restarted replication forks after APH (30 μM) mediated fork stalling (DigU-BioU tracts), compared with the total number of DigU-labeled tracts (DigU plus DigU-BioU). Statistical significance at $p < 0.05$, $p < 0.01$, and $p < 0.001$ are indicated as *, **, ***, respectively. (C) FANCD2 plays a more crucial role than FANCI in suppressing new origin firing in the presence of stalled replication forks. WT, $D2^{-/-}$ (clone #39), $I^{-/-}$ (clone #28) , and *ID2* DKO (clone #1), as well as the complemented cells were analyzed for the fraction of newly fired replication origins during the 40 min post-APH recovery period. Fractions were measured as the number of green-only (BioU) tracts compared with the total number of spreading replication tracts (BioU plus DigU-BioU). Statistical significance at $p < 0.05$,

$p < 0.01$, and $p < 0.001$ are indicated as *, **, ***, respectively. (D) Schematic of the DNA combing assay with representative images of stretched DNA fibers. Green tracks: CldU; red tracks: IdU. (E) FANCD2 plays a more crucial role than FANCI in promoting the restart of HU-stalled replication forks. The efficiency of replication restart in WT, *D2*$^{-/-}$(clones #29 and #39), *I*$^{-/-}$ (clones #28 and #30) and *ID2* DKO (clones #1 and #2) was measured as the number of restarted replication forks after HU-mediated fork stalling (CldU-IdU tracts), compared with the total number of CldU-labeled tracts (CldU plus CldU-IdU). Data points were averaged between clones of identical genetic backgrounds. Statistical significance at $p < 0.05$, $p < 0.01$, and $p < 0.001$ are indicated as *, **, ***, respectively.

Figure 7. Over-expressed FANCD2 fully promotes replication fork restart in the absence of FANCI

(A) Human wild type FANCD2 can be stably overexpressed in *I*$^{-/-}$ cells. A PiggyBac transposon containing the *FANCD2* codon-optimized cDNA was introduced into *I*$^{-/-}$ cells (clone #28), and two FANCD2-overexpressing *I*$^{-/-}$ cell lines (named *I*$^{-/-:D2o/e}$, clones #2 and #12) were generated. To determine the level of FANCD2 overexpression, WCEs were prepared from WT (lanes 1 and 2), *I*$^{-/-}$ (lanes 3 and 4), and *I*$^{-/-:D2o/e}$ (lanes 5 to 8) cells that were untreated (lanes 1, 3, 5, 7) or treated with 4 mM HU for 4 hr (lanes 2, 4, 6, and 8) and analyzed for the presence of FANCD2 by western blot analysis. Actin was used as a loading control. (B) Overexpression of FANCD2 leads to an increase in FANCD2 chromatin binding in the absence of FANCI. In parallel to the preparation of WCEs described in (A) above, chromatin fractions were isolated from these same WT (lanes 1 and 2), *I*$^{-/-}$ (lanes 3 and 4), and *I*$^{-/-:D2o/e}$ (lanes 5 to 8) cells that were untreated

(lanes 1, 3, 5, 7) or treated with 4 mM HU for 4 hr (lanes 2, 4, 6, and 8) and analyzed for the presence of FANCD2 by western blot analysis. H3 was used as a loading control. (C) FANCD2 overexpression rescues the replication fork restart defects in FANCI null cells. The efficiency of replication fork restart in WT, $D2^{-/-}$, $I^{-/-}$, and $I^{-/-:D2o/e}$ cells was measured as the number of restarted replication forks after HU-mediated fork stalling (CldU-IdU tracts), compared with the total number of CldU-labeled tracts (CldU plus CldU-IdU). Statistical significance at $P<0.05$, $P<0.01$, and $P<0.001$ are indicated as *, **, ***, respectively.

Figure 8. FANCD2 plays a crucial role to promote HDR-mediated, RAD51-dependent DNA DSB repair.

(A) A GFP-HDR DNA repair assay was used to determine the HDR efficiency in WT, $D2^{-/-}$(clones #29 and #39), $I^{-/-}$ (clones #28 and #30) and *ID2* DKO (clones #1 and #2), as well as in the complemented cells. $RAD54B^{-/-/-}$ cells were included in the assay as a control cell line that is severely HDR deficient. In this assay, I-SceI restriction enzyme digestion creates a DSB in the HDR reporter plasmid (DR-GFP). Repair of the DSB by HDR restores GFP expression. The repair efficiency was determined by dual GFP and mCherry positive cells divided by the mCherry positive cells (transfection control). Results were averaged from a minimum of 3 replicates and normalized to the average repair efficiency in the WT cells. Data points were averaged between clones of identical genetic backgrounds. Statistical significance at $p < 0.05$, $p < 0.01$, $p < 0.001$ and $p < 0.0001$ are indicated as *, **, ***, **** respectively. (B) The HDR assay shown in (A) was repeated for the WT, $D2^{-/-}$, $I^{-/-}$ and *ID2* DKO cells in the absence or presence of the RAD51 stabilizer, RS-1 (7.5 mM). Results were averaged from a minimum of 3

replicates and normalized to the average repair efficiency in the WT cells. Statistical significance at $p < 0.05$, $p < 0.01$, $p < 0.001$ and $p < 0.0001$ are indicated as *, **, ***, **** respectively.

Figure 9. Model of common and independent functions of FANCD2 and FANCI

(A)FANCD2 and FANCI act in concert during the cellular response to DNA ICLs in S-phase to promote ICL removal and cell survival. (B and C) FANCD2 and FANCI have separate roles during the cellular response to APH- or HU- stalled replication forks. (B) FANCD2 – but not FANCI – is crucial to recruit RAD51 and promotes RAD51 filament formation to mediate fork recovery. (C) Simultaneously, FANCD2 promotes cell survival by inhibiting a FANCI-dependent lethal response.

Supplementary Figure S1. CRISPR/Cas9-mediated gene targeting to create additional D2$^{-/-}$ clone 29 and DKO clones 3 and 4

(A) Schematic of the CRISPR/Cas9-mediated gene targeting to knockout *FANCD2* in WT cells to create D2$^{-/-}$ clone #29. A guide RNA was designed targeting *FANCD2* exon 11 with the Cas9 cut site overlapping with an endogenous BpuEI restriction enzyme recognition site. Indels introduced at the Cas9 cut site (red arrow) would disrupt the BpuEI cut site. Sequence confirmation of biallelic frameshift inducing mutations. (B) Schematic of the CRISPR/Cas9-mediated gene targeting to knockout *FANCI* in D2$^{-/-}$ clone #29 cells to create ID2$^{-/-}$ clone 3. A guide RNA was designed targeting *FANCI* exon 9 with the Cas9 cut site overlapping with an endogenous AcuI restriction enzyme recognition site. Indels introduced at the Cas9 cut site (red arrow) would disrupt the AcuI recognition sequence. Bottom: Sequence confirmation of biallelic frameshift-inducing mutations. (C) Schematic of the CRISPR/Cas9-mediated gene targeting to knockout

FANCI in $D2^{-/-}$ clone #39 cells to create the $ID2^{-/-}$ DKO clone #4. A guide RNA was designed targeting *FANCI* exon 9 with the Cas9 cut site overlapping with an endogenous AcuI restriction enzyme recognition site. Indels introduced at the Cas9 cut site (red arrow) would disrupt the AcuI recognition sequence. Sequence confirmation of biallelic frameshift inducing mutations. (D-E) No truncated FANCD2 or FANCI proteins are observed in the null cell lines. (D) WCE from WT, $D2^{-/-}$, and $ID2^{-/-}$ were analyzed for the presence of FANCD2 (Santa Cruz; sc-20022, 1:1000). Tubulin was used as a loading control. (E) WCE from WT, $I^{-/-}$, and $ID2^{-/-}$ were analyzed for the presence of FANCI (Bethyl; A300-212, 1: 1000).

Supplementary Figure S2. $D2^{-/-}$, $I^{-/-}$ and $ID2^{-/-}$ G2/M arrest in response to MMC

Percentage of cells in each phase of the cell cycle to accompany Figure 4C. WT, $D2^{-/-}$, $I^{-/-}$, $ID2^{-/-}$ and complemented cell lines were untreated or treated with 10 nM MMC 24 hr, followed by propidium iodine (PI) staining and FACS analysis to determine the percentage of cells in each phase of the cell cycle, in triplicate. The average from two independent clones for $D2^{-/-}$, $I^{-/-}$ and $ID2^{-/-}$ cells is reported.

Supplementary Figure S3. FANCD2, but not FANCI, promotes cellular resistance to APH and HU in additional independent clones for $D2^{-/-}$, $I^{-/-}$ and $ID2^{-/-}$ to accompany Figure 5.

FANCD2, but not FANCI, promotes cellular resistance to APH and HU in additional independent clones for $D2^{-/-}$, $I^{-/-}$ and $ID2^{-/-}$ to accompany Figure 5. WT, $D2^{-/-}$, $I^{-/-}$, and $ID2^{-/-}$ cell lines were plated at low density and incubated in absence or presence of HU (50, 100 and 150 μM) or APH (10, 25 or 50 nM) for 12 to 14 days to allow for single cell colony formation. Plates were fixed and stained with Coomassie, and colonies with a

minimum of 50 cells were scored. Results were averaged from a minimum of 3 replicate wells for each cell line and normalized to the respective untreated cells. Error bars represent the standard deviation and significance was determined by t-test. Statistical significance at $P<0.05$, $P<0.01$, and $P<0.001$ are indicated as *, **, ***, respectively, and is in comparison to normalized WT survival under the same conditions.

Supplementary Figure S4. CtIP foci images

Defective induction of CtIP in $D2^{-/-}$, $I^{-/-}$ and $ID2^{-/-}$ cell lines. Cells from the indicated cell lines were either left untreated or treated with 4 mM HU for 20 hr. The cell nuclei (blue) were then identified by staining with DAPI. The cells were also stained (green) with an antibody that detects CtIP followed by incubation of the cells with a fluorescent secondary antibody. For statistical analysis of nuclear foci formation, images were taken using a Leica DM LB2 microscope with a Hamamatsu Orca-ER camera. Quantification of CtIP foci was carried out using ImageJ.

Supplementary Figure S5. RAD51 foci images

Normal induction of RAD51 foci in $D2^{-/-}$, $I^{-/-}$ and $ID2^{-/-}$ cell lines. Cells from the indicated cell lines were either left untreated or treated with 4 mM HU for 20 hr. The cell nuclei (blue) were then identified by staining with DAPI. The cells were also stained (green) with an antibody that detects RAD51 followed by incubation of the cells with a fluorescent secondary antibody. For statistical analysis of nuclear foci formation, images were taken using a Leica DM LB2 microscope with a Hamamatsu Orca-ER camera. Quantification of RAD51 foci was carried out using ImageJ.

Supplementary Figure S6. FANCD2 is dispensable for replication stress-induced RAD51 foci formation in a human fibroblast cell line.

An FA-D2 patient-derived cell line (PD20) and its complemented counterpart (PD20+D2) were left untreated or treated with 2 mM HU for 20 hr. Cellular nuclei were analyzed for the presence of RAD51 foci. Nuclei with >5 foci were considered positive for RAD51 foci formation.

Supplementary Figure S7. FANCD2 and FANCI both have a role in maintaining normal cell cycle response to APH

FANCD2 and FANCI both have a role in maintaining normal cell cycle response to APH. WT, $D2^{-/-}$, $I^{-/-}$, $ID2^{-/-}$ and complemented cell lines were untreated or treated with 100 nM APH for 24 hr, followed by propidium iodine (PI) staining and FACS analysis to determine percentage of cells in each phase of the cell cycle, in triplicate. (A) Representative histograms of the cell cycle profile are shown for each cell line. Blue shading represents G1 phase cells, orange shading represents S phase cells and grey shading represents G2/M phase cells. (B) Percentage of cells in each phase of the cell cycle. The average from two independent clones for $D2^{-/-}$, $I^{-/-}$ and $ID2^{-/-}$ cells is reported.

Supplementary Figure S8. FANCD2, but not FANCI, functions to promote ANHEJ-mediated DNA DSB repair

FANCD2, but not FANCI, functions to promote A-NHEJ-mediated DNA DSB repair. WT, $D2^{-/-}$, $D2^{-/-}$+D2, $I^{-/-}$, $I^{-/-}$+I, and $ID2^{-/-}$ cells were used. In this assay, I-Scel digestion creates a DSB in the A-NHEJ reporter plasmid (EJ2-GFP). Repair of the DSB by microhomology-mediated repair restores GFP expression. The repair percentage was determined by the number of dual GFP and mCherry positive cells divided by the number of mCherry positive cells (transfection control). Results were averaged from a minimum

of 3 replicates. Error bars represent the standard deviation and significance was determined by t-test. Statistical significance at $P < 0.05$, $P < 0.01$, $P < 0.001$, $P < 0.0001$ are indicated as *, **, ***, **** respectively.

Figure 1

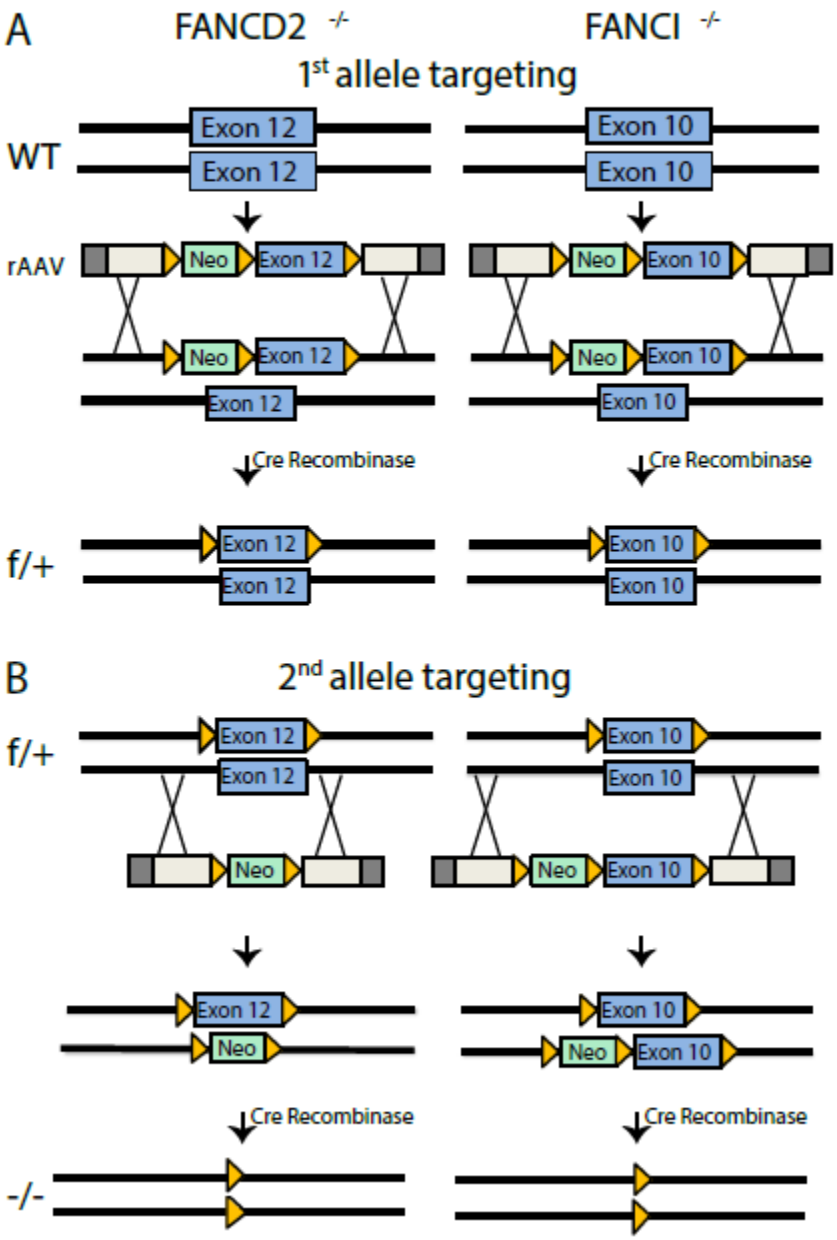
A
FANCD2 -/-
FANCI -/-
1st allele targeting
WT
Exon 12
Exon 12
Exon 10
Exon 10
rAAV
Neo
Exon 12
Neo
Exon 12
Exon 12
Neo
Exon 10
Neo
Exon 10
Exon 10
Cre Recombinase
Cre Recombinase
f/+
Exon 12
Exon 12
Exon 10
Exon 10
B
2nd allele targeting
f/+
Exon 12
Exon 12
Neo
Exon 10
Exon 10
Neo
Exon 10
Exon 12
Neo
Exon 10
Neo
Exon 10
Cre Recombinase
Cre Recombinase
-/-

Figure 2

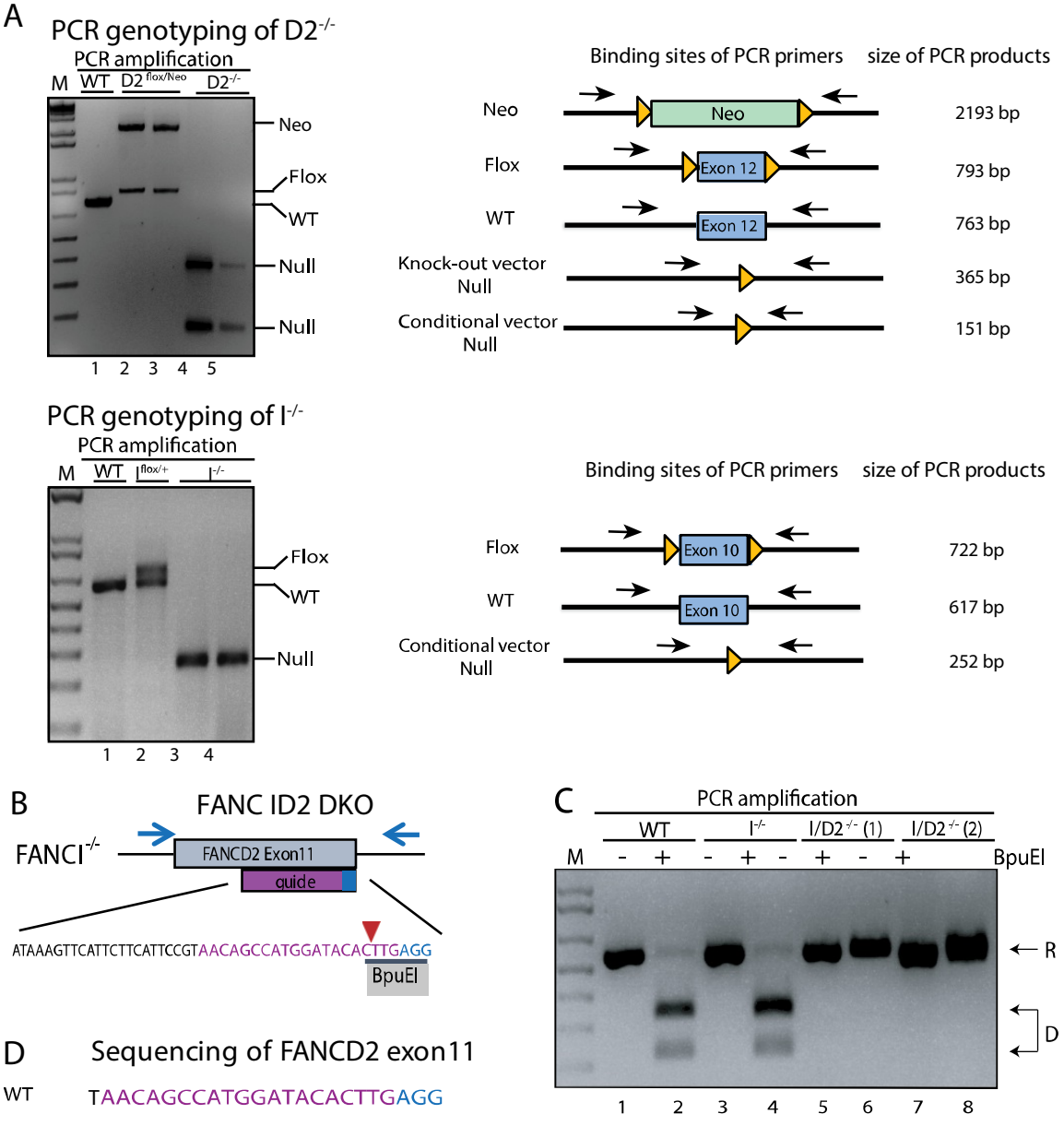
A
PCR genotyping of D2-/-
PCR amplification
M WT D2flox/Neo D2-/-
Neo
Flox
WT
Null
Null
1 2 3 4 5
Binding sites of PCR primers
size of PCR products
Neo
Neo
2193 bp
Flox
Exon 12
793 bp
WT
Exon 12
763 bp
Knock-out vector
Null
365 bp
Conditional vector
Null
151 bp
PCR genotyping of I-/-
PCR amplification
M WT Iflox/+ I-/-
Flox
WT
Null
1 2 3 4
Binding sites of PCR primers
size of PCR products
Flox
Exon 10
722 bp
WT
Exon 10
617 bp
Conditional vector
Null
252 bp
B
FANC ID2 DKO
FANCI-/-
FANCD2 Exon11
guide
ATAAAGTTCATTCTTCATTCCGTAACAGCCATGGATACACTTGAGG
BpuEI
C
PCR amplification
WT
I-/-
I/D2-/- (1)
I/D2-/- (2)
M - + - + - + - + BpuEI
R
D
1 2 3 4 5 6 7 8
D
Sequencing of FANCD2 exon11
WT TAACAGCCATGGATACACTTGAGG
ID2 DKO (#1)
allele 1 TAACAGCCATG----------TTGAGG (7 bp deletion)
allele 2 TAACAGCCATGGATACACTTTGAGG (1 bp insertion)
ID2 DKO (#2)
allele 1 TAACAGCCATGGATACAC-TGAGG (1 bp deletion)
allele 2 TAACAGCCATGGATACACATTGAGG (1 bp insertion)

Figure 3

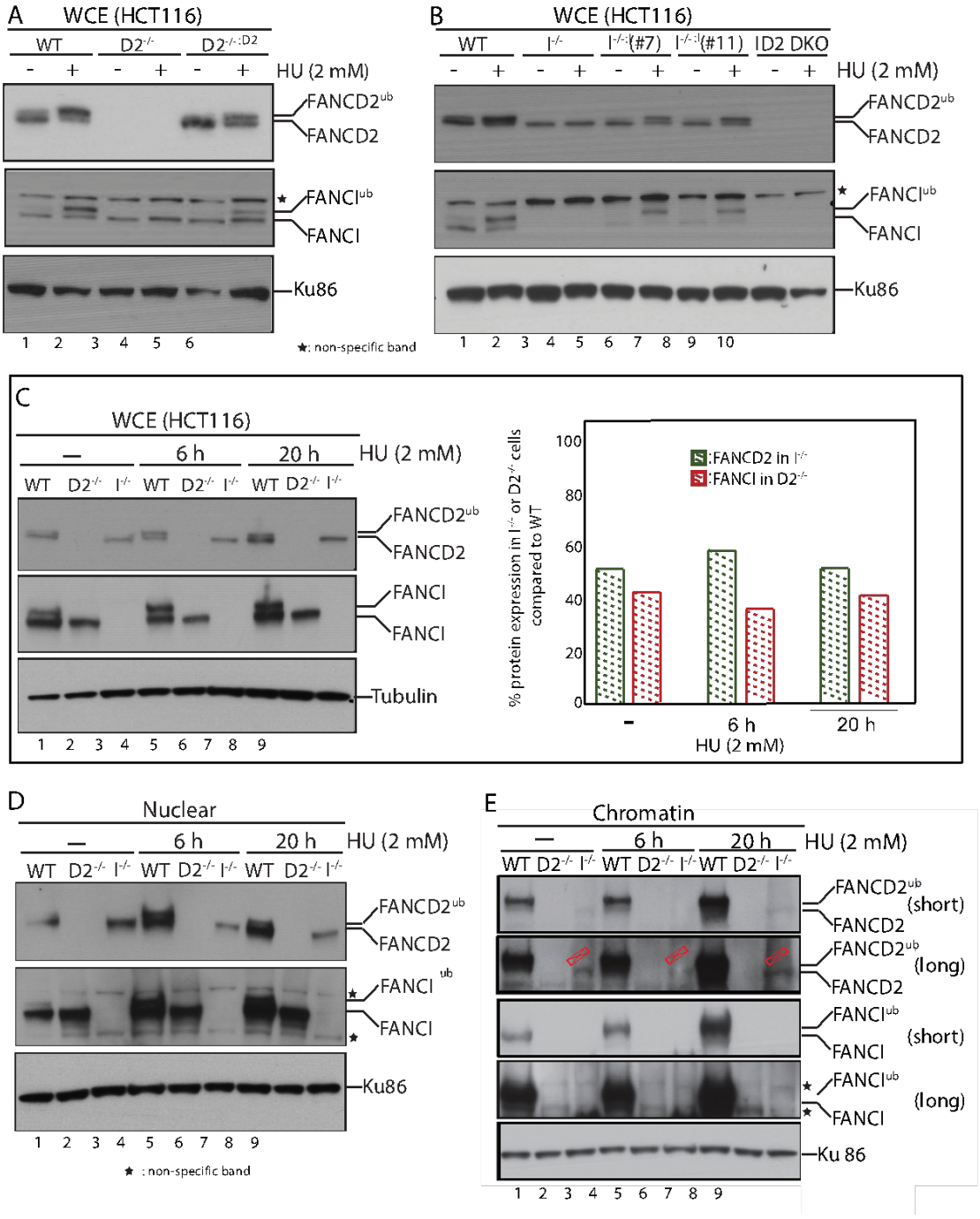

Data generated in Figure 3 by Jung Eun Yeo

Figure 4

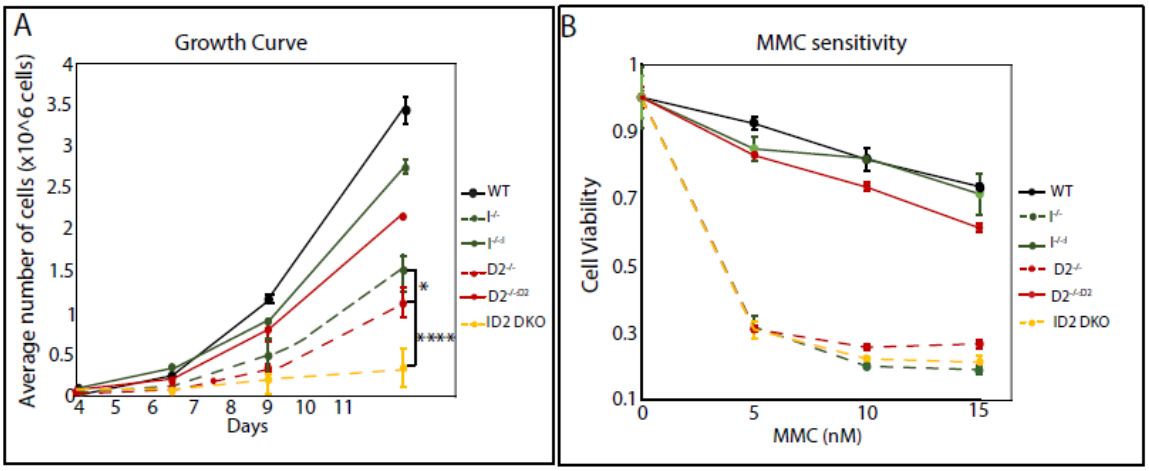
A
Growth Curve
Average number of cells (x10^6 cells)
Days
WT
I-/-
I-/-I
D2-/-
D2-/-D2
ID2 DKO
*
****
B
MMC sensitivity
Cell Viability
MMC (nM)
WT
I-/-
I-/-I
D2-/-
D2-/-D2
ID2 DKO

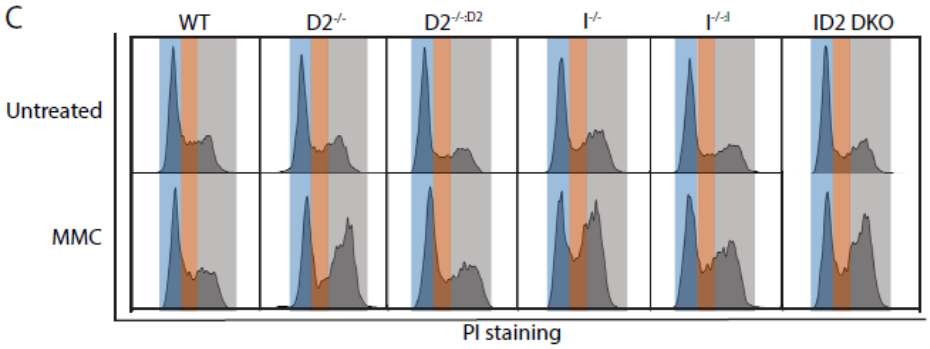
C
WT
D2-/-
D2-/-D2
I-/-
I-/-I
ID2 DKO
Untreated
MMC
PI staining

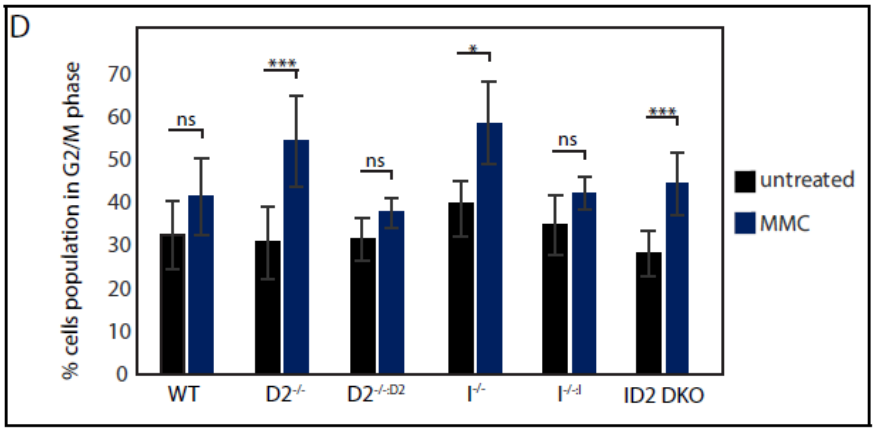
D
% cells population in G2/M phase
ns
***
ns
*
ns
***
untreated
MMC
WT
D2-/-
D2-/-D2
I-/-
I-/-I
ID2 DKO

Figure 5

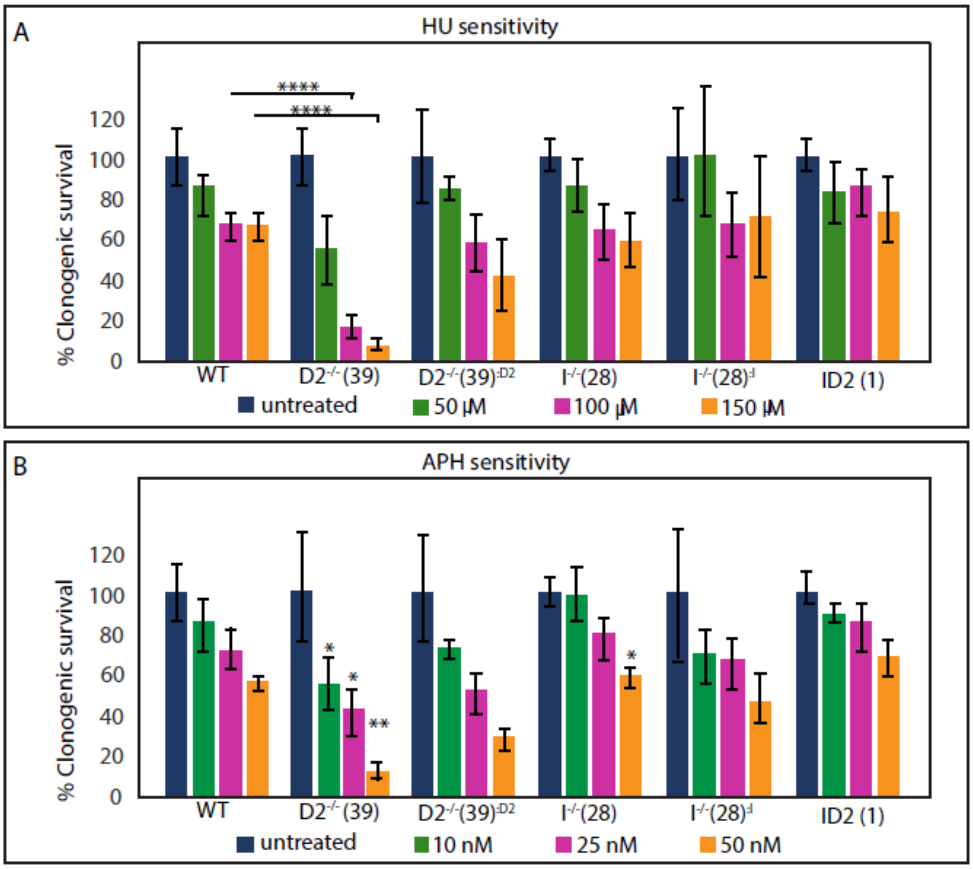

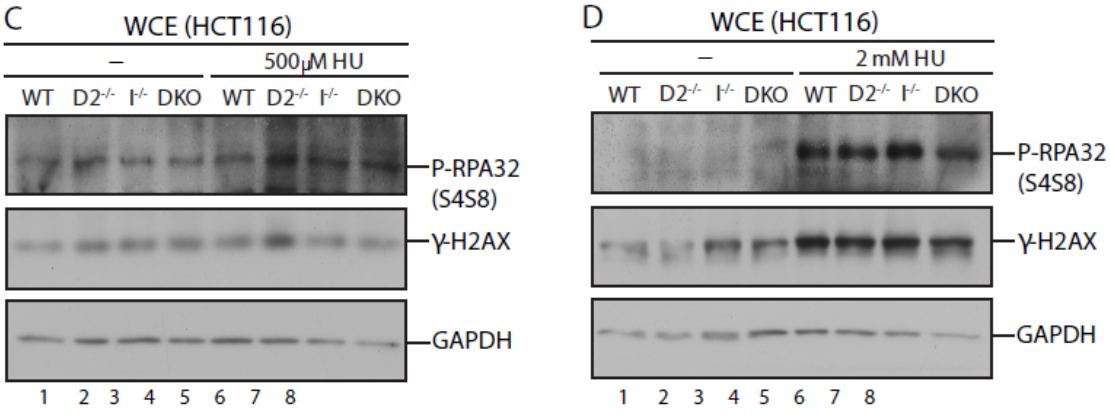

Data generated in Figure 5 A, B by Elizabeth Thompson and C, D by Jung Eun Yeo

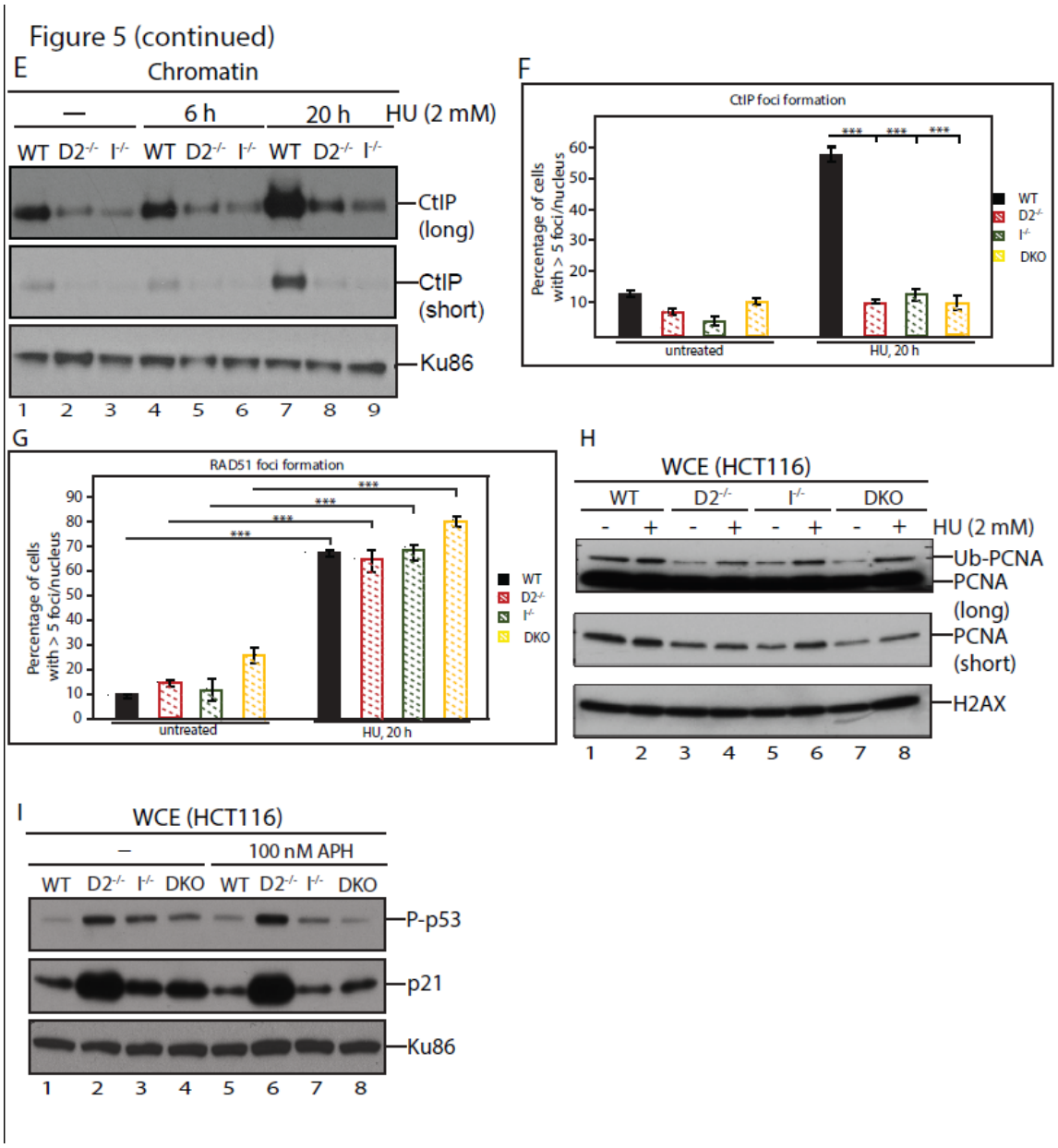

Data generated in Figure 5 E-I by Jung Eun Yeo

Figure 6

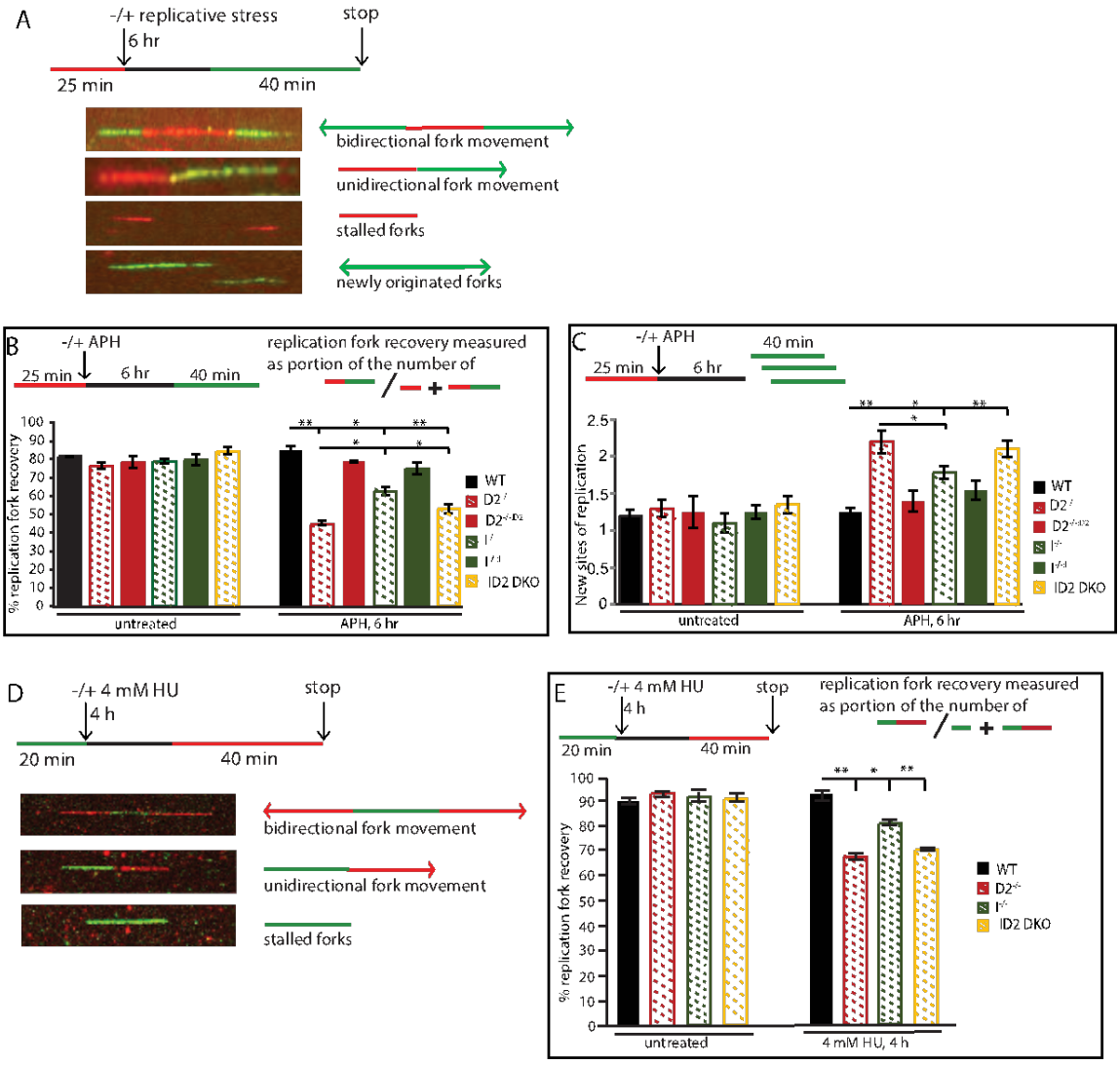

Data generated in Figure 6 by Jung Eun Yeo

Figure 7

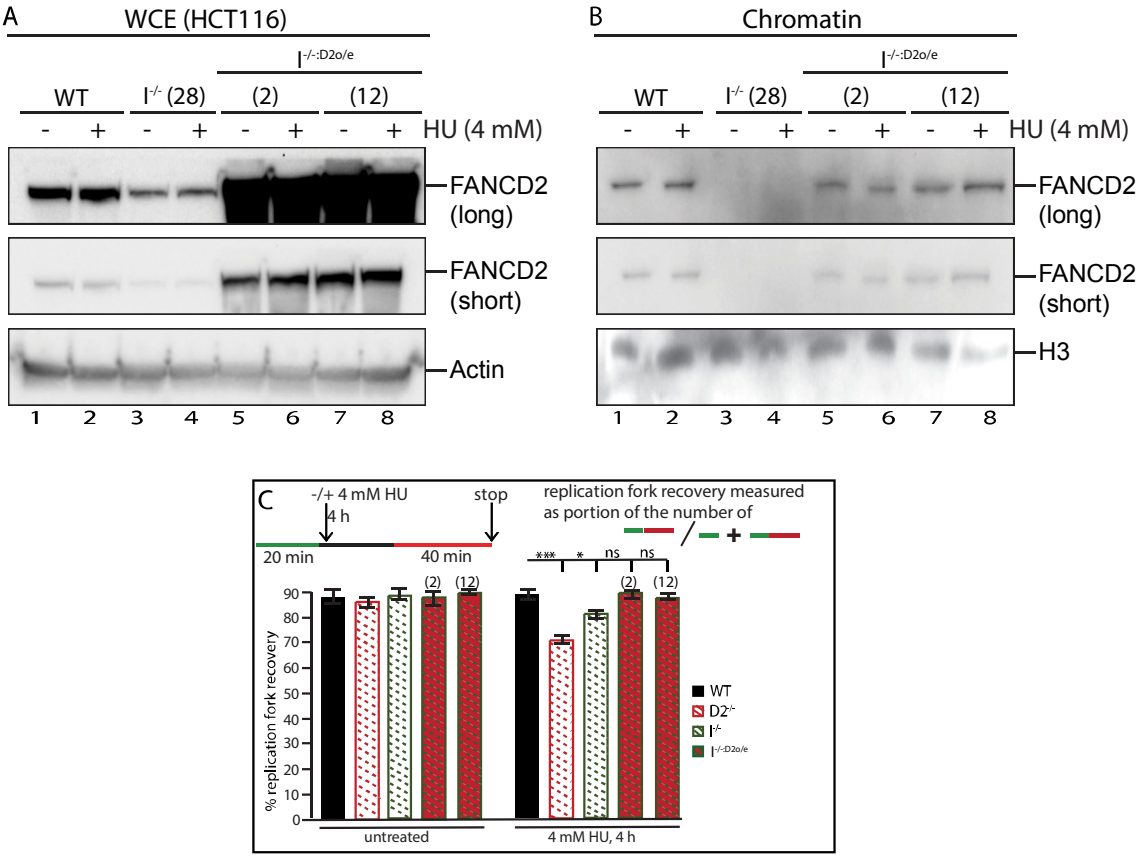

Data generated in Figure 7 by Jung Eun Yeo

Figure 8

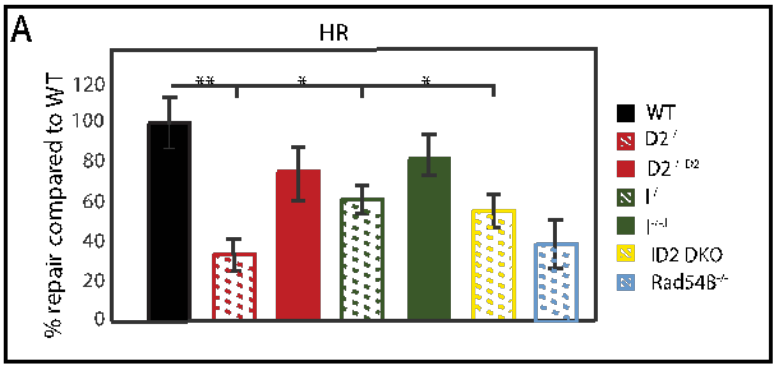
A
HR
% repair compared to WT
120
100
80
60
40
20
0
**
*
*
WT
D2-/-
D2-/-D2
I-/-
I-/-I
ID2 DKO
Rad54B-/-

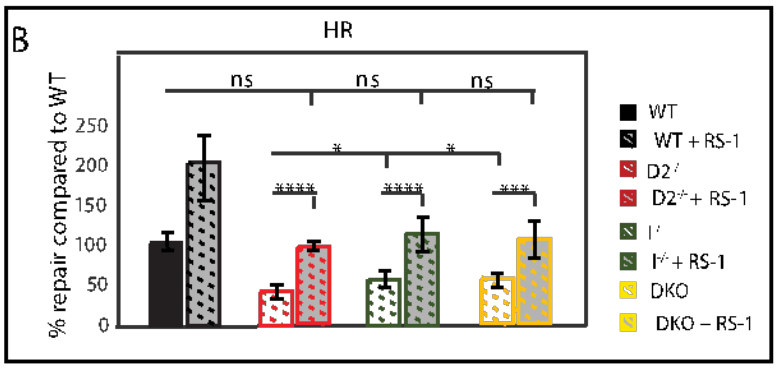
B
HR
% repair compared to WT
250
200
150
100
50
0
ns
ns
ns
*
*
****
****
***
WT
WT + RS-1
D2-/-
D2-/- + RS-1
I-/-
I-/- + RS-1
DKO
DKO – RS-1

Figure 9

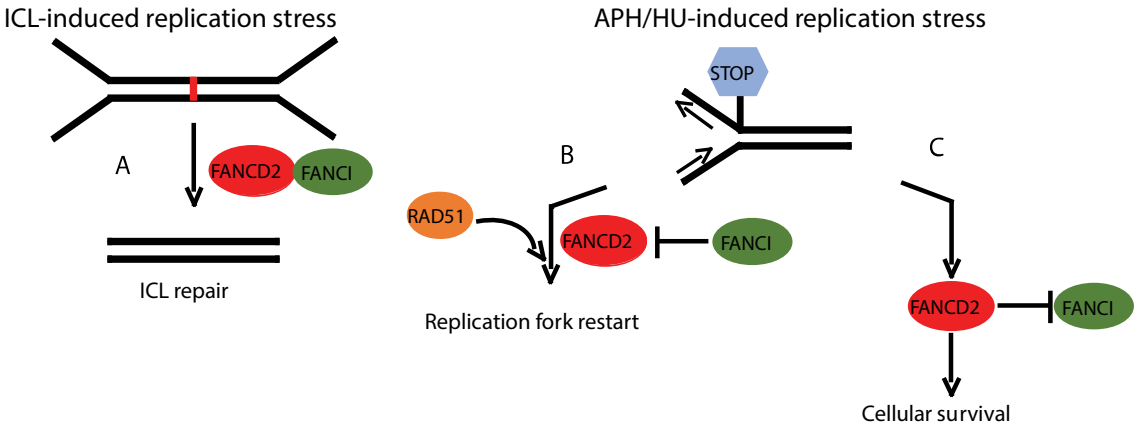
ICL-induced replication stress
A
FANCD2
FANCI
ICL repair
APH/HU-induced replication stress
STOP
B
RAD51
FANCD2
FANCI
Replication fork restart
C
FANCD2
FANCI
Cellular survival

Supplementary Figure S1

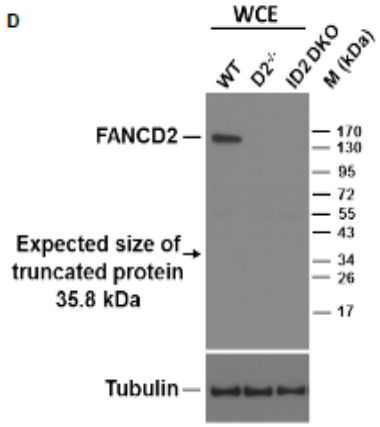

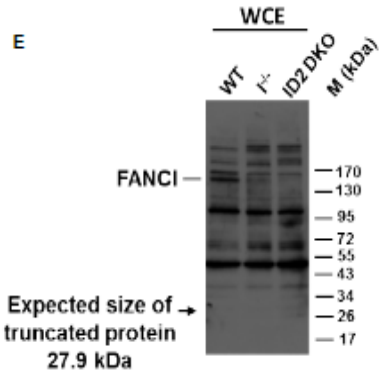

Supplementary Figure S2

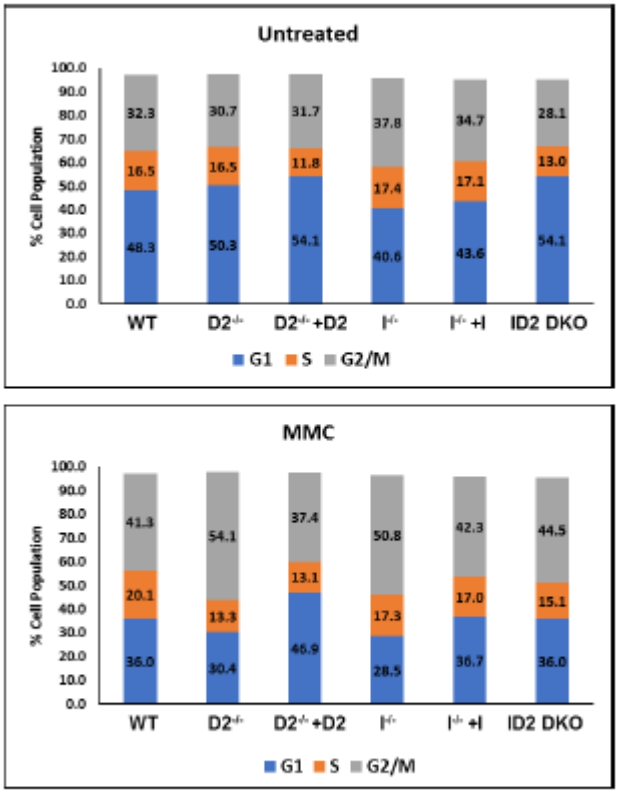

Supplementary Figure S3

A

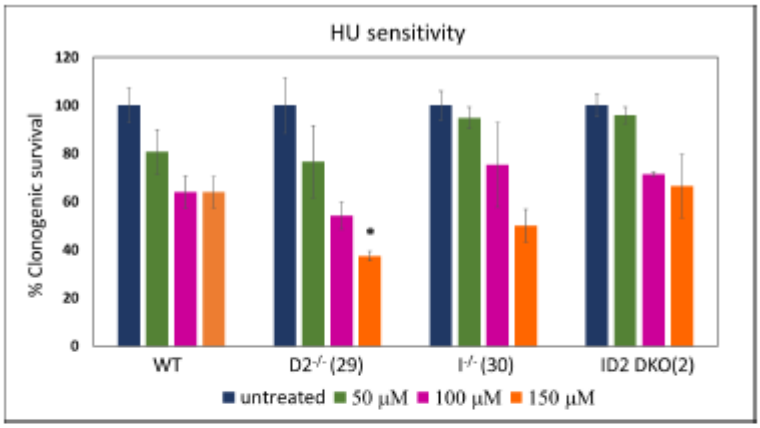

B

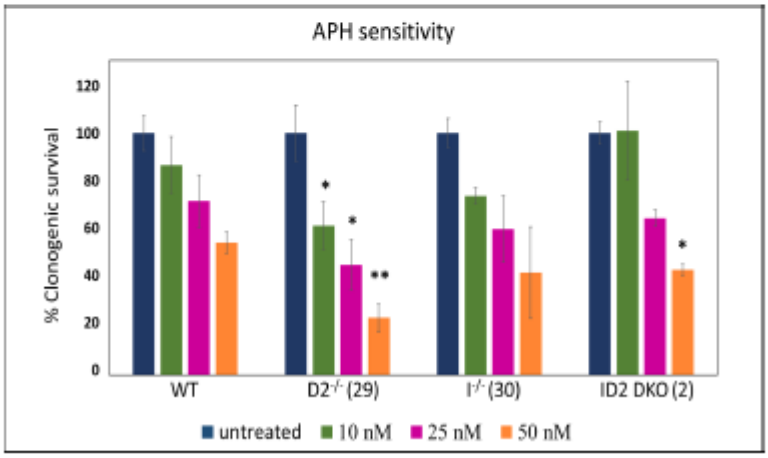

Supplementary Figure S4

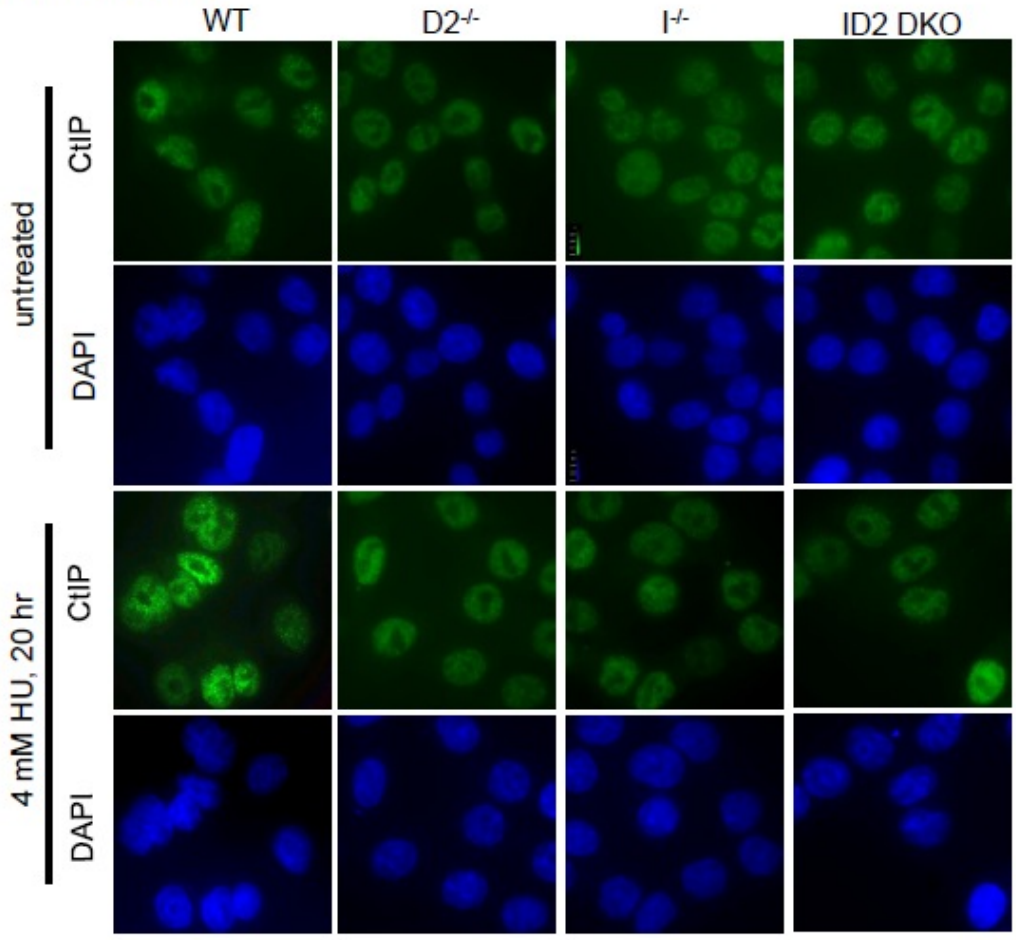

Data generated in Supplementary Figure S4 by Jung Eun Yeo

Supplementary Figure S5

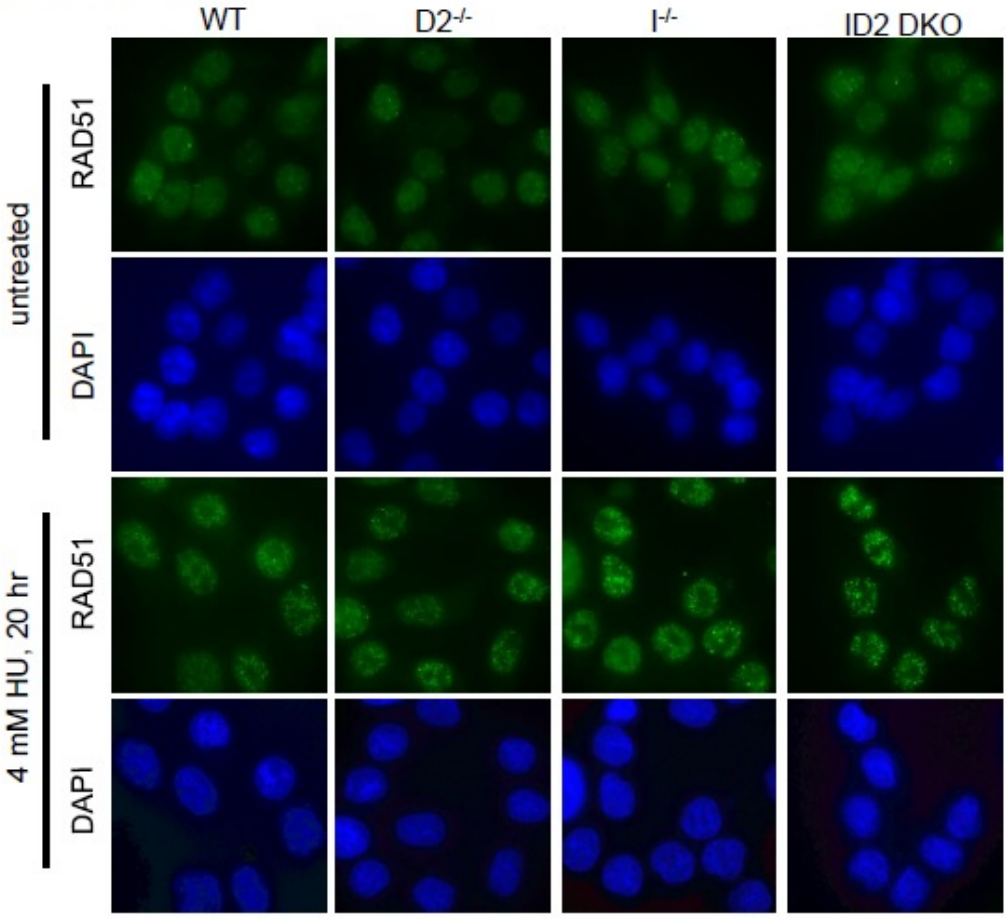

Data generated in Supplementary Figure S5 by Jung Eun Yeo

Supplementary Figure S6

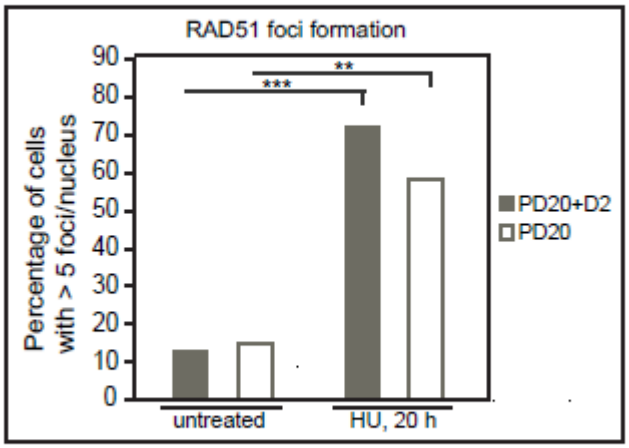

Data generated in Supplementary Figure S6 by Jung Eun Yeo

Supplementary Figure S7

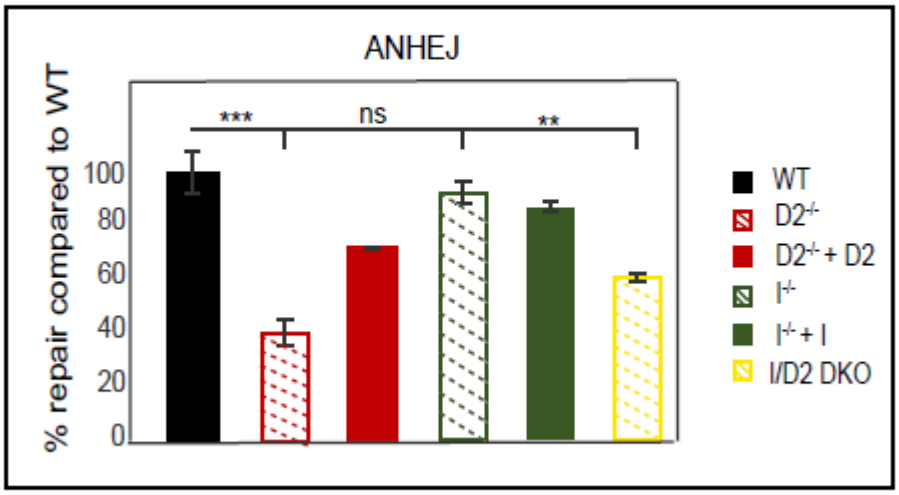

Supplementary Table S1

Primers

FANCD2 rAAV Conditional Vector Targeting Exon 12: Golden Gate Cloning primers

hFANCD2_LF_GG	GACGCTCTTCACCGTGACCCAAACTTCCTATTGA
hFANCD2_LR_GG	GACGCTCTTCTGAGGTTGCTTTATCTAGGTGTGA
hFANCD2_RF_GG	GACGCTCTTCGGCACAGACTAACTGAGAATACTGAC
hFANCD2_IR_GG	GACGCTCTTCGGTATGCTATACGAAGTTATGGATTGATCTGAATGGCTAAG
hFANCD2_IF_GG	GACGCTCTTCCTACATTATACGAAGTTATCAGACGACAGTGCAAGTT
hFANCD2_RR_GG	GACGCTCTTCCCGCCGCCACCTCAGATTATCTT

FANCD2 rAAV Knockout Vector Targeting Exon 12: Golden Gate Cloning primers

FANCD2-St KO-LF	GACGCTCTTCACCG GTGACCTACTGATAGAGAATAC
FANCD2-St KO-LR	GACGCTCTTCTGAG TAAGAGCATACCTCAAGTGT
FANCD2-ST KO-RF	GACGCTCTTCGTCAAAGAGCTCATCCTCACAC
FANCD2-ST KO-RR	GACGCTCTTCCATGTTGACAGTGGACAGATTGA

FANCD2 Allele Determination rAAV Targeting

FANCD2_EX11SF	ATTCTTCATTCCGTAACAGC
FANCD2_LoxP SR	GACAACCTCATGTATAAGATGG

FANCI rAAV Conditional Vector Targeting Exon 10: Golden Gate Cloning primers

FancI_GG_LF	GACGCTCTTCACCGGCTCAGGAGTTCAAGACC
FancI_GG_LR	GACGCTCTTCTGAGTCAAGACCAGCCTCTACTAA
FancIcond_GG_RF	GACGCTCTTCGTCACTCCTGGGATCAAGTGAT
FancIcond_GG_IR	GACGCTCTTCGGTATGCTATACGAAGTTATGAGTGTGGTAACATCATGTA
FancIcond_GG_IF	GACGCTCTTCCTACATTATACGAAGTTATTAATGTCCTCACTTTAGCAG
FancIcond_GG_RR	GACGCTCTTCCATGGAACAACCAAATGCAATGC

FANCI Allele Determination rAAV Targeting

FancIc_GG_LIF	GCAATGGCACAATCTTGG
FancIcond_GG_LoxR	ATAGGACTTTCTGGCTTGCT

CRISPR/Cas9 Targeting of FANCD2 Exon 11

FANCD2 gRNA sequence	AACAGCCATGGATACACTTG
FancD2_CC_ F2	GGAAGATGGAGTAAGAGAAGT
FancD2_CC_ R2	TGCTCATTCATAGTGGGTAG

CRISPR/Cas9 Targeting of FANCI Exon 9

FANCI gRNA sequence	CTTATCTAGTGCACTGAAGA
FancI_CC _F3	TTCTCTGCTCCCAAGTTTC
FancI_CC _R3	TGTGCTGAGGTGAAGGTA

Supplementary Table S2 P-Values from student t-test analysis

Figure	samples	p-value (two tales)
4A	$D2^{-/-}$ vs $I^{-/-}$	0.033561
	$D2^{-/-}$ vs ID2 DKO	0.0000029
	$I^{-/-}$ vs ID2 DKO	0.0000065
	WT vs $I^{-/-}$	0.0000115
	WT vs $D2^{-/-}$	0.0000308
5A-B	WT vs $D2^{-/-}$ + HU 50 μM	ns
	WT vs $D2^{-/-}$ + HU 100 μM	0.0018921
	WT vs $D2^{-/-}$ + HU 150 μM	0.0019495
	WT vs $D2^{-/-}$ + APH 10 nM	0.0310029
	WT vs $D2^{-/-}$ + APH 25 nM	0.0204921
	WT vs $D2^{-/-}$ + APH 50 nM	0.0004985
	WT vs $I^{-/-}$ + HU 50 μM	ns
	WT vs $I^{-/-}$ + HU 100 μM	ns
	WT vs $I^{-/-}$ + HU 150 μM	ns
	WT vs $I^{-/-}$ + APH 10 nM	ns
	WT vs $I^{-/-}$ + APH 25 nM	ns
	WT vs $I^{-/-}$ + APH 50 nM	0.0120932
	WT vs ID2 DKO + HU 50 μM	ns
	WT vs ID2 DKO + HU 100 μM	ns
	WT vs ID2 DKO + HU 150 μM	ns
	WT vs ID2 DKO + APH 10 nM	ns
	WT vs ID2 DKO + APH 25 nM	ns
	WT vs ID2 DKO + APH 50 nM	ns
5F	WT + HU vs $D2^{-/-}$ + HU	0.00021854
	WT + HU vs $I^{-/-}$ + HU	0.00040459
	WT + HU vs ID2 DKO + HU	0.00062153
5G	WT vs WT + HU	0.000731473
	$D2^{-/-}$ vs $D2^{-/-}$+ HU	0.00065732
	$I^{-/-}$ vs $I^{-/-}$ + HU	0.000321296
	ID2 DKO vs ID2 DKO + HU	0.0001602
6B	WT + APH vs $D2^{-/-}$ + APH	0.000595
	WT + APH vs $I^{-/-}$ + APH	0.009439
	WT + APH vs ID2 DKO + APH	0.000594
	$D2^{-/-}$ + APH vs $I^{-/-}$ + APH	0.001009
	$D2^{-/-}$ + APH vs ID2 DKO + APH	0.011695
6C	WT + APH vs $D2^{-/-}$ + APH	0.002453
	WT + APH vs $I^{-/-}$ + APH	0.014428
	WT + APH vs ID2 DKO + APH	0.003668
	$D2^{-/-}$ + APH vs $I^{-/-}$ + APH	0.013982
6E	WT + HU vs $D2^{-/-}$ + HU	0.004277

Figure	samples	p-value (two tales)
6E	WT + HU vs $I^{-/-}$ + HU	0.015219
	WT + HU vs ID2 DKO + HU	0.00449912
7C	WT + HU vs $D2^{-/-}$ + HU	0.0002692
	WT + HU vs $I^{-/-}$ + HU	0.0195361
	WT + HU vs $I^{-/-}$ (2)+ HU	ns
	WT + HU vs $I^{-/-}$ (12)+ HU	ns
8A	WT vs $I^{-/-}$	0.0240309
	WT vs ID2 DKO	0.012311962
	$D2^{-/-}$ vs $I^{-/-}$	9.91012E-06
	$D2^{-/-}$ vs ID2 DKO	0.00055944
8B	WT vs $D2^{-/-}$ + RS-1	0.00020194
	WT vs $I^{-/-}$ + RS-1	ns
	WT vs ID2 DKO + RS-1	ns
	$D2^{-/-}$ vs $I^{-/-}$	0.01322908
	$D2^{-/-}$ vs ID2 DKO	0.01258901
	$D2^{-/-}$ vs $D2^{-/-}$ + RS-1	1.8008E-09
	$I^{-/-}$ vs $I^{-/-}$ + RS-1	0.000040968
	ID2 DKO vs ID2 DKO + RS-1	0.00031077
S3A-B	WT vs $D2^{-/-}$ + HU 50 μM	ns
	WT vs $D2^{-/-}$ + HU 100 μM	ns
	WT vs $D2^{-/-}$ + HU 150 μM	0.013007
	WT vs $D2^{-/-}$ + APH 10 nM	0.025805
	WT vs $D2^{-/-}$ + APH 25 nM	0.022563
	WT vs $D2^{-/-}$ + APH 50 nM	0.001225
	WT vs $I^{-/-}$ + HU 50 μM	ns
	WT vs $I^{-/-}$ + HU 100 μM	ns
	WT vs $I^{-/-}$ + HU 150 μM	ns
	WT vs $I^{-/-}$ + APH 10 nM	ns
	WT vs $I^{-/-}$ + APH 25 nM	ns
	WT vs $I^{-/-}$ + APH 50 nM	ns
	WT vs ID2 DKO + HU 50 μM	ns
	WT vs ID2 DKO + HU 100 μM	ns
	WT vs ID2 DKO + HU 150 μM	ns
	WT vs ID2 DKO + APH 10 nM	ns
	WT vs ID2 DKO + APH 25 nM	ns
	WT vs ID2 DKO + APH 50 nM	0.0293818
S6	PD20+D2 vs PD20+D2 + HU	0.00052779
	PD20 vs PD20 + HU	0.00204948

Figure	samples	p-value (two tales)
S8	WT vs $D2^{-/-}$	0.001209
	WT vs $I^{-/-}$	ns
	WT vs ID2 DKO	0.012742

Data generated in Supplementary Table S2 by Elizabeth Thompson and Jung Eun Yeo

CHAPTER 3

PALB2 IS AN ESSENTIAL GENE AND PROTECTS THE GENOME FROM CATASTROPHIC INSTABILITY

A version of this chapter is to be submitted for publication in the near future

SUMMARY

Partner and localizer of BRCA2 (PALB2) is an important tumor suppressor that is associated with Fanconi anemia (FA) and breast cancer susceptibility. Indeed, FA patients with mutations in *PALB2* (the FA-N subtype; FANCN) typically have more severe disease with earlier onset of cancer. PALB2 is known to promote homology dependent recombination (HDR) by complexing with both breast cancer allele 1 and 2 (BRCA1 and BRCA2) and facilitating radiation sensitive 51 (RAD51) strand invasion. To further investigate the function of PABL2, we used recombinant adeno-associated virus (rAAV)-mediated gene targeting techniques to make a conditionally null human *PALB2* cell line. Removal of the conditional allele resulted in spontaneous chromosomal breaks and rearrangements that ultimately lead to chromosomal catastrophe within two cell cycles. Successful complementation of the *PALB2*-null cell line was accomplished using cDNAs encoding three FA-associated truncating mutations and three PALB2 single nucleotide polymorphisms (SNPs) identified in breast cancer patients. These experiments demonstrated that the *PALB2* patient mutations were hypomorphic because they could rescue the viability of the *PALB2* null cell line and that PALB2's essential role in genomic stability is replication dependent. Furthermore, we confirmed that the PALB2 mutants (all of which did not express the C-terminal WD40 domain) could still bind BRCA2, but were defective in RAD51 foci formation and were HDR deficient. These experiments identified several novel important separation-of-function characteristics: PALB2's essential activity is separable from its ability to interact with BRCA2 and with its HDR activity. Similarly, the analysis of the SNP mutants proved informative. All of the SNP mutants were capable of forming a complex with RAD51.

Importantly, however, two of the three SNP mutants were as sensitive to mitomycin C (MMC), poly(ADP-ribose) polymerase 1 (PARP1) inhibitors and replication stress as the pathogenic FA mutations. Thus, we identified two cancer-associated *PALB2* SNPs that are sensitive to interstrand crosslinks and defective in DNA repair and are thus potentially pathogenic mutations. In conclusion, this research has revealed a mechanistic understanding of PALB2 function and how *PALB2* patient mutations result in disease.

INTRODUCTION

PALB2/FANCN is an important tumor suppressor and DNA repair protein with roles in repairing two of the most toxic DNA lesions, ICL (interstrand cross links) and DSB (double strand breaks) (129,130) that can occur in human cells. PALB2 was first described as a binding partner for BRCA2 (134), but has since been recognized as a molecular scaffold coordinating HDR with BRCA1, BRCA2, RAD51 and RAD51C (129,130,196). As a well-established tumor suppressor, biallelic mutations of *PALB2* are associated with the chromosomal instability disorder FA (138,197) and monoallelic mutations are associated with predisposition to hereditary breast, ovarian, prostate and pancreatic cancer (198-205). Thus, a mechanistic understanding of PALB2 function(s) and how patient mutations lead to disease should provide valuable insight into cancer etiology and prevention.

The characterization of the structural and protein binding domains of PALB2 have helped define PALB2 as a "molecular scaffold" in coordinating HDR and DSB repair (129,130,206). The N-terminus contains a coiled-coil domain that is the site of BRCA1 interaction and has been identified as the PALB2 homo-oligomerization domain as well (207,208). The N-terminus also contains binding domains for DNA, RAD51, and Kelch-like ECH-associated protein 1 (KEAP1). KEAP1 is an E3 ubiquitin ligase that has been implicated in the detection and cellular response to oxidative stress (209,210). In addition, KEAP1 can ubiquitinate N-terminal PABL2 lysines that prevent BRCA1 binding to PALB2 in a cell cycle dependent manner, and this ubiquitination can suppress HDR in G1 phase of the cell cycle (211). The central region of PALB2 contains a chromatin associated motif (ChAM), a second DNA binding domain, and a binding site

for MORF-related gene on chromosome 15 (MRG15), which is a transcription factor and part of a chromatin modifying complex. The ChAM domain and MRG15 work together to localize PALB2 to chromatin and promote HDR (212-214). The C-terminus of PALB2 contains a tryptophan-aspartic acid 40 (WD40) domain that mediates interaction with proteins involved in HDR and replication stress including BRCA2, RAD51, RAD51C, X-ray cross-complementing 3 (XRCC3) and DNA polymerase eta (pol η) (196,215). This WD40 domain forms a protein:protein binding structure called a 7-bladed *beta*-propeller (128,216) that is especially important for the localization of BRCA2 and RAD51 (131,132,196,217,218).

FA patients with the FA-N subtype typically have a severe clinical phenotype, similar to the BRCA2 subtype FA patients, with an early onset of cancer, including embryoid tumors such as Wilm's tumor, medulloblastoma and neuroblastoma (138,219,220). Interestingly — from a molecular genetics' perspective — most of the pathogenic PALB2/FANCN mutations are truncating mutations resulting in the loss of the C-terminus and WD40 domain where BRCA2 binds (130,138,197). The importance of the PALB2's C-terminus is additionally reinforced by the observation that heterozygous inheritance of a C-terminal truncating mutation in PALB2 can result in a six-fold increase in the incidence of breast cancer (136,221,222). In contrast, and somewhat surprisingly, very few missense mutations in PALB2 have either been described or characterized (130,223).

To address the function of PALB2, and especially to advance our understanding of PALB2's roles in cellular viability and HDR, we set out to a create a conditionally-null PALB2 knockout in the human HCT116 cell line. We choose a conditionally-null

approach for two reasons. First, the attempted creation of a PALB2 knockout mouse resulted only in embryonic lethality (224), and second, while several PALB2 patient cell lines have been established they all have detectable (albeit mutant) protein expression (197,201,225,226), suggesting strongly that the mutations are hypomorphic. Here, we demonstrate that the removal of PALB2 from human cells is lethal and results in a rapid and extremely profound chromosome fragmentation phenotype. In addition, we then utilized this cell line in a functional rescue approach to evaluate the function of known PALB2 pathogenic patient mutations and SNPs of unknown significance. Importantly we were able to identify mutations that genetically separated the essential activity of PALB2 from its activity required for HDR. Thus, quite unexpectedly, we have demonstrated that HDR is likely not the essential activity of PALB2. Just as importantly — from a clinical perspective — we were able to demonstrate that cell lines expressing two of the three PALB2 SNPs are sensitive to mitomycin C (MMC), aphidicolin (APH), and olaparib and have HDR defects, suggesting they are potentially pathogenic mutations. *In toto*, these studies significantly advance our mechanistic understanding of the role(s) that PALB2 is required for in human somatic cells.

MATERIALS AND METHODS

Generating a PALB2 inducible, conditionally-null cell line by rAAV-mediated gene targeting

A conditional PALB2 knockout was generated using rAAV-mediated gene targeting (Figure 1A). Two targeting rAAV vectors were made using Golden Gate cloning techniques as described (152,153,181). Based on their proximity and the small size of the exons, we selected both exons 2 and 3 for targeting. In addition, deletion of both exons 2 and 3 should result in a frameshift mutation and very premature truncation of any possible protein product. Thus, a conditional vector was designed to introduce a neomycin (NEO) selection cassette and loxP sites flanking exons 2 and 3. This conditional rAAV PALB2 vector was transduced into the HCT116 cell line. G418 selection and PCR were used to identify correctly targeted subclones ($PALB2^{floxNEO/+}$). Correctly targeted cells were subsequently transduced with a transient Cre recombinase-expressing adenovirus (AdCre). The resulting subclones were screened for the loss of the NEO selection cassette, but retention of the floxed exons 2 and 3 to create the conditional allele ($PALB2^{flox/+}$). The second round of targeting was then performed with a knockout vector that simply replaced exons 2 and 3 with a NEO selection cassette ($PALB2^{flox/NEO}$). AdCre was used again to remove the NEO selection cassette and subclones were screened by PCR to identify cell lines with the correct allelic configuration ($PALB2^{flox/-}$) (Figures 1A & 1B). The sequences for all primers used in these reactions can be found in Supplementary Table S1.

An inducible gene knockout of PALB2 was created with a Cre recombinase fused to the estrogen receptor ligand-binding domain (CreER) system. A PiggyBac transposon

containing the Cre-ER systems and a puromycin resistance gene (PURO) was used to isolate clones in which the vector had stably integrated. Loss of the conditional allele could then be obtained at the experimenter's discretion with the addition of tamoxifen or 5 nM of 4-hydroxytamoxifen (4-OHT) (227). The loss of the conditional PALB2 allele upon 4-OHT treatment could be confirmed by PCR amplification with allele-specific primers flanking the targeted locus (Figure 1B).

Growth curves

Wild type (WT) HCT116 cells and two independent clones of the PALB2$^{flox/-:Cre-ER}$ cell line (clones 3 and 31) were plated in 6-well plates. WT cells were subcultured at 3,500 cells/well. PALB2$^{flox/-:Cre-ER}$ cells were subcultured at 5,000 cells/well for untreated wells and 20,000 cells/well for PALB2$^{flox/-:Cre-ER}$ + 4-OHT wells. 4-OHT (10 nM) [you said 5 in the paragraph above] was added to one half of the plates. Cell counts were derived in triplicate on the indicated days (3, 5, 7 and 11) from both the 4-OHT-treated and untreated wells.

Cytogenetics

PALB2$^{flox/-:Cre-ER}$ cells and PALB2$^{-/-}$ + WT cDNA cells untreated or treated with 10 nM 4-OHT for 24, 48, or 72 hr were subjected to cytogenetic analysis at the University of Minnesota's cytogenomics core laboratory. Thirty metaphases were analyzed by G-banding karyotyping for all samples except that only 20 metaphases were scored for PALB2$^{flox/-}$ cells treated with tamoxifen at 48 and 72 hr due to their low mitotic index. The results are summarized in Supplementary Table S3.

Replication assay

Two independent clones of the PALB2$^{flox/-:Cre\text{-}ER}$ cell line were tested in complete media (10% fetal bovine serum; FBS) and low serum (1% FBS) to determine if reducing the growth rate could also reduce the amount of cell death of PALB2-deficient cells. Cells were subcultured in 6-well plates at 50,000 cells/well for complete media samples and 150,000 cells/well for low serum samples. The next day the complete media was removed and then complete media or low serum media, either with or without 10 nM 4-OHT was added to the wells in triplicate. Cell counts were derived at two and four days after tamoxifen treatment. The change in cell number was determined between day 2 and day 4 by subtracting day 4 cell counts from the average cell count on day 2 for each condition. The percent change in cell number was then determined based on the average cell count from day 2. Data was combined from the two independent clones.

PALB2 mutations

Fanconi anemia patient mutations

Mutation c.1653T>A, p.Tyr551* (**Y551X**) is a nonsense mutation resulting in a premature truncation in exon 4 of PALB2. This truncation results in the loss of the WD40 and MRG15 binding domains. This mutation was the first PALB2 mutation associated with an FA patient (197) and the patient was a compound heterozygote who had this mutation and c.(?_200)_(3113+1_3114-1)del, a large deletion (presumed to be a null allele) encompassing exons 1 to 10 on the other PALB2 allele (228). The patient's clinical presentation included skin, heart, thumb and kidney abnormalities, growth retardation, and anemia. The patient died at the age of 2 due to a rare and aggressive form of endothelia cancer, kapsosiform hemangioendothelioma (197).

Mutation c.2257C>T, p.Arg753* (**R753X**) is a nonsense mutation resulting in a premature truncation in PALB2 exon 5. This truncation results in the loss of the WD40 domain and the majority of the MRG15 binding domain. This mutation is a *bona fide* FA and breast cancer associated mutation (130). The patient was a compound heterozygote with this mutation and Y1183X. The patient's clinical presentation included a Wilms tumor diagnosis at age 1, severe intrauterine growth retardation, growth retardation, microcephaly, microphthalmia, and skin hyperpigmentation (138).

Mutation c.3549C>G, p.Tyr1183* (**Y1183X**) is a nonsense mutation resulting in a premature truncation in PALB2 exon 13. This 4 amino acid truncation of the C-terminus has been implicated as destabilizing to the 7-bladed β-propeller WD40 domain (128). This mutation is associated with FA, breast cancer and pancreatic cancer (130) and was found in three unrelated FA patients, all compound heterozygous with this mutation and R753X, Q988X or N1039fs. Each of these FA patients had a diagnosis of cancer before the age of 3 including the following: Wilms tumor (patient 1), medulloblastoma (patient 2), and neuroblastoma and acute myelocytic leukemia (AML; patient 3). Common clinical presentation for all 3 patients included growth retardation and microcephaly. Two patients also presented with skin hyperpigmentation and two with thumb anomalies (138).

Breast cancer variants of unknown significance (VUS) mutations

A recent study using a next generation sequencing screen of breast cancer-associated genes in a population of 2,158 breast cancer patients found PALB2 VUS mutations in 56 patients (2.6%) (139). The three VUS missense mutations described below are SNPs that

were selected for further analysis because they either occurred in more than one patient within this cohort, or because they were associated with high-risk based on family history (139).

Mutations c.298C>T, p.Leu100Phe (**L100F**) affects the last amino acid in the KEAP1 binding domain and is located within a putative DNA binding domain in exon 4. This mutation was associated with 3/2158 breast cancer patients.

Mutation c.656A>G, p.Asp219Gly (**D219G**) is located in exon 4 between the two DNA binding domains, but is otherwise not within any known binding or structural domains. This mutation was associated with 3/2158 breast cancer patients and high-risk.

Mutation c.1699C>T, p.His567Tyr (**H567Y**) is located in exon 5 between the ChAM domain and the MRG15 binding domain, but not within any known binding or structural domains. This mutation was associated with 1/2158 breast cancer patients and high-risk.

Structural domain mutation

A delta coiled-coil mutation (ΔCC). One structural domain deletion mutant was constructed and tested. The coiled-coil domain (amino acids 9 to 44) was deleted to test if the BRCA1 binding and PALB2 homodimerization domains were essential for viability.

Patient mutation complementation

A PALB2 cDNA was PCR amplified and Gateway cloned into a pDONR 221 plasmid and subsequently into a PiggyBac transposon expression vector containing a NEO selection cassette and a CAGs promoter. Site-directed mutagenesis was performed with either a QuickChange II Site-Directed Mutagenesis Kit or a Q5 Site-Directed Mutagenesis Kit to incorporate a FLAG epitope tag and the patient mutations. All

primer sequences utilized for these experiments are listed in Supplementary Table S1. Flag-tagged WT and patient mutation-containing cDNAs were introduced into the PALB2$^{flox/-:CreER}$ cell line by PiggyBac-meidated transposition and G418 selection was used to confirm integration. The remaining floxed PALB2 genomic allele was the removed by the addition of 10 nM 4-OHT to the media for 2 days. Cells were subcloned and clones which had lost the endogenous PALB2 allele were identified by PCR screening. One tamoxifen treatment was sufficient to obtain the L100F, D219G, H567Y and Y1183X cell lines with the loss of the floxed allele. However, 3 subsequent tamoxifen treatments and cell recovery cycles were necessary to obtain the complemented Y551X, R753X and ΔCC cell lines containing the loss of the floxed PALB2 allele.

Generating the PALB2 delta C-terminus cell line by CRISPR/Cas9 mediated gene targeting

A gRNA targeting PALB2 exon 5 was designed and incorporated in the CRISPR/Cas9 plasmid hSpCas9-2A-Puro/px458 as described (Supplementary Figure S1)(229). A single-stranded DNA oligonucleotide (ssODN) was designed to "knock-in" the patient mutation R753X along with a novel BseYI restriction enzyme recognition site. WT HCT116 cells were electroporated with 5 ug of the CRISPR/Cas9 plasmid and 1.5 uL of 100 μM ssODN and allowed to recover for 2 days. Cells were sorted by fluorescence activated cell sorting (FACS) to obtain the green fluorescent protein (GFP; *i.e.*, transfected) cell population. The GFP-positive cells were then subcloned and screened by PCR with FancN_Ex5_F1 and FancN_Ex5_R3 primers and a subsequent restriction

enzyme digestion with BseYI. The WT sequence contains one BseYI enzyme recognition site in the PCR product and can be digested to two fragments of different sizes (342 and 172 bp), whereas a heterozygous knock-in should generate 4 restriction enzyme digestion fragments (342, 240, 172 and 92 bp), and a homozygous knock-in should produce 3 digestion fragments (250, 172 and 92 bp). After PCR amplification and BseYI restriction enzyme digestion, clones 17 and 67 and 83 indicated that they contained possible heterozygous knock-ins and the clones were further analyzed by TOPO-TA cloning for allele sequence confirmation. This analysis showed that two of the clones were useful. Clone 83 contained indeed a heterozygous knock-in of the R753X mutation. Interestingly, Clone 17 contained biallelic mutations consisting of a frameshift and C-terminal truncating mutation on one allele (c.2279insT, p.760fs*11) and a 65 bp deletion plus a 2 bp insertion resulting in a 21 amino acid in-frame deletion with flanking missense mutations on the other allele (c.2268_2332delinsGG, p.C757W_S778Gdel) (hereafter referred to as PALB2* cell line). See Supplementary Table S2 for primer, guide and ssODN sequences used in these experiments.

Drug sensitivity testing

WT and PALB2$^{-/-}$ complemented cells were subcultured in 6-well plates according to their plating efficiency. WT cells were subcultured at 300 cells/well, PALB2$^{-/-}$ complemented cells (L100F, D219G, H567Y) were plated at 1,000 to 3,000 cells/well, and PALB2$^{-/-}$ complemented cells (Y551X, R753X, Y1183X and ΔCC) were subcultured at 5,000 to 8,000 cells/well. After 24 hr, the old media was removed and new media containing 0, 1, 2, 5 nM MMC, 0, 25, 50, 75 nM APH, or 0, 50, 100, 250 nM olaparib

was added in triplicate. Cells were incubated for 12 to 14 days, washed in phosphate buffered saline (PBS), fixed in 10% acetic acid/10% methanol and stained with Coomassie as described (158). Colonies reaching a minimum size of 50 cells were counted and normalized to the average colony number in untreated wells. Data is averaged from a minimum of 2 independent experiments with a minimum of 3 replicates per experiment.

DNA HDR repair assay

The HDR reporter assay was performed with the DR-GFP plasmid as described (159). Briefly, three plasmids including the reporter plasmid (DR-GFP), an I-SceI expression plasmid, and a mCherry expression plasmid (which was used as a transfection control) were co-transfected into cells using Lipofectamine 3000. Cells were fixed with 4% paraformaldehyde 72 hr after transfection and sorted by FACS. The number of dual GFP-positive and mCherry-positive cells divided by the number of mCherry-positive cells was calculated to determine repair efficiencies. The values were normalized to the repair efficiency observed in WT cDNA complemented PALB2$^{-/-}$ cells.

For the RS-1 treatment used during the HDR assay, 7.5 nM RS-1 was added to the media 2 hr prior to plasmid transfection. Fresh media containing 7.5 nM RS-1 was added again 24 hr after transfection. Normalized repair efficiency with RS-1 was subtracted from the normalized repair efficiency without RS-1 and the percent change in efficiency from untreated was reported. Data is averaged from a minimum of 6 replicates from 2 independent experiments.

Immunoblotting

Untreated WT and PALB2$^{flox/-:CreER}$ cells untreated and treated with 10 nM 4-OHT for 24, 48, 72, and 96 hr were lysed in radioimmunoprecipitation assay (RIPA) buffer containing a Complete Protease Inhibitor cocktail. Protein concentrations determined and 80 μg of each lysate in 1X NuPAGE LDS sample buffer were electrophoresed on a Criterion 4 to 20% gradient gel and then transferred to Hybond P, polyvinylidene fluoride (PVDF) membranes. Primary antibodies used were a rabbit anti-PALB2 (obtained from B. Xia, 1:1000) and a mouse anti-Ku86 and secondary goat anti-mouse IgG HRP conjugate or donkey anti-rabbit IgG HRP.

Co-immunoprecipitation

Cells were collected from 75% confluent 10 cm plates with trypsin and washed in PBS. All the following steps were performed on ice or at 4^{o}C. The cells were lysed in 50 mM TRIS, 2 mM EDTA, 0.5% NP-40, 150 mM NaCl (NTEN buffer) containing Complete Protease Inhibitor Cocktail and subsequently incubated on ice for 15 min. The samples were then centrifuged for 15 min at 14,000 rpm and the supernatant was transferred to a new tube. Lysates were then pre-cleared with mouse IgG-Agarose beads for 1 hr using a rotator. Immunoprecipitation (IP) was performed overnight on a rotator with either mouse IgG-Agarose (IgG IP control) or anti-FLAG M2 affinity gel (FLAG IP). The next day, the beads were washed 3 times with NTEN buffer and protein eluted from beads with 1X NuPAGE lithium dodecyl sulfate (LDS) sample buffer at 95^{o}C for 5 min. The samples were then loaded on a Criterion 4 to 20% gradient gel and transferred to a

Hybond P membrane. Immunoblotting was performed with a mouse anti-BRCA2, rabbit anti-RAD51, mouse anti-Flag M2, rabbit anti-PALB2 and secondary goat anti-mouse IgG HRP conjugate (or donkey anti-rabbit IgG HRP.

Immunofluorescence

Cells were plated in 4-chamber slides at 100,000 to 200,000 cells per chamber. The day after plating, irradiated samples were exposed to 10 Gy of ionizing radiation (IR). After 6 hr of recovery, the cells were fixed in 4% paraformaldehyde/PBS for 15 min and permeabilized with 0.2% Triton X-100/PBS for 15 min. Fixed cells were blocked in 7% bovine serum albumin (BSA)/PBS for 60 min. The primary antibody was diluted in 0.5% BSA/PBS and incubated overnight at 4^{o}C. The primary antibody was rabbit anti-RAD51 and the secondary antibody was an Alexa Fluor 555 anti goat and rabbit antibody. DNA repair foci quantification was performed using ImageJ.

RESULTS

Generation of an inducible-conditionally-null *PALB2* knockout cell line

We used rAAV-mediated gene targeting to generate a *PALB2* knockout in the HCT116 cell line as described (Figure 1)(152,153,181). A conditional knockout cell line approach was used because of two informative precedents: first, the direct disruption of *PALB2* in the mouse resulted in embryonic lethal (224). Second, the FA patients reported to date with *PALB2* biallelic mutations are not null, but express truncated proteins with potential hypomorphic function (197). Together, these two pieces of data suggested that the complete absence of PALB2 expression might not be compatible with viability. To begin to experimentally address this hypothesis, an adenovirus expressing Cre recombinase (AdCre) was introduced into the *PALB2*$^{flox/NEO}$ cell line in an attempt to remove the NEO selection cassette and the floxed conditional allele. However, while 9 of 40 clones demonstrated removal of the NEO selection cassette, all of the subclones retained the floxed allele (data not shown). Moreover, when two of the *PALB2*$^{flox/-}$ cell lines were treated with AdCre and 96 clones were screened, all of the viable subclones still retained the floxed allele (data not shown). These two preliminary experiments circumstantially confirmed that the isolation of a human cell line lacking the expression of PALB2 was likely not biologically possible. This prompted us to introduce the CreER system into the cell line as an inducible way to force the removal of the floxed allele (227). With the addition of tamoxifen or 4-OHT, the CreER translocates to the nucleus and can facilitate recombination of the floxed *PALB2* allele. Indeed, the *PALB2*$^{flox/-:CreER}$ cells effectively removed the floxed allele following the addition of 4-OHT to the cell culture media, and PCR did not detect any residual floxed allele 24 hr after CreER induction (Figure 1B,

lanes 4-7). The loss of PALB2 protein expression with the addition of tamoxifen further confirmed the functionality of the CreER system and establishment of the *PALB2*$^{-/-}$ genotype (Figure 1C). While the PALB2$^{flox/-:CreER}$ cells have reduced PALB2 expression compared to WT (Figure 1C, lanes 1 and 2), the induced *PALB2*$^{-/-}$ cells had no detectable PALB2 protein expression (Figure 1C, lanes 3 to 6).

PALB2 is essential for cell viability and genomic stability

To document the effect of the lack of PALB2 expression on cell proliferation, a growth curve of the *PALB2*$^{flox/-:CreER}$ cells compared to WT cells with and without tamoxifen treatment was performed (Supplementary Figure S1). Untreated *PALB2*$^{flox/-:CreER}$ cells had a growth defect compared to WT, suggesting that *PALB2* is haploinsufficient. Even more striking, when tamoxifen was added to the cultures the cells no longer expanded but instead began to die. These observations unequivocally demonstrated that PALB2 is essential for cell viability and explained why no *PALB2*$^{-/-}$ subclones could ever be obtained from single cells. PALB2's tight association with BRCA1 and BRCA2 and its involvement in HDR led us to investigate the genomic stability of *PALB2*-null cells. Thus, metaphase spreads were derived from either *PALB2*$^{flox/-:CreER}$ or *PALB2*$^{-/-}$ +WT cDNA cells 24, 48, and 72 hr after tamoxifen treatment or from cells that were untreated. The resulting karyotypes demonstrated that within 24 hr of inducing the *PALB2*$^{-/-}$ genotype with tamoxifen, that highly characteristic FA radial chromosome formations could already be observed along with an increased frequency of breaks and fragmented chromosomes (Figure 2). Strikingly, by 48 hr after tamoxifen addition, massive chromosomal catastrophe had occurred in 75% of the metaphase cells and an additional 10% of the metaphase spreads were simply too fragmented to quantitate (Figure 2 and

Supplementary Table S1). Not surprisingly, a low mitotic index was noted for the *PALB2*$^{flox/-:CreER}$ cells at 48 and 72 hr after tamoxifen treatment (data not shown).

This type of chromosome shattering can be caused by aberrant DNA replication (230,231). To examine if the severe genomic instability in the absence of PALB2 was replication dependent, the cells were grown in complete media and in low serum (1% FBS) media. The low serum conditions reduced cell proliferation by 56% and when tamoxifen was added, low serum conditions also reduced the cell death resulting from the loss of PALB2 by 47% (Supplementary Figure S1). Therefore, the reduction in cell growth and replication was proportional to the reduction in cell death, suggesting that the genomic instability observed in the absence of PALB2 was replication dependent. Taken together, these results support the hypothesis that PALB2 is essential for preventing replication-dependent genomic instability.

Complementation with *PALB2* patient mutations rescues cell viability

Few FA patients of the FA-N subtype have been reported and these patients typically have a severe form of FA associated with an early onset of cancer (138,197). Interestingly, even though the patient sample size is small, most of these FA-N patients have *PALB2* frameshift and/or nonsense mutations that truncate or destabilize the C-terminus of the protein. Thus, after establishing that PALB2 function was essential for cell viability and genome stability, we set out to understand how these potentially hypomorphic patient mutations functioned in the cell. Three of the FA-N known pathogenic *PABL2* mutation were selected for analysis: c.1653T>A, p.Tyr551* (Y551X); c.2257C>T, p.Arg753* (R753X); and c.3549C>G, p.Tyr1183* (Y1183X) (Figure 3A).

Mutations Y551X and R753X are both truncations that eliminate the PALB2 WD40 domain, which is the binding site for BRCA2, RAD51 and RAD51C. Y1183X is a PALB2 truncation of just the last 4 amino acids of the protein, but has been reported to destabilize the 7-bladed β-propeller protein structure formed by the WD40 domain (128).

In addition to the 3 naturally-occurring *PALB2* mutations described above, a recent study using next generation sequencing performed on breast cancer patients identified several breast cancer patients with VUS mutations resulting from SNPs in *PABL2*. This study identified 13/2158 (0.6%) breast cancer patients with known pathogenic PALB2 mutations, but another 56/2158 (2.6%) that had *PALB2* VUS mutations (139). Three of the VUSs that resulted in single amino acid substitutions were selected for analysis: c.298C>T, p.Leu100Phe (L100F); c.656A>G, p.Asp219Gly (D219G); and c.1699C>T, p.His567Tyr (H567Y) (Figure 3A). Two of the VUS mutations, L100F and D219G, were each found in 3 patients from this study, indicating a potentially higher population occurrence or pathogenicity. In addition, two of the VUS mutations, D219G and H567Y, were associated with high-risk based on family history. High-risk was defined as a family history of breast cancer before the age of 50 or ovarian cancer at any age or with corresponding mutations in a first- or second-degree relative (139). When these mutations were evaluated by the MutationTaster2 web-based software to classify the pathogenicity of these SNPs, all three were predicted to just be polymorphisms (*i.e.,* non-pathogenic) (232).

Both the FA authentic, *PALB2*-truncating mutations as well as the breast cancer SNP mutations were engineered into a WT *PALB2* cDNA and the respective mutant cDNAs were then used to complement the $PALB2^{flox/-:CreER}$ cells. Tamoxifen was subsequently

used to remove the floxed *PALB2* allele and *PALB2*$^{-/-}$ complemented cell lines with the 6 different patient mutation (and a WT cDNA) were successfully obtained, confirming that all of the mutant cDNAs were capable of rescuing cellular viability. Of note, however, the Y551X and R753X PALB2 truncating mutations did not complement easily, and multiple rounds of tamoxifen treatment were required before complemented cells with the loss of the conditional allele could be isolated. A priori and quite importantly, the successful *PALB2*$^{-/-}$ complementation with Y551X and R753X *PALB2* cDNAs (which both truncate the C-terminal WD40 domain) strongly and surprisingly implied that the BRCA2, RAD51, and RAD51C binding domains were not essential for viability. Therefore, it was hypothesized that the N-terminal coiled-coil domain containing the BRCA1 binding and PABL2 homodimerization activities was perhaps the essential portion of PALB2 that was required for cellular viability. To test this hypothesis, we constructed an additional mutant *PALB2* cDNA lacking the coiled-coil domain (ΔCC). Surprisingly, complementation was also successful with this cDNA, although establishing the cell line also required several rounds of tamoxifen treatment to obtain the relevant clones. In all instances, complementation of viability was confirmed by loss of the chromosomal conditional (floxed) allele (Figure 3B, lanes 4-11).

CRISPR/Cas9-mediated targeting to generate a *PALB2* mutant cell line

As further confirmation that viable, hypomorphic mutations can be generated in *PALB2*, a CRISPR/Cas9-mediated gene editing strategy was used to create another PALB2 mutant cell line. A guide RNA was designed close to the R753X mutation site in exon 5 (Supplementary Figure S2)(157). The CRISPR/Cas9-containing plasmid was transfected

along with a ssODN as a donor template for the knock-in of the R753X mutation and a novel restriction enzyme recognition site for BseYI. Screening was performed of the edited cells by PCR amplification of the target site, BseYI restriction enzyme digestion and subsequently by confirmatory DNA sequencing. One of the resulting clones (#17) had biallelic mutations of *PALB2* in exon 5. One allele of clone 17 contained a one base pair insertion resulting in a frameshift and premature truncation in exon 5 (very similar, but not identical to R753X). The other allele had an in-frame, 21 amino acid deletion flanked by missense mutations, p.C757W_S778Gdel. Theoretical expression of the second allele should produce a protein containing intact N- and C-terminal domains. This biallelic *PALB2* mutant cell line is hereafter referred to as the PALB2* cell line and was also characterized in the experiments described below.

PALB2 VUS mutations D219G and H567Y are potentially pathogenic

To confirm the utility of the FA mutant cell lines and to assess the breast cancer VUS for pathogenicity, all of the complemented and genetically engineered *PALB2* cell lines were tested with three different drugs that will induce different types of cellular stress. The hallmark of FA cells is a sensitivity to interstrand DNA crosslinks, such as those introduce by the chemotherapeutic MMC. Therefore, all the complemented cell lines were first tested for MMC sensitivity in a colony forming assay. The cells were plated at low density according to their plating efficiency and colony formation was evaluated in MMC-treated cells at increasing concentrations (1, 2, and 5 nM) compared to untreated cells. The WT complemented *PABL2*$^{-/-}$ cells were as equally resistant to MMC as WT cells demonstrating that a WT cDNA can completely rescue this phenotype (Figure 4A).

In contrast, all but one of the derived mutations demonstrated significant sensitivity to MMC at all three concentrations. The one exception was the breast cancer associated VUS, L100F, which was not significantly sensitive to MMC at 1 nM, but was sensitive at the two higher concentrations (2 and 5 nM MMC) as compared to WT HCT116 cells (Figure 4A). Thus, all of the mutant cDNAs, some more so than others, were incapable of restoring a MMC-resistant phenotype to *PABL2*$^{-/-}$ cells.

Replication stress is a known contributor to genomic instability due to the resulting DSBs caused by the collapse of stalled replication forks. Therefore, the ability of the *PALB2* mutant cell lines to handle replication stress was evaluated by using colony forming assays with increasing concentrations (25, 50 and 75 nM) of APH exposure. Again, the WT-complemented *PALB2*$^{-/-}$ cells were as equally resistant to APH as WT cells demonstrating the possibility of full complementation (Figure 4B). All of the PALB2 mutant cell lines except L100F were sensitive to the highest dose (75 nM) of APH. However, only H567Y and ΔCC were significantly sensitive to all 3 concentrations of APH (Figure 4B).

Lastly, *BRCA1* and *BRCA2* cancer cells have a demonstrated synthetic lethality with PARP1 inhibitors such as olaparib. Olaparib inhibits PARP1 activity, which is involved in single-strand DNA break repair as well as alternative non-homologous end joining (233). To test the sensitivity of the *PALB2* mutations, the mutant cell lines were evaluated by a colony forming assay with increasing concentrations (50, 100, and 250 nM) of olaparib compared to untreated cells. As before, the WT-complemented PALB2$^{-/-}$ cells were equally resistant to olaparib as WT cells. Likewise, similar to the MMC sensitivity experiments, all of the mutant-complemented cell lines, except L100F, were

significantly sensitive to olaparib at all three concentrations tested. Interestingly, the *PALB2** cell line had some resistance to olaparib and was only significantly sensitive at the highest concentration (250 nM) tested (Figure 4C).

Taken together, these data indicate that the PALB2 WD40 domain (with the BRCA2/RAD51/RAD51C binding activities) and the coiled-coil domain (with the BRCA1 binding and PALB2 homodimerization activities) are essential for MMC, APH and olaparib resistance. In contrast, the breast cancer VUS, L100F, had only mild MMC sensitivity and no increased sensitivity to APH or olaparib suggesting that it was (or nearly so) as functional as a WT cDNA. Strikingly, however, and of significant clinical significance, the other two breast cancer VUS mutations, D219G and H567Y, both demonstrated drug sensitivities comparable to the *bona fide* FA pathogenic mutations. These VUSs do not disrupt any known PALB2 domain, but are apparently highly debilitating. Of additional interest, the *PALB2** mutant had only intermediate phenotypes for MMC and especially for olaparib sensitivity, indicating that it maintains significant PABL2 function, most likely because this allele contains intact N- and C-terminal domains.

All *PALB2* mutants are defective in HDR and a full-length PALB2 is essential for HDR

PALB2 has been implicated as the molecular scaffold for HDR repair proteins and a coordinator of HDR repair. Thus, a recombination assay was used to determine the ability of the mutant cell lines to carry out HDR (159). Briefly, 3 plasmids: a DR-GFP reporter plasmid, an I-SceI expression plasmid, and a mCherry expression plasmid as a transfection control were transfected into the relevant cell lines. The DR-GFP plasmid

contains two non-functional GFP cassettes, one has been inactivated by the inclusion of an integrated I-SceI enzyme recognition site along with stop codons and the other is inactivated because it is truncated on both the 5' and 3' ends. The I-SceI enzyme can thus be used to create a DSB in the first GFP cassette and if HDR is used with the truncated GFP cassette, then GFP expression can be restored and HDR positive cells can be quantitated by FACS analysis. The percent repair is determined by the number of mCherry and GFP doubly-positive cells within the total mCherry-positive cell population (Figure 5A). Importantly, all of the *PALB2* mutants were found to have a significantly reduced HDR repair compared to the WT complemented cell line (Figure 5A). With that said, all three of the VUS mutations and Y1183X had a significantly higher percentage of HR compared to the FA patient mutations Y551X and R753X, and the ΔCC and PABL2* mutants. A parsimonious interpretation of these results is that rather than a functional N- or C-terminus being required for HDR what may be more important is the expression of a full length (or mostly intact, as Y1183X lacks just the last 4 amino acids) PALB2 protein — a view that is consistent with a putative scaffolding role.

A RAD51 stabilizing small molecule, RS-1, is known to help stabilize RAD51 filament formation (183). To evaluate if RS-1 could improve the HDR rates of the *PALB2* mutant cell lines, 7.5 nM RS-1 was next included while performing the HDR assay. RS-1 improved the percentage of HDR repair in the WT-complemented *PALB2*$^{-/-}$ cells by 30%, whereas all *PALB2* mutants except Y1183X showed little to no improvement in HDR efficiency. RS-1 increased the Y1183X mutant HDR efficiency by 28%, which was not significantly different from the improvement observed in WT-complemented cells. These results indicate that PABL2 is playing an important role in

RAD51 filament formation and/or that strand invasion cannot be compensated for by RAD51 filament stabilization. It also implies that the Y1183X mutant is somewhat uniquely defective in stabilizing RAD51 filaments and that RS-1 can improve HDR specifically for this *PALB2* mutant.

Pathogenic PABL2 mutants can complex with BRCA2 and RAD51

Most of the confirmed FA-N group mutations in PALB2 are nonsense or frameshift mutations resulting in premature truncation of the protein's C-terminus and consequently encode proteins that do not bind BRCA2 and have reduced binding to RAD51 (131,196). To evaluate whether the *PALB2* mutations studied here could still bind BRCA2 and RAD51, a co-immunoprecipitation was performed (Figure 6). Detectable amounts of FLAG-tagged PALB2 were successfully pulled down using FLAG antibody beads for immunoprecipitation in all of the complemented cell lines except R753X and ΔCC, indicating these two proteins may be more unstable than the other mutants (Figure 6, lanes 7, 9, 12). With that said, it is important to remember that these two mutant cell lines, while not expressing detectable immunoprecipitable PALB2 protein, are nonetheless viable, indicating that some protein must perforce be expressed. In addition, BRCA2 was pulled down in WT-complemented cells (Figure 6, lane 2) and in all the VUS mutants (L100F, D219G, H567Y) (Figure 6, lanes 3 to 5) and even in the FA mutation Y1183X (Figure 6, lane 8). As expected, the *PALB2* mutant cell lines expressing the Y551X, R753X truncations of the WD-40 domain did not bind BRCA2 (Figure 6, lanes 6, 7, 11). Interestingly, the ΔCC mutant did not co-immunoprecipitate BRCA2 either (Figure 6, lanes 9 and 12), but that could be due to insufficient quantities

of stable PALB2 mutant protein. Intriguingly, RAD51 was pulled down in all of the cell lines (Figure 6, lanes 2 to12). WT HCT116 cells not expressing a FLAG-tagged PALB2 were used a negative control and, as expected, no detectable BRCA2, PALB2, or RAD51 protein was pulled down (Figure 6, lane 1). Since there are two binding domains for RAD51, one in the N-terminus and one in the C-terminus of PALB2 that could explain how the truncating mutations are still binding RAD51 (Figure 3). The RAD51 pull down also supports the contention that some PALB2 protein is expressed for the R753X and ΔCC mutants even if it is below the antibody detection level.

PABL2 facilitates RAD51 function and PALB2 truncation mutants of the WD40 domain generally disrupt the formation of RAD51 foci following exposure of cells to DNA damage (118,197). Therefore, since all the PALB2 mutants bound RAD51 as defined by co-immunoprecipitation, immunofluoresence was used to investigate if the PALB2 mutant cell lines could still form RAD51 foci after 10 Gy of IR exposure (Figure 7). As reported, the two PALB2 mutants that truncate the WD40 domain (Y551X and R753X) were unable to form RAD51 foci, nor was the ΔCC mutant. The three VUS mutants (L100F, D219G and H567Y) appear to have fewer RAD51 foci than the WT-complemented cells. Most interesting was the ability of the Y1183X and PALB2* to form RAD51 foci. This demonstration was especially interesting in light of the previous demonstration (Figure 5A) that both of these mutants are defective in HDR. Taken together these results strikingly suggest that BRCA2 and RAD51 binding are not sufficient for the normal function of PALB2 in facilitating RAD51 localization, filament formation or HDR.

DISCUSSION

The importance of DSB repair and resolution of stalled replication forks in preventing cancer, particularly breast cancer, is reinforced by the fact that many genes involved in HDR are cancer predisposition genes. In this study, we created a tamoxifen-inducible knockout of PALB2, and demonstrated that it is essential for genomic stability and viability. Indeed, the loss of PALB2 resulted in a rapid and catastrophic genomic instability (Figure 2). We then demonstrated that *PALB2* FA-associated mutations are hypomorphic and can rescue cellular viability and yet they are still defective in DNA repair and sensitive to ICLs and replication stress. These latter observations are important because they define a novel separation-of-function that was previously unappreciated in terms of PALB2's role(s) in cellular viability and DNA repair. We have also characterized the function of three *PALB2* VUSs that were discovered in breast cancer patients. While most *PALB2* pathogenic mutations identified so far are truncations, our results indicate that even single amino acid changes — even ones not located in critical structural domains in PALB2 — can significantly alter the ability of the protein to enable DNA repair and the response to replication stress.

FA pathogenic mutations

The three FA-associated mutations, Y551X, R753X and Y1183X, all demonstrated significant sensitivity to ICLs, replication stress and PARP1 inhibition, and all were defective in HDR, as expected. However, the Y1183X mutation did have some residual drug resistance and HDR function that was not observed with the other two, larger truncating mutations. In addition, the Y1183X mutation was the only PALB2 mutant

with increased HR efficiency when the RAD51 stabilizer, RS-1, was used, and the only FA truncating mutant that was capable of binding BRCA2 and forming RAD51 foci. One possible explanation for these results is that the loss of the C-terminal four amino acids does not destabilize the protein as much as had been predicted (128). Alternatively, it is also possible that the instability predicted to be imparted by this mutation does in fact occur but that it is overcome by overexpression in our system (*e.g.*, Figure 6), allowing for some protein folding and binding of BRCA2. Regardless, what is perhaps mechanistically most important is that this binding of BRCA2, and the recruitment of RAD51 to DNA damage foci improved HDR over the full WD40 truncation mutants, Y551X and R753X (Figure 6), and (modestly) improved drug resistance (Figure 4). Purified PALB2 binds preferentially to ssDNA and D-loop structures and facilitates RAD51 filament formation and strand invasion (118,234). Therefore, the observed result that RS-1 improved HR efficiency for Y1183X leads to the conclusion that this mutant may be predominately defective in RAD51 filament formation or strand invasion. Therefore, the PALB2-mediated binding of BRCA2 and recruitment of RAD51 to DNA damage foci is not only insufficient for full HDR activity but it may also not be predictive of the pathogenicity for a PALB2 mutation.

The PALB2* and ΔCC mutants

The PALB2* and ΔCC mutants provided some additional insight into PALB2 function. Since many of FA-associated mutations truncated the BRCA2 binding domain, but retained the BRCA 1 binding domain, we had hypothesized that the BRCA1 binding domain was the PALB2 feature that was essential for viability. In addition, BRCA1 has been implicated as functioning upstream of PALB2, and that it is required for MMC

resistance, HDR and RAD51 foci formation (131,132,134,235). Therefore, it was surprising that the ΔCC mutant, which completely lacks the BRCA1 binding domain, rescued the viability of the *PALB2*$^{-/-}$ cell line. These experiments surprisingly demonstrated that the coiled-coil is not required for viability. This conclusion must be tempered somewhat since there no detectable protein expression for the ΔCC mutant. However, the fact that the viability of the *PALB2*$^{-/-}$ cell line could be complemented by this mutation argues strongly that there must be some protein functioning in the cells. The observation of RAD51 binding in the ΔCC mutant also argue for some functioning residual protein. As expected, the ΔCC mutant demonstrated severe sensitivity to ICLs, replication stress and olaparib, and was defective in HDR indicating that the coiled-coil domain (and BRCA1 binding and homo-dimerization domain) were essential for these functions. It is unclear whether the undetectable binding of BRCA2 to PALB2 ΔCC was due to the ΔCC domain being essential for BRCA2 binding or, as we believe the more likely scenario if it was due to low PALB2 mutant protein levels making detection difficult (Figure 6, lanes 9 and 12).

The PALB2* mutant was also illustrative. One allele of PALB2* contains a mutation that results in a frame shift and truncation (p.760fs*11) comparable in location (seven amino acids C-terminal) to the R753X mutant. However, this mutant performed better than R753X in all the drug sensitivity assays, indicating that the other allele, an in-frame deletion of 21 amino acids with an intact WD40 domain (p.C757W_S778Gdel) was likely functioning to some extent. With that said, the putative intact WD40 domain and the demonstrable RAD51 foci formation did not correlate with efficient HDR. In addition, RS-1 did not improve HDR in the PALB2* mutant. Indicating possible defects

with D-loop stabilization or DNA binding considering the deletion occurs near the MRG15 binding site and may affect chromatin association. Interestingly, internal protein deletions of PALB2 have been found before to rescue functionality of the protein before. A revertant clone from Y551X was found that deletes exon 4 completely and provides rescue of MMC sensitivity and RAD51 foci formation. Also, a hypomorphic PALB2 mutation associated with a patient with a more mild form of FA-N had C-terminal truncation mutation (c.1676_1677dleAAinsG; p.Gln559ArgfsTer2) and second mutation that results in an in-frame skipping of exon 6 (c.3586+1G>A;p.Thr839_Lys862del). The cells from the FA-N patient can bind BRCA2 and form RAD51 foci. Therefore, it interesting that PALB2* mutant with an in-frame 21 amino acid deletion in exon 5 is still sensitive to ICL, APH and olaparib. However, PALB2* has some partial resistance to olaparib compared to the other pathogenic mutations (PALB* is only significantly sensitive at the highest concentration of Olaparib) which is similar to a report by Bleuyard et al., that reported MMC sensitivity but not olaparib sensitivity when ChAM motif was deleted (214). In summary, central deletions of PALB2 can recover some functionality of the protein in experimental assays, and could result in less severe clinical phenotypes.

Breast cancer SNPs

The three breast cancer associated PALB2 SNPs from this study were selected based on association with high family history or repeated occurrence in the breast cancer patients tested in the study by Tung *et. al*.(139). The SNPs were all classified as variants of unknown significance (VUS) and had not been previously reported. All three of the SNPs produced full length PALB2 protein that was well expressed (Figure 6). However,

the defective phenotype for the D219G and H567Y mutants observed in the drug sensitivity assays (MMC, APH and olaparib, Figure 4) was surprising and comparable to the sensitivity of the highly pathogenic WD40 truncating mutations. Further analysis revealed that all three of the mutants were defective in HR, and the HR efficiency could not be improved with RS-1. In addition, all the SNPs were capable of binding BRCA2 and forming RAD51 foci (Figures 6-7). However, as seen with the Y1183X, even pathogenic mutations can bind BRCA2 and form RAD51 foci. Therefore, the experimental data along with a strong family history for breast/ovarian cancer for the D219G and H567Y mutations supports the conclusion that they are potentially pathogenic. In conclusion, we have developed a cellular model system that is being used successfully to evaluate PALB2 cellular functions and screen variants for pathogenicity.

FIGURE LEGENDS

Figure 1. Generation of the inducible-conditional PALB2 knockout (A) rAAV targeting scheme for PALB2. The first round of targetin used a conditional rAVV vector to knock-in a NEO selection cassette (green rectangle) and flank PALB2 exons 2 and 3 with lox P sites (yellow triangles). AdCre was used to remove the NEO selection cassette creating the $PALB2^{flox/+}$ cell line. The second round of targeting used a knock-out rAAV vector to knock-out PALB2 exons 2 and 3 and replace them with a NEO selection cassette. AdCre was used again to remove the NEO selection cassette and to remove the floxed exons 2 and 3 on the conditional allele. However, only clones that retained the floxed exon were recovered after subcloning creating the $PALB2^{flox/-}$ cell line. Therefore, an inducible Cre recombinase system, CreER, was introduced to the cells to force the removal of the conditional allele with the addition of tamoxifen (4-OHT), creating the $PALB2^{flox/-:CreER}$ cell line. The addition of tamoxifen to the culture media results in forced removal of the conditional allele and creation of the $PALB2^{-/-}$ cell line. (B) Schematic of the different alleles and sizes that can be detected with the primers used in the PCR. The untreated PCR panel shows the WT HCT116 parental cells with a single band across exons 2 and 3 (Lanes 2-3) while the two independent clones of $PALB2^{flox/-:CreER}$ cells (3 and 31) amplify two alleles, the flox and null bands (Lanes 4-7). The tamoxifen treated panel (+4-OHT) shows that tamoxifen does nothing to WT cells (Lanes 2-3), but within 24 hours of adding 10 nM tamoxifen to the $PALB2^{flox/-:CreER}$ cells, the floxed allele is no longer detectable and only the null alleles are amplified, confirming the inducible $PALB2^{-/-}$ cell line (Lanes 4-7). Negative control (Lane 8). 1Kb Plus DNA

Ladder (Invitrogen) (Lanes 1 and 9) (C) Western blot analysis demonstrating reduced PALB2 expression in the PALB2$^{flox/-:CreER}$ cells and loss of PALB2 after the addition of tamoxifen. 80 ug of whole cell lysates from WT HCT116 cell (Lane1), and PALB2$^{flox/-:CreER}$ clone 3 (Lanes 2-6), untreated (0) and 24, 48, 72 and 96 hours after the addition of tamoxifen. Ku86 was used a loading control.

Figure 2. PALB2 is essential for genomic stability (A) Example metaphase spreads from cytogenetic analysis of PALB2$^{flox/-:CreER}$ cells untreated, 24 and 48 hours after 10 nM tamoxifen added to the cells to induce the loss of PALB2. The untreated cells demonstrate the PALB2$^{flox/-:CreER}$ cells have a stable and diploid karyotype of the HCT116 parental cell line. 24 hours after 4-OHT added to the media, radial chromosomes (red arrows) that are characteristic of FA patient cells can be found. 48 hours after 4-OHT is added, chromosomal catastrophe has occurred in 75% of the metaphases analyzed.

Figure 3. PALB2 structure and location of patient mutations that rescue cell viability (A) PALB2/FANCN cDNA exons and bp (base pairs) and the FANCN protein aa (amino acids) are numbered and aligned with the binding and structural domains of the protein. The location of the PABL2 patient mutations selected for analysis are plotted. (B) The same PCR primers from Figure 1B were used to confirm that all the PALB2 mutant cDNAs had complemented viability of the PALB2$^{-/-}$ cell line. WT HCT116 cell have a single band across exons 2 and 3(Lane 2), the PALB2$^{flox/-:CreER}$ cells have the flox and null bands (Lane 3), and the complemented clones only have null bands and no endogenous PALB2 (Lanes 4-11). The null bands are different sizes due to the conditional and knock-out rAAV vectors being designed with different size deletions of

intronic sequence surrounding the targeted exons. No template negative control (Lane 12) 1Kb Plus DNA Ladder (Invitrogen) (Lanes 1 and 13)

Figure 4. Drug sensitivity assays demonstrate PALB2 VUS mutations D219G and H567Y are potentially pathogenic. Colony formation assays were performed to test drug sensitivity for MMC, APH and Olaparib. Cells were plated at low density in 6-well plates according to their plating efficiencies. The next day, media untreated or with drug was added to the cells. The cells were allowed to grow for 12-14 days then fixed, stained, and counted. The percent clonogenic survival was determined from the average number of colonies from the untreated wells. The reported results are the average from a minimum of 6 replicates from a minimum of 2 independent experiments. Error bars represent the SEM (standard error of the mean) (A) MMC sensitivity of the PALB2 mutants was tested in 0, 1, 2, and 5 nM MMC added to the media. (B) APH sensitivity of the PALB2 mutants was tested in 0, 25, 50 and 75 nM APH added to the media. (C) Olaparib sensitivity of the PALB2 mutants was tested in 0, 50, 100 and 250 nM Olaparib. P-values are provided in Supplementary Table 3.

Figure 5. All PALB2 mutants are defective in HR (A) HR (homologous recombination) repair assay was performed on all PALB2 mutant cell lines. The percent repair was normalized to the average repair efficiency determined from the PALB2$^{-/-}$ +WT cDNA (WT) complemented cell line. (B) 7.5 nM RS-1 was added to the media 2 hours prior to transfection with HR assay plasmids, and replenished 24 hours later. Otherwise, the HR assay was performed the same as in (A). The change in repair efficiency was determined by subtracting the normalized repair efficiency with RS-1 from the normalized untreated repair efficiency and determining the percentage based on

the normalized untreated repair efficiency. Data is averaged from a minimum of 6 replicates from 2 independent experiments. Error bars represent the SEM (standard error of the mean). P-values are provided in Supplementary Table 3.

Figure 6. Pathogenic PABL2 mutants can complex with BRCA2 and RAD51 Co-immunoprecipitation of FLAG-tagged PALB2 immunoblotted with anti-BRCA2, anti-PALB2 and anti-RAD51 antibodies. (Lane 1) negative control of WT HCT116 cells without expression of FLAG-tagged PALB2, and has no BRCA2, PALB2 or RAD51 binding. (Lanes 2-5) PALB2 complemented cell lines with WT, L100F, D219G, H567Y all express a full length PALB2 protein, and bind BRCA2 and RAD51. (Lanes 6 and 11) Y551X clones 1 and 13 express a truncated protein and is variably expressed between the two clones. Neither Y551X clone binds BRCA2, but both bind RAD51. (Lane 7) R753X has no visible PALB2 protein detected and no BRCA2 binding, but RAD51 is pulled down (Lane 8) Y1183X has PALB2 expression, BRCA2 and RAD51 binding (Lanes 9 and 12) ΔCC has no visible PALB2 protein detected and no BRCA2 binding, but RAD51 is pulled down (Lane 10) MWM (molecular weight marker)

Figure 7. WD40 domain is essential for RAD51 foci formation, but RAD51 foci are not sufficient for efficient HR WT HCT116 cell and PALB2$^{-/-}$ complements were plated in 4 chamber slides. Cells were exposed to 10 gy IR and allowed to recover for 6 hours prior to fixing and staining by immunofluorescence. 50 cells were evaluated per cell line for RAD51 foci.

Supplementary Figure S1. PALB2 is essential for cellular viability and cell death is replication dependent (A) Growth curve of WT HCT116 cells and PALB2$^{flox/-:CreER}$ cells clones 3 and 31 with and without tamoxifen (4-OHT) treatment. Cells were plated in 6 well plates with or without tamoxifen. Cell counts were collected at day 3, 5, 7 and 11 after tamoxifen treatment in triplicate. Error bars represent SD (standard deviation). (B) The loss of PALB2 results in replication dependent cell death was confirm by a replication assay. PALB2$^{flox/-:CreER}$ cells were grown in complete media (10% FBS) or in low serum media (1% FBS) and either with or without tamoxifen. Cell counts were collected in triplicate on day 2 and day 4 after tamoxifen treatment. The change in cell count between days 2 and 4 was determined and the percent change was determined from the average cell count on day 2. Results from two, independent PALB2$^{flox/-:CreER}$ clones were averaged. Error bars represent SEM (Standard error of the mean). Low serum conditions reduced cell proliferation by 56% and when tamoxifen was added, the low serum conditions also reduced the cell death resulting from the loss of PALB2 by 47%. The reduction in cell growth was proportional to the reduction in cell death, confirming that cell death was replication dependent.

Supplementary Figure S2. CRISPR/Cas9 targeting of PALB2 exon 5 demonstrates biallelic mutations are hypomorphic and rescue viability

A) Schematic of the CRISPR/Cas9-mediated gene targeting to knockout *PALB2* in WT cells to create biallelic mutations. A guide RNA was designed targeting *PALB2* exon 5 with the Cas9 cut site in proximity to the R753X mutation (c.2257C>T;p.Arg753*). A ssODN (single stranded DNA oligo) donor was provided for knock-in of the R753X

mutation, a novel restriction site of BpuEI, and a codon optimized mutation of the PAM sequence. After transfection with Cas9, guide RNA, and ssODN transfected cells were FACS sorted for transient Cas9-GFP positive cells and subcloned. Subclones were screened for targeting by PCR amplification of the targeted region and subsequent BpuEI digestion. WT sequence will cut once with BpuEI resulting in two bands (342 and 172 bp) a heterozygous knock-in would have 4 bands (342, 250, 172, and 92- not visible). No clones with possible homozygous knock-in were found. Alleles were sequenced from clones with potential heterozygous knock-in. Sequence confirmation of alleles revealed a heterozygous KI of R753X in clone 83 and biallelic hypomorphic mutations in clone 17.

Figure 1

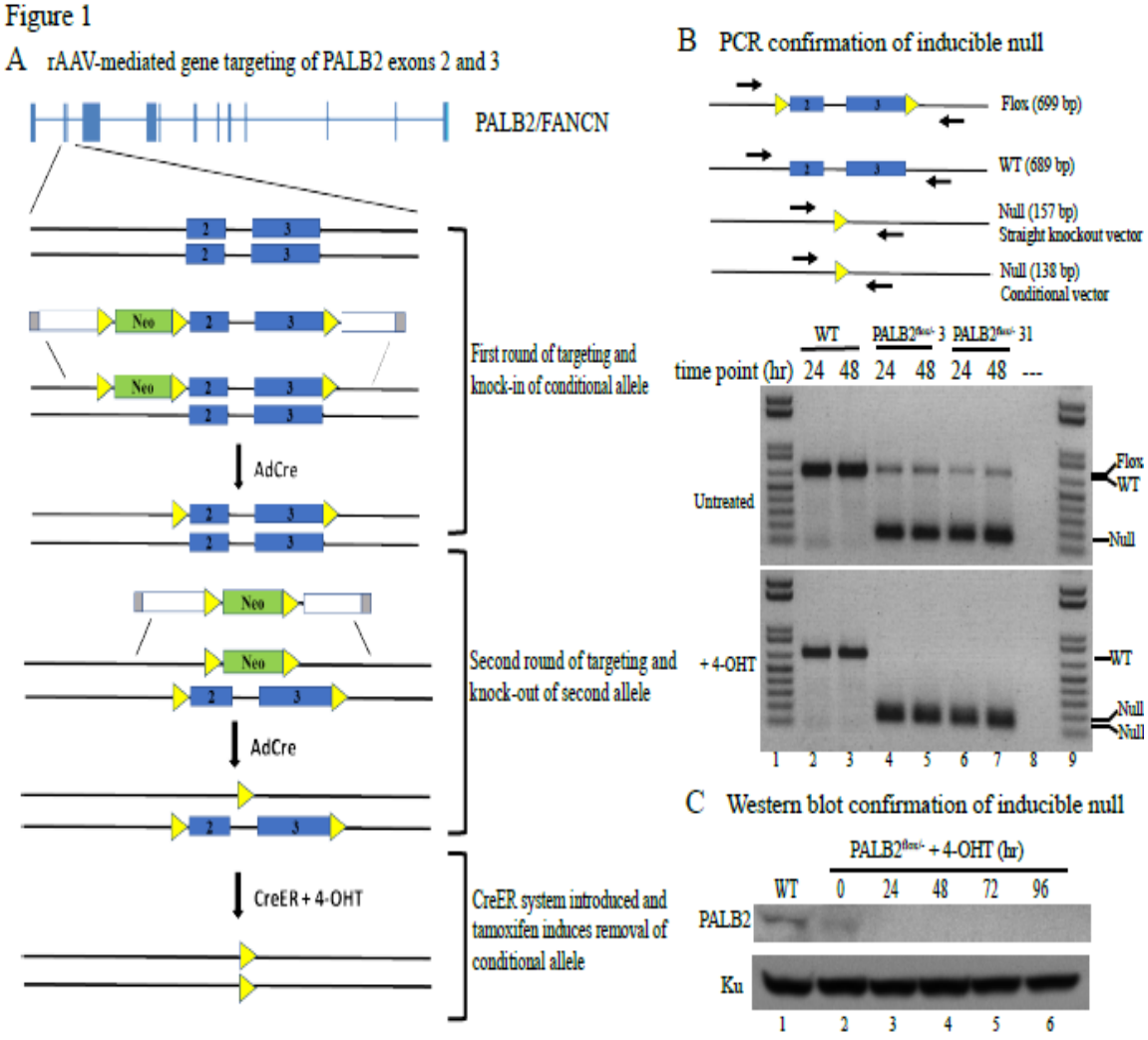
A rAAV-mediated gene targeting of PALB2 exons 2 and 3
PALB2/FANCN
Neo
AdCre
First round of targeting and knock-in of conditional allele
Second round of targeting and knock-out of second allele
CreER + 4-OHT
CreER system introduced and tamoxifen induces removal of conditional allele
B PCR confirmation of inducible null
Flox (699 bp)
WT (689 bp)
Null (157 bp)
Straight knockout vector
Null (138 bp)
Conditional vector
WT
time point (hr) 24 48 24 48 24 48 ---
Untreated
+4-OHT
Flox
WT
Null
1 2 3 4 5 6 7 8 9
C Western blot confirmation of inducible null
PALB2 + 4-OHT (hr)
WT 0 24 48 72 96
PALB2
Ku
1 2 3 4 5 6

Figure 2 PALB2$^{flox/-}$ CreER cells

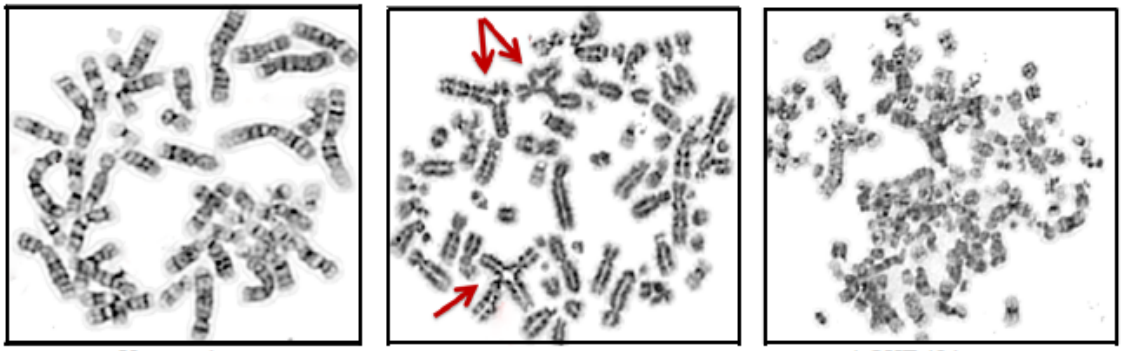

Untreated + 4-OHT 24 hours + 4-OHT 48 hours

Figure 3

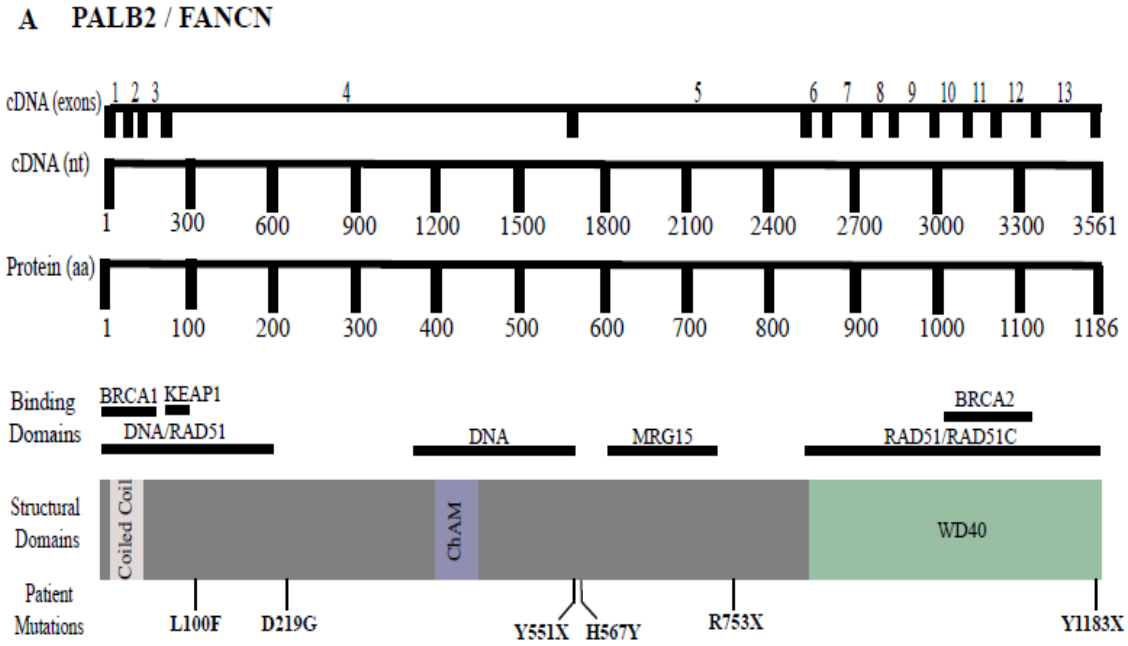
A PALB2 / FANCN
cDNA (exons)
cDNA (nt)
Protein (aa)
Binding Domains
BRCA1
KEAP1
DNA/RAD51
DNA
MRG15
BRCA2
RAD51/RAD51C
Structural Domains
Coiled Coil
ChAM
WD40
Patient Mutations
L100F
D219G
Y551X
H567Y
R753X
Y1183X

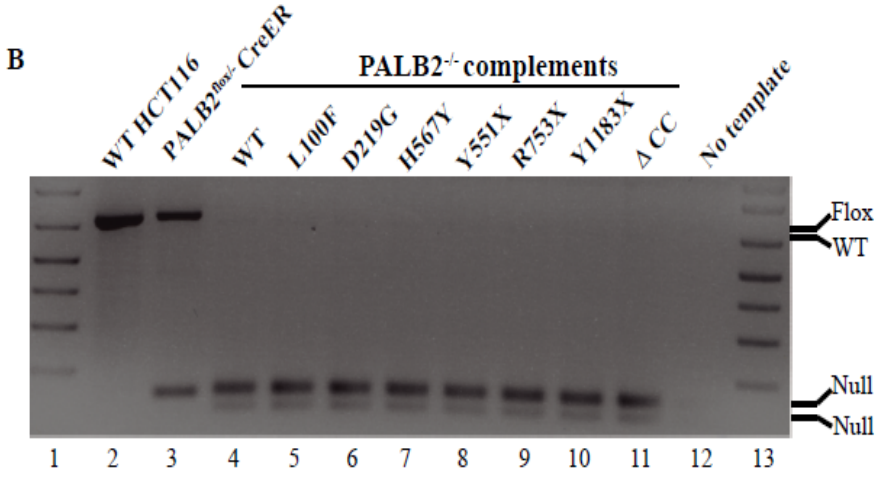
B
WT HCT116
PALB2flox/- CreER
PALB2-/- complements
WT
L100F
D219G
H567Y
Y551X
R753X
Y1183X
Δ CC
No template
Flox
WT
Null
Null
1 2 3 4 5 6 7 8 9 10 11 12 13

Figure 4

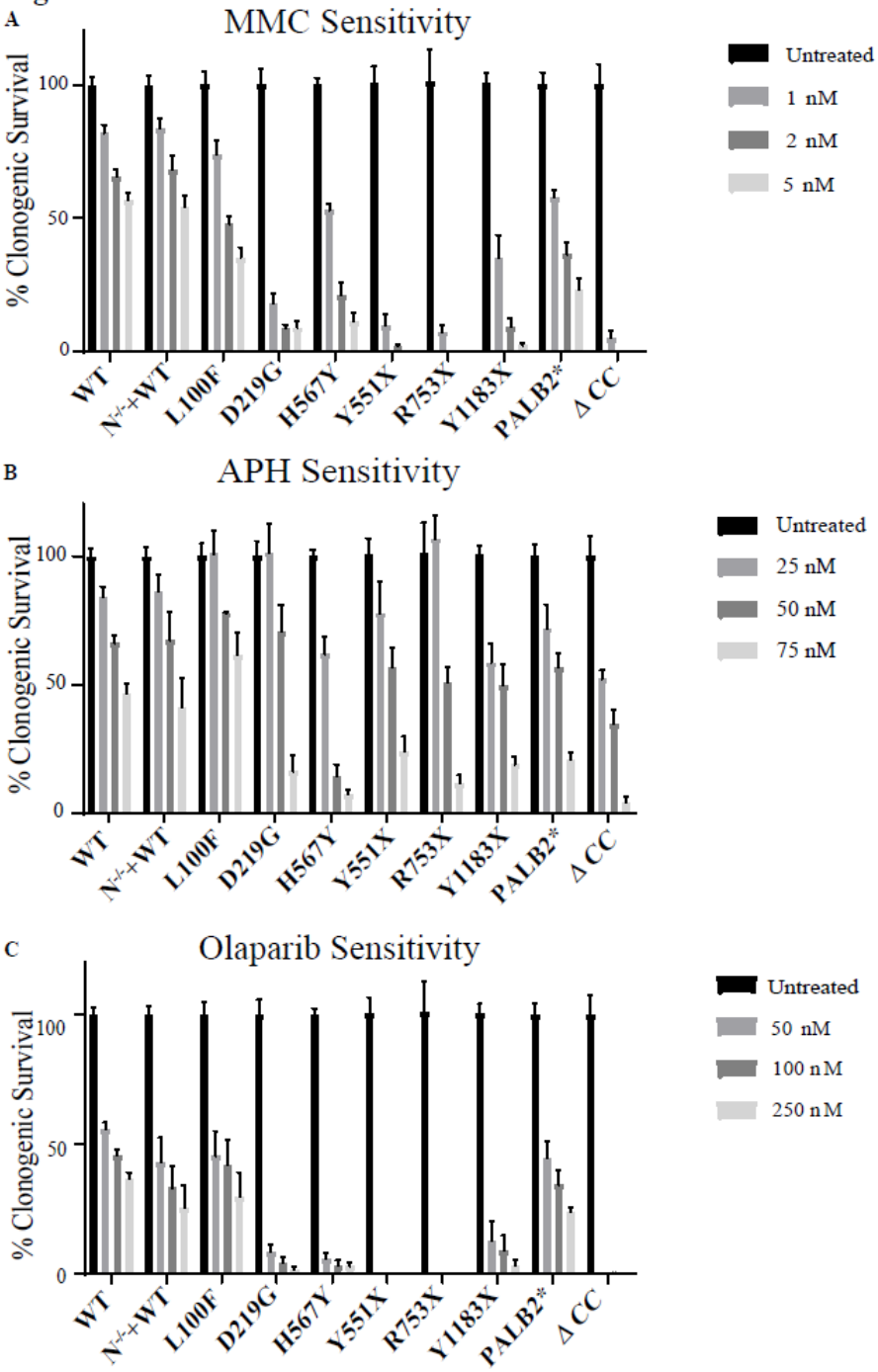
A
MMC Sensitivity
% Clonogenic Survival
100
50
0
Untreated
1 nM
2 nM
5 nM
WT
N-/-+WT
L100F
D219G
H567Y
Y551X
R753X
Y1183X
PALB2*
ΔCC
B
APH Sensitivity
% Clonogenic Survival
100
50
0
Untreated
25 nM
50 nM
75 nM
WT
N-/-+WT
L100F
D219G
H567Y
Y551X
R753X
Y1183X
PALB2*
ΔCC
C
Olaparib Sensitivity
% Clonogenic Survival
100
50
0
Untreated
50 nM
100 nM
250 nM
WT
N-/-+WT
L100F
D219G
H567Y
Y551X
R753X
Y1183X
PALB2*
ΔCC

Figure 5

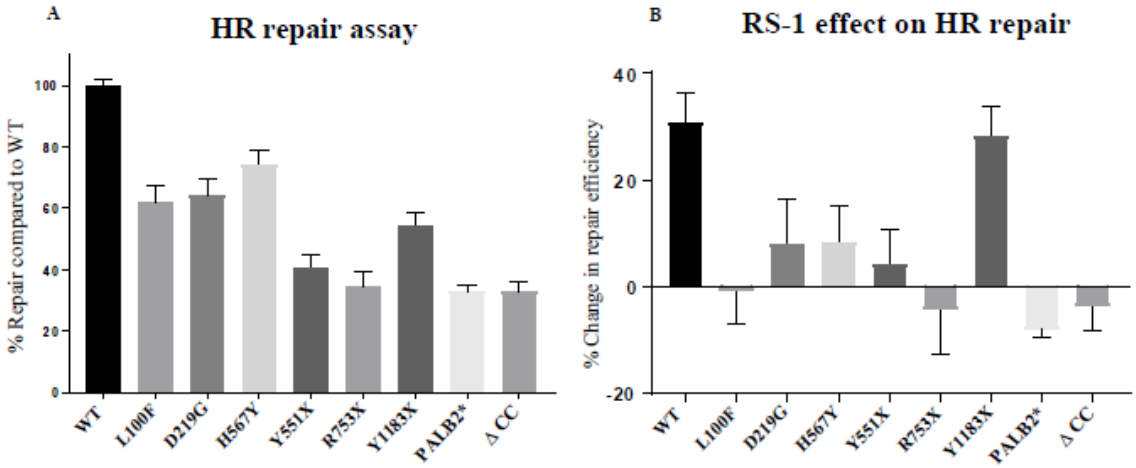
A
HR repair assay
% Repair compared to WT
100
80
60
40
20
0
WT
L100F
D219G
H567Y
Y551X
R753X
Y1183X
PALB2*
Δ CC
B
RS-1 effect on HR repair
% Change in repair efficiency
40
20
0
-20
WT
L100F
D219G
H567Y
Y551X
R753X
Y1183X
PALB2*
Δ CC

Figure 6

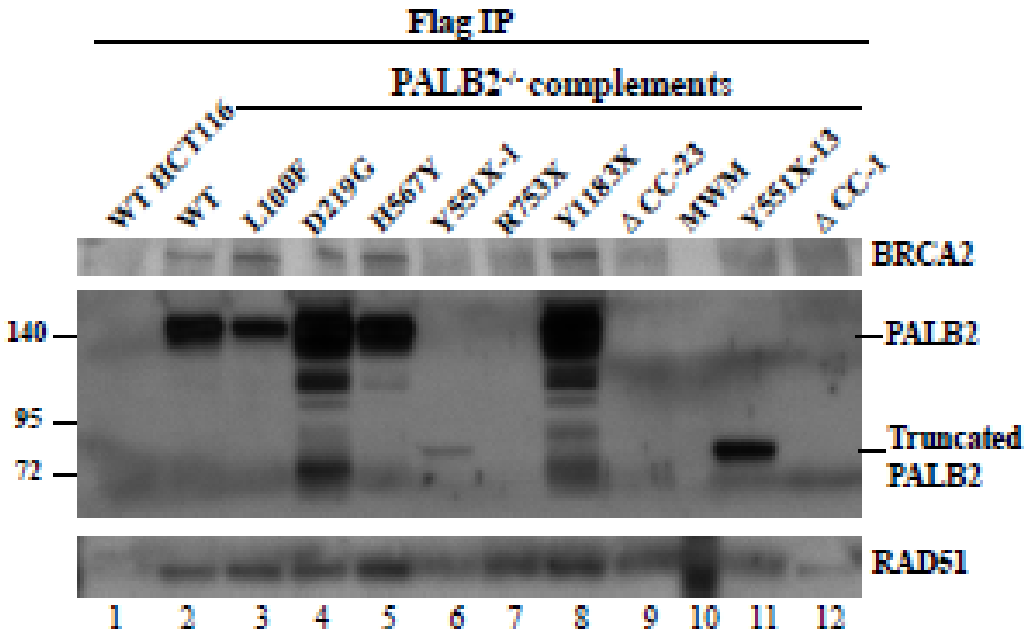
Flag IP
PALB2-/- complements
WT HCT116
WT
L1008F
D219G
H567Y
Y551X-1
R753X
Y1183X
Δ CC-23
MWM
Y551X-13
Δ CC-1
BRCA2
PALB2
Truncated PALB2
RAD51
140
95
72
1 2 3 4 5 6 7 8 9 10 11 12

Figure 7

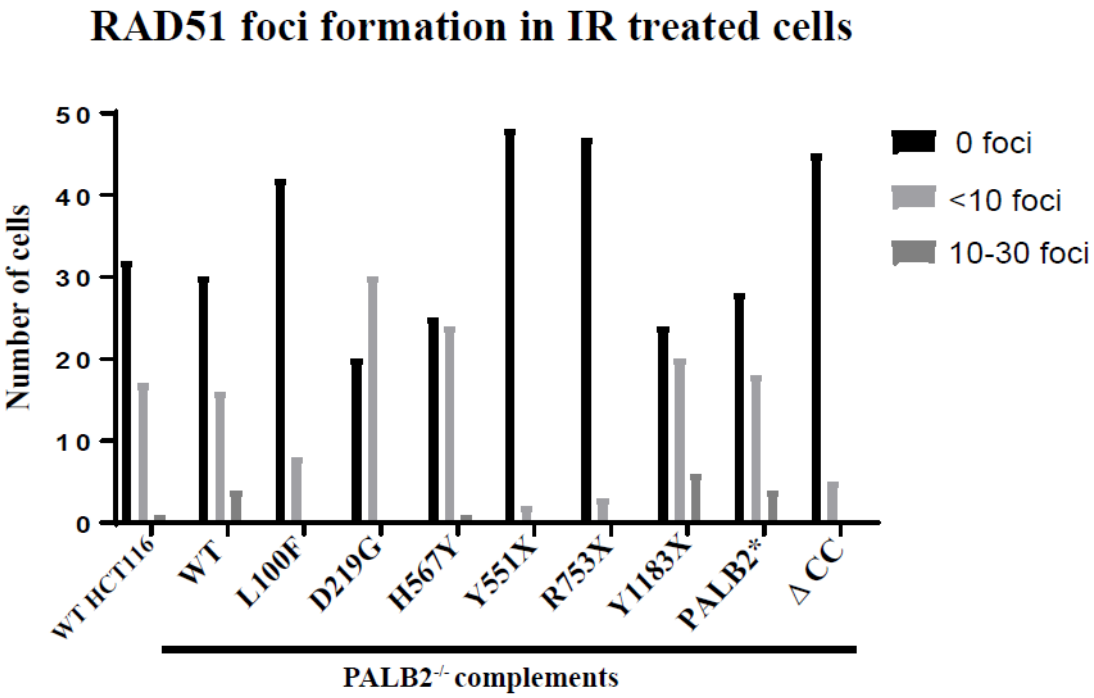

Data generated in Figure 7 by Avani Gosalia and Elizabeth Thompson

Supplementary Figure S1

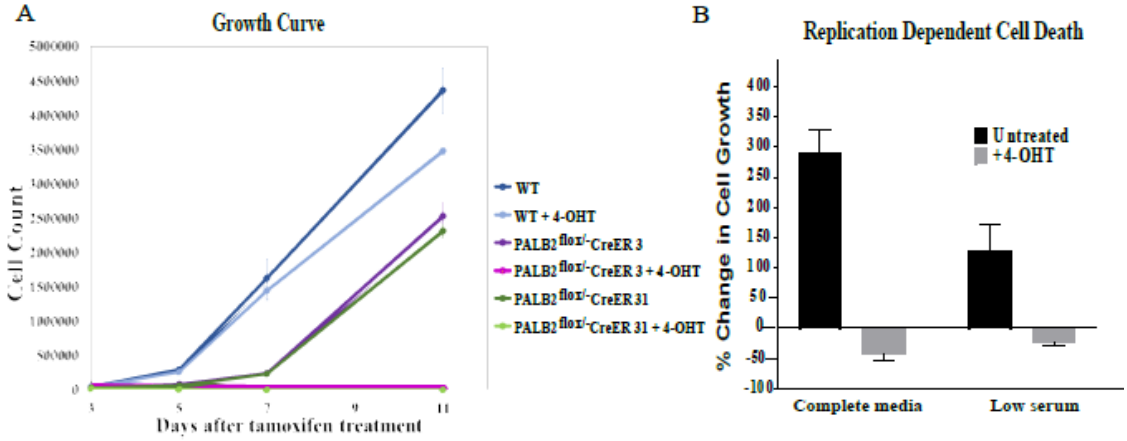

Suplementary Figure S2

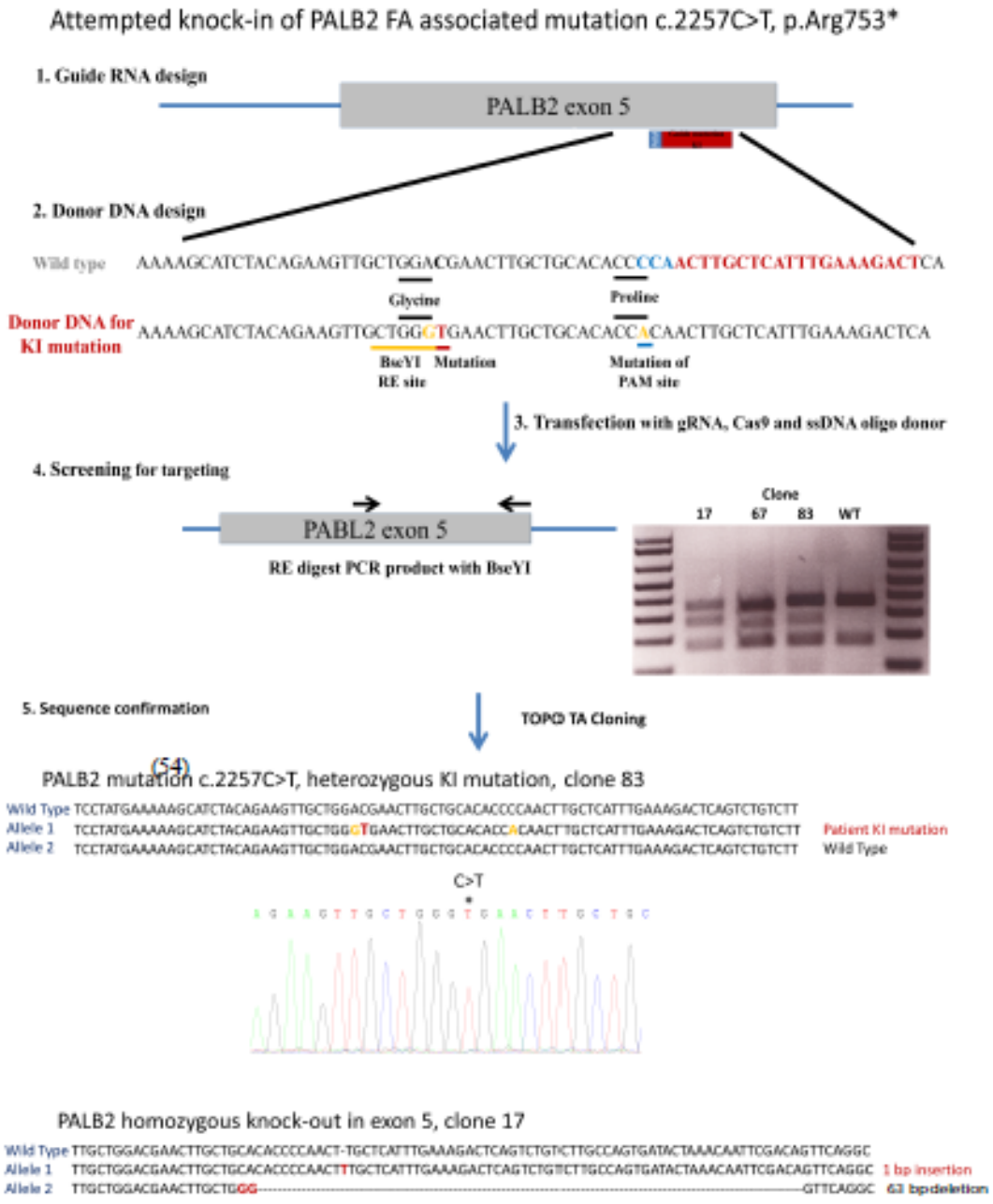

(54)

Supplementary Table S1

PALB2$^{flox/-}$

Cytogenetic scoring	Untreated	+4-OHT 24hr	+4-OHT 48hr	+4-OHT 72hr
Breaks/metaphase	0.033 (n=30)	7 (n=23)	8.3 (n=3)	2 (n=1)
Too fragmented to quantitate	0%	23%	10%	30%
Extremely fragmented	0%	0%	75%	65%
Tetraploid	0%	20%	5%	5%

PALB2$^{-/-}$+WT cDNA

Cytogenetic scoring	Untreated	+4-OHT 24hr	+4-OHT 48hr	+4-OHT 72hr
Breaks/metaphase	0 (n=30)	2.55 (n=29)	2.7 (n=30)	3.1 (n=29)
Too fragmented to quantitate	0%	3%	0%	3%
Extremely fragmented	0%	0%	0%	0%
Tetraploid	0%	6%	6%	0%

Supplementary Table S2

PALB2/FANCN conditional rAAV targeting vector construction primers

Primer	Sequence
FancN_GG_LF	GACGCTCTTCACCGGCATGTATGGAGGATGGAA
FancN_GG_LR	GACGCTCTTCTGAGCACCAAGCTCTGACCATT
FancN_GG_RF	GACGCTCTTCGGCATTGTTATGGACCAGTGCTAC
FancN_GG_IR	GACGCTCTTCGGTATGCTATACGAAGTTATGCGTCTATTGCTAGTCATTATC
FancN_GG_IF	GACGCTCTTCCTACATTATACGAAGTTATACAATCTTGGCTCACTACA
FancN_GG_RR	GACGCTCTTCCCACACACTCCCATTTCAATAACC

PALB2/FANCN knock-out rAAV targeting vector construction primers

Primer	Sequence
FancN_KO_GG_LF	GACGCTCTTCACCGGCAGGATTTCACCATGTTG
FancN_KO_GG_LR	GACGCTCTTCTGAGCACCAAGCTCTGACCATT
FancN_KO_GG_RF	GACGCTCTTCGGCAACAATCTTGGCTCACTACA
FancN_KO_GG_RR	GACGCTCTTCCCGC GGTGTTGACTACTTCTACTATC

Allele confirmation primers

Primer	Sequence
FancN_GG_LIF	ATGATAGGAACAGGTTATGC
FancN_GG_LoxR	GGAGTTGGAGGTTGTAGT

Site Directed Mutagenesis primers for flag tag PALB2/FANCN cDNA and patient mutations

Primer	Sequence
Q5_FANCN_flagtag_F	gatgatgataaaCCCGGGAAGCCCCTCAGC
Q5_FANCN_flagtag_R	atctttataatcAGGCTCGTCCATCGGGCAG

Mutation	Primer	Sequence
L100F	Q5FANCN_flagcDNA_298T_F	ATCTATCACAtTTGATGTTGGGC
	Q5FANCN_flagcDNA_298T_R	GTCTTTTCTCCAGTTTCTTC
D219G	Q5FANCN_flagcDNA_656G_F	ATTAATGAAGgCAGTGTATTAATTCC
	Q5FANCN_flagcDNA_656G_R	TTCTGTAACTGGTTCTGG
H567Y	Q5FANCN_flagcDNA_1699T_F	GAAAAGTCGTtATCAAAAAGAGGATTC
	Q5FANCN_flagcDNA_1699T_R	TTCCCTTTCACTTGAATAAATAATTTTTC
Y511X	FancN_Mut 1653F	GTCACCTCACACAAATAACAGCACGAAAAATTATTTATTCAAGTG
	FancN_Mut 1653R	CACTTGAATAAATAATTTTTCGTGCTGTTATTTGTGTGAGGTGAC
R753X	FancN_Mut2257F	GTCACCTCACACAAATAACAGCACGAAAAATTATTTATTCAAGTG
	FancN_Mut2257R	GTGCAGCAAGTTCATCCAGCAACTTCTGTAG
Y1183X	FancN_Mut3549F	GATGGAAATATATTTGTATAGCACTATTCATAAGTTAGGG
	FancN_Mut3549R	CCCTAACTTATGAATAGTGCTATACAAATATATTTCCATC
Delta cc	FancN_CoilCoildel_F2	AAGAAAACAGTAGAAGAACAAGATTGTTTG
	FancN_CoilCoildel_R2	GGGCTTCCCGGGTTTATC

PALB2/FANCN cDNA sequencing primers and Golden Gate Cloning primers (FancN_cDNA_F/R)

Primer	Sequence
FancN_cDNA_F	GGGGACAAGTTTGTACAAAAAAGCAGGCTGCCACCGCCTGCCCGATGGACGAGCCT
FancN_cDNA_R	GGGGACCACTTTGTACAAGAAAGCTGGGTCCCTAACTTATGAATAGTGGTATAC
FancN_cDNA_504R	TCTTGGGTGTCATCTGTTC
FancN_cDNA_885F	TATCAGATAGCGGTAGTAGT

Supplemental Table S3

Figure 4 P-values: Student t-test p-values of complemented PALB2$^{-/-}$ cells % clonogenic survival compared to wild type HCT116 cells
Significance determined by a p-value < 0.05.

		WT	L100F	D219G	H567Y	Y551X
MMC (nM)	1	0.708196566	0.233075894	9.37458E-09	8.22583E-05	1.36537E-09
	2	0.658772329	0.000768705	9.98806E-10	1.42819E-05	1.14808E-09
	5	0.606043028	0.001016554	7.50158E-09	1.65997E-07	2.8187E-08
APH (nM)	25	0.805679443	0.19441804	0.261601728	0.017858531	0.627962482
	50	0.929475379	0.006007037	0.697765333	3.97824E-06	0.281936764
	75	0.680121672	0.225226723	0.016640243	1.02897E-06	0.007910471
Olaparib (nM)	50	0.271573755	0.344433141	3.10832E-08	3.72694E-10	2.34258E-08
	100	0.193770472	0.727660303	7.50273E-09	1.61506E-09	8.78795E-08
	250	0.262101636	0.500414114	3.65266E-08	3.94671E-08	2.82115E-07

		R753X	Y1183X	PALB2*	Δ CC
MMC (nM)	1	6.21609E-11	0.000974043	6.18838E-05	5.25554E-12
	2	9.00034E-09	6.71009E-09	0.000269849	9.00034E-09
	5	2.8187E-08	9.20166E-09	7.66098E-05	2.8187E-08
APH (nM)	25	0.082632059	0.012893544	0.279873891	1.00715E-05
	50	0.05720131	0.105150686	0.167633834	0.000208662
	75	6.90168E-06	4.82886E-05	7.81448E-05	2.81295E-07
Olaparib (nM)	50	2.34258E-08	0.000794986	0.147631206	2.34258E-08
	100	8.78795E-08	0.000351662	0.104309126	8.08041E-08
	250	2.82115E-07	5.10853E-08	0.000899993	2.82115E-07

Figure 5A P-values: Student t-test p-values of mutant cell line % HR vs the specified cell line.
Significance determined by a p-value < 0.05.

Cell line	vs. PABL2$^{-/-}$+WT	vs. Y551X	vs. R753X	vs. PALB2*	vs. ΔCC
L100F	7.66E-06	0.00602262	0.001282	0.000163	4.3225E-05
D219G	7.74E-06	0.00206898	0.000456	4.07E-05	1.03905E-05
H567Y	8.85E-05	1.6193E-05	5.95E-06	1.64E-07	4.29638E-08
Y551X	4.69E-10	1	0.315541	0.095157	0.021162685
R753X	3.57E-09	0.31554095	1	0.775961	0.33788409
Y1183X	6.77E-10	0.01986022	0.003936	6.33E-05	1.2605E-05
PABL2*	5.53E-21	0.09515671	0.775961	1	0.284624511
ΔCC	1.73E-16	0.02116268	0.337884	0.284625	1

Figure 5A P-values: Student t-test p-values of change in % HR with RS-1 treatment for PABL2$^{-/-}$ + WT cDNA vs the specified cell line. Significance determined by a p-value < 0.05.

CHAPTER 4

DISCUSSION AND FUTURE DIRECTIONS

DISCUSSION

Fanconi anemia is a challenging disease to treat due to the heterogeneity in severity and symptoms of the individual patients. In addition, the DNA repair defect in FA is a double edge sword, resulting in cancer predisposition, but also making them intolerant to the typical cancer treatments of chemotherapy and radiation. Through my PhD work, I have created five isogenic knockout cell lines in FA proteins representing the 3 different groups of the FA pathway in order to study the different cellular phenotypes. My overall goal was to gain mechanistic insight at the cellular level that could lead to a better understanding of the disease heterogeneity and potentially improved treatment options for FA.

FANCD2 and FANCI in the replication stress response

The monoubiquitination of FANCD2 is a key functional step in the FA pathway in ICL repair, and is dependent on the presence of FANCI(145,166). In addition, FANCD2 and FANCI co-localize together at the sites of DNA damage (145,166). Therefore, the concept of FANCD2 and FANCI having separate function from the ID2 complex and without monoubiquitination was, and still is paradigm changing. Some of the initial evidence for this came from the Sobeck laboratory utilizing *Xenopus* extracts revealing that FANCD2 had functions independent of FANCI in stalled replication fork restart and in interaction with BLM, a HJ resolvase (69,151). Therefore, we created the FANCD2, FANCI, and FANCI/FANCD2 double knockout isogenic cell lines for the investigation of FANCD2 and FANCI in the replication stress response to further clarify any separation of function.

Important to establishing these null cell lines as cellular models for FA disease, we needed to establish they were consistent with FA patient cell lines and previous studies. Consistent with previous reports, we found that FANCD2 and FANCI were co-dependent for monoubiquitination and ICL repair, and partially dependent for protein stability, nuclear import and chromatin localization (87,145,236). We confirmed previous work in the Sobeck laboratory, that non-monoubiquitination FANCD2 could be recruited to chromatin and aid in stalled replication fork restart and new origin firing, independently of FANCI (69,150).

We made several novel contributions, including the establishment of the isogenic FANCD2, FANCI and FANCI/FANCD2 double knockout cell lines, since to our knowledge there had been no previous reports of such cell lines. Our novel findings also include that the $D2^{-/-}$, $I^{-/-}$ and the ID2 double knockout cell lines are viable, therefore neither FANCD2 nor FANCI is essential for viability. However, both FANCI and FANCD2 contribute to cell proliferation. In addition, we found that FANCD2 has a more vital role in HDR than FANCI, and FANCD2 is involved in RAD51 filament formation and/or stabilization to promote HDR. Furthermore, we found that FANCD2 deficient cells were highly sensitive to low dose replication stress, and surprisingly, FANCI deficient and FANCI/FANCD2 double deficient cells were not. The sensitivity of the FANCD2 deficient cells to replication stress was not due to increased DNA damage, reduced recruitment of HDR repair factors, or activation of DDT pathway. Instead, we found evidence that FANCD2 may negatively regulate FANCI-mediated cell death

following replication stress. Altogether deducing important functional differences between FANCI and FANCD2 and how they regulate each other in alternative functions.

PALB2/FANCN is an essential gene and patient mutations are hypomorphic

PALB2/FANCN is an important tumor suppressor and is associated with both FA and breast cancer susceptibility. It has been implicated as a molecular scaffold for HDR that coordinates the function of multiple proteins including BRCA1, BRCA2, and RAD51 (129,130). Taking into consideration that FA-N subtype patients with PALB2 mutations often have residual or truncated protein expression (197,225), and the attempted mouse *PALB2* knockout was embryonic lethal (224), led us to hypothesis that *PALB2* was an essential gene. Therefore, we generated a novel PALB2 conditional null cell line, and incorporated an inducible Cre recombinase systems, CreER. With the addition of tamoxifen, the CreER system induces the removal of the conditional allele, resulting in a PALB2 null cell line. Using this inducible PALB2 null cell line, we confirmed that loss of *PALB2* results in replication dependent chromosomal catastrophe. Unequivocally, demonstrating that *PALB2* is an essential gene for genomic stability. This conditional PALB2 null cell line allowed us to investigate the function of PALB2 mutations through complementation with mutated *PABL2* cDNAs and subsequent removal of the floxed allele with tamoxifen. Three truncating FA-N subtype (PALB2) patient mutations were capable of rescuing cell viability and confirmed that these truncated PALB2 proteins were in fact hypomorphic. Two of the FA-N mutations completely removed the C-terminal WD40 domain and the other was predicted to destabilize this WD40 motif (128,138,197). Therefore, complementation by these three FA-N patient mutations

demonstrated that the C-terminal WD40 domain, which is the BRCA2, RAD51, RAD51C, and POLη binding domain(128,196), is not essential for viability. We then hypothesized that it was potentially the N-terminal coiled-coil domain, which is the BRCA1 binding and PALB2 homo-oligomerization domain (132,208) that may be performing the essential function for viability. Therefore, we tested if PALB2 with deletion of the coiled-coil domain could complement the PALB2 null cell line. Surprisingly, this Δ coiled-coil PALB2 mutant was also able to complement viability, therefore the N-terminal coiled-coil domain and BRCA1 binding domain is not essential for viability either. Finally, we complemented the PALB2 null cell line with three PALB2 SNP mutations identified in breast cancer patients through a next generation sequencing study(139). These 3 SNPs all result in single amino acid substitutions with unknown pathogenicity, and were classified as variants of unknown significance (VUSs). All three of the breast cancer associated SNPs complemented viability of the PALB2 null cell line as well. In conclusion, neither the WD40 nor the coiled-coil domain are essential for viability indicating that the ability to form the BRCA1:PALB2:BRCA2 complex is not the essential function of PALB2 for cellular viability.

We further characterized the patient mutations and determined that the WD40 and coiled-coil domain are essential for resistance to ICLs, replication stress and PARP1 inhibition. In addition, the WD40 and coiled-coil domains are essential for BRCA2 binding, RAD51 localization, and efficient HDR. Interestingly, all three of the breast cancer associated SNPs were also defective in HDR, despite the ability to bind BRCA2 and form RAD51 foci. Furthermore, two of the breast cancer associated SNPs were equally sensitive to ICLs, replication stress and PARP1 inhibition as the truncating and pathogenic FA-N

associated mutations. Thus, indicating that two of the VUSs (D219G and H567Y) are potentially pathogenic, which are the same two VUSs that were assessed as high risk based on family history (139).

In summary, the WD40 and coiled-coil domains are required for resistance to ICLs, replication stress, and PARP1 inhibition, and for efficient HDR, but not for cellular viability. Furthermore, we have developed a novel cellular system for determining the mechanistic function of PALB2, functionally evaluating PABL2 mutations and characterizing potential pathogenicity.

FUTURE DIRECTIONS

The generation of these isogenic cell lines from the three different protein groups of the FA pathway provide an opportunity to study the pathway in more holistic approach. All of the cell lines are sensitive to ICL inducing agent, MMC, however, these cell lines have varied sensitivity to replication stress. The ability to investigate the different responses of the FA cell lines to different cellular stresses could lead to better insight into disease heterogeneity and possibly to improved or personalized treatment based on the gene mutations. The following outlined projects have already been started with my collection of isogenic FA cell lines.

Fanconi anemia proteins in replication stress

In chapter 2, we investigated the separation of function for FANCD2 and FANCI proteins in replication stress and found that FANCD2 null cells are highly sensitive to low levels

of replication stress, but FANCI null cells were not (Chapter 2, Figure 5 A, B). Furthermore, when the FANCD2/FANCI DKO was made, it took on the FANCI null phenotype of not being sensitive to low level replication stress. We chased down several possible explanations for this observation, such as increased DNA damage, recruitment of HDR factors and activation of DNA damage tolerance pathway, however none of these were any different in any of the knockout cell lines. We did find an elevated phopho-p53 and p21 expression in the FANCD2 deficient cells which seemingly indicates that in the absence of FANCD2, FANCI is inducing apoptotic cell death in response to low level replication stress. Also, this would explain why the FANCD2/FANCI DKO took on the FANCI null phenotype for survival, because FANCI was not present to induce the apoptotic response. A recent study has also implicated FANCI as a negative regulator of AKT, and when FANCI was depleted, resulted in reduced apoptosis (237). Therefore, I am using RNAseq to further clarify the different responses between FANCD2 and FANCI deficient cells to replication stress. WT, $D2^{-/-}$, $I^{-/-}$ and ID2 DKO cells (two independent clones of each cell line) were either untreated or treated for 24 hours with 100 nM APH. This treatment and time frame is sufficient for an observable cell cycle alteration in response to the APH (data not shown). RNA was isolated and prepared for RNAseq analysis. Sequencing of the samples has just been completed and analysis is pending. We expect this investigation to help clarify the different replication stress responses of these cell lines.

However, in addition to FANCI and FANCD2, there are differences in other FA proteins in sensitivity or resistance to low level replication stress. In Chapter 3 we demonstrate that FANCN mutations are also sensitive to APH induced replication stress (Chapter 3,

Figure 4B). In addition, my preliminary data with the FANCA null cell line indicates that it is not sensitive to low level APH-induced replication stress (data not shown). Inferring that FANCD2 and FANCN may have active roles in the replication stress response and FANCI and FANCA may not. Therefore, FANCA null (two clones) and FANCN (PALB2*, Y1183X, and R753X) were treated with and without 100 nM APH for 24 hours, and prepared for RNAseq analysis. Sequencing of the samples has just been complete and analysis is pending.

We are collaborating with Dr. Filip Zelezny at the Czech Technical University in Prague for bioinformatic analysis. We expect that comparison of this RNAseq analysis of the different FA pathway proteins (FANCA, FANCI, FANCD2, and FANCN) in replication stress response will reveal mechanistic insight into their differing responses and possibly lead to potential drug targets to investigate for FA patients.

PALB2 VUS screen

Next generation sequencing is becoming more common for breast cancer susceptibility genes (125,139). While the discovery of a pathogenic mutation is informative for a patient and can help guide preventative or cancer treatments, the diagnosis of a VUS is not beneficial. Therefore, we have been developing a large-scale screen of VUS mutation for breast cancer using the PALB2 conditional null cell line to determining the function of PALB2 VUS mutations and define potential pathogenicity.

Creation of PALB2 variant cDNA Library: We selected over 90 different PALB2 variants including the following: VUS mutations identified in breast cancer patients(139), known pathogenic mutations associated with either breast cancer or FA-N subtype, and

general population SNPs. Next, we used site directed mutagenesis to incorporate the mutations into the PALB2 cDNA. In collaboration with the Chad Myers laboratory at the University of Minnesota, we have designed DNA barcoded primers and we are currently in the process of barcode labeling each of the individual patient mutation containing cDNAs. After the cDNAs are barcoded, they will be cloned into a FLP-in system expression vector to create an expression library of barcoded cDNAs.

Creating the FLP-In PALB2$^{flox/-;CreER}$ cell line: We have also been working to incorporate the FLP-In System (Invitrogen), FRT site into the PALB2$^{flox/-;CreER}$ cell line. The FLP-in system works by using the FLP recombinase to site specifically integrate the expression vector, containing the PALB2 cDNAs into the genome through a FRT site. We are currently using CRISPR/Cas9 to site specifically integrate the FRT site into the AAVS1, safe harbor locus, in the PALB2$^{flox/-;CreER}$ cell line.

Screening PALB2 mutations: We will then transfect the barcoded PALB2 cDNA expression library along with a Flp recombinase expression plasmid into the FLP-In PALB2$^{flox/-;CreER}$ cell line and select for cDNA integration with hygromycin. Subsequently, the conditional PALB2 allele will be removed with tamoxifen, however an untreated population (no tamoxifen) will be collected to determine baseline of incorporated cDNAs. The tamoxifen treated transfected population will then be divided into 4 treatment populations including the following: untreated, MMC treatment (ICL inducing agent), APH treatment (replication stress), and olaparib treatment (PARP1 inhibitor). After treatment, cells from each treatment group and baseline will be PCR amplified over the cDNA barcoded region with indexing primers to identify the treatment groups and baseline. These samples will then be sequence for identification of the

PALB2 barcoded cDNA. Proportions of barcoded cDNAs for each variant can be compared to the baseline transfected population for each treatment condition to determine viability with drug treatment. Risk stratification can be accomplished by the shear number of individual cells that can be screened by sequencing.

We expect this variant screen to identify and provide evidence of potential pathogenic mutations within the VUS population.

PALB2 post-translational modifications for improved gene targeting

Two recent studies have implicated PALB2 post-translational modification as having a strong influence in the efficiency of HDR and its cell cycle control. In the first study, Buisson *et al.* found that the ATR promotes HR through PALB2 by facilitating a S59-S64 phosphorylation switch on PALB2 (238). The phosphorylation of PALB2 S59 by ATR promoted the PALB2:BRCA1 interaction and PALB2 localization, and the hypo-phosphorylation of PALB2 S64, a CDK phosphorylation site, also promoted this interaction. Therefore, the PALB2 S59E/S64A mutant increased HR efficiency over WT PALB2. In the second study, Orthwein *et al.* found that PALB2 N-terminal lysines (K20, K25, and K30) are critical for cell cycle regulation of the BRCA1:PALB2 interaction (211). Ubiquitination of these critical lysines by the E3 ubiquin ligase composed of KEAP1 is sufficient for preventing the BRCA1:PALB2 interaction in G1 phase of the cell cycle. They also found that they could increase HDR in G1 cells by deleting the KEAP1 binding motif (ETGE) in the PALB2 N-terminus or by mutating the N-terminal lysines (K20R, K25R, and K30R). Therefore, based on these two studies, site directed mutagenesis on the PALB2 cDNA was used to create the following mutations: PALB2

S59E/S64A, PALB2 K20R, PALB2 K25R, PALB2 K30R, PALB2 K20/25/30R, PALB2 ΔETGE. All of the PALB2 mutations listed were able to complement the PALB2 null cell line, and therefore rescued viability. Further experiments are pending to investigate the effect of these mutations on gene targeting frequency and their ability to influence gene targeting in G1 cells.

BIBLIOGRAPHY

1. Lobitz, S. and Velleuer, E. (2006) Guido Fanconi (1892-1979): a jack of all trades. *Nat Rev Cancer*, **6**, 893-898.
2. Mamrak, N.E., Shimamura, A. and Howlett, N.G. (2017) Recent discoveries in the molecular pathogenesis of the inherited bone marrow failure syndrome Fanconi anemia. *Blood Rev*, **31**, 93-99.
3. Wang, A.T., Kim, T., Wagner, J.E., Conti, B.A., Lach, F.P., Huang, A.L., Molina, H., Sanborn, E.M., Zierhut, H., Cornes, B.K. *et al.* (2015) A Dominant Mutation in Human RAD51 Reveals Its Function in DNA Interstrand Crosslink Repair Independent of Homologous Recombination. *Mol Cell*, **59**, 478-490.
4. Knies, K., Inano, S., Ramírez, M.J., Ishiai, M., Surrallés, J., Takata, M. and Schindler, D. (2017) Biallelic mutations in the ubiquitin ligase RFWD3 cause Fanconi anemia. *J Clin Invest*, **127**, 3013-3027.
5. Ceccaldi, R., Sarangi, P. and D'Andrea, A.D. (2016) The Fanconi anaemia pathway: new players and new functions. *Nat Rev Mol Cell Biol*, **17**, 337-349.
6. Cheung, R.S. and Taniguchi, T. (2017) Recent insights into the molecular basis of Fanconi anemia: genes, modifiers, and drivers. *Int J Hematol*.
7. Sawyer, S.L., Tian, L., Kähkönen, M., Schwartzentruber, J., Kircher, M., Majewski, J., Dyment, D.A., Innes, A.M., Boycott, K.M., Moreau, L.A. *et al.* (2015) Biallelic mutations in BRCA1 cause a new Fanconi anemia subtype. *Cancer Discov*, **5**, 135-142.
8. Bluteau, D., Masliah-Planchon, J., Clairmont, C., Rousseau, A., Ceccaldi, R., Dubois d'Enghien, C., Bluteau, O., Cuccuini, W., Gachet, S., Peffault de Latour, R. *et al.* (2016) Biallelic inactivation of REV7 is associated with Fanconi anemia. *J Clin Invest*, **126**, 3580-3584.
9. Ameziane, N., May, P., Haitjema, A., van de Vrugt, H.J., van Rossum-Fikkert, S.E., Ristic, D., Williams, G.J., Balk, J., Rockx, D., Li, H. *et al.* (2015) A novel Fanconi anaemia subtype associated with a dominant-negative mutation in RAD51. *Nat Commun*, **6**, 8829.
10. Park, J.Y., Virts, E.L., Jankowska, A., Wiek, C., Othman, M., Chakraborty, S.C., Vance, G.H., Alkuraya, F.S., Hanenberg, H. and Andreassen, P.R. (2016) Complementation of hypersensitivity to DNA interstrand crosslinking agents demonstrates that XRCC2 is a Fanconi anaemia gene. *J Med Genet*, **53**, 672-680.
11. Rickman, K.A., Lach, F.P., Abhyankar, A., Donovan, F.X., Sanborn, E.M., Kennedy, J.A., Sougnez, C., Gabriel, S.B., Elemento, O., Chandrasekharappa, S.C. *et al.* (2015) Deficiency of UBE2T, the E2 Ubiquitin Ligase Necessary for FANCD2 and FANCI Ubiquitination, Causes FA-T Subtype of Fanconi Anemia. *Cell Rep*, **12**, 35-41.
12. Neveling, K., Endt, D., Hoehn, H. and Schindler, D. (2009) Genotype-phenotype correlations in Fanconi anemia. *Mutat Res*, **668**, 73-91.
13. Kee, Y. and D'Andrea, A.D. (2012) Molecular pathogenesis and clinical management of Fanconi anemia. *J Clin Invest*, **122**, 3799-3806.
14. Arber, D.A., Orazi, A., Hasserjian, R., Thiele, J., Borowitz, M.J., Le Beau, M.M., Bloomfield, C.D., Cazzola, M. and Vardiman, J.W. (2016) The 2016 revision to

the World Health Organization classification of myeloid neoplasms and acute leukemia. *Blood*, **127**, 2391-2405.
15. Kutler, D.I., Auerbach, A.D., Satagopan, J., Giampietro, P.F., Batish, S.D., Huvos, A.G., Goberdhan, A., Shah, J.P. and Singh, B. (2003) High incidence of head and neck squamous cell carcinoma in patients with Fanconi anemia. *Arch Otolaryngol Head Neck Surg*, **129**, 106-112.
16. Giampietro, P.F., Adler-Brecher, B., Verlander, P.C., Pavlakis, S.G., Davis, J.G. and Auerbach, A.D. (1993) The need for more accurate and timely diagnosis in Fanconi anemia: a report from the International Fanconi Anemia Registry. *Pediatrics*, **91**, 1116-1120.
17. Soulier, J. (2011) Fanconi anemia. *Hematology Am Soc Hematol Educ Program*, **2011**, 492-497.
18. Clauson, C., Schärer, O.D. and Niedernhofer, L. (2013) Advances in understanding the complex mechanisms of DNA interstrand cross-link repair. *Cold Spring Harb Perspect Biol*, **5**, a012732.
19. Auerbach, A.D. (2015) Diagnosis of Fanconi anemia by diepoxybutane analysis. *Curr Protoc Hum Genet*, **85**, 8.7.1-17.
20. Gregory, J.J., Wagner, J.E., Verlander, P.C., Levran, O., Batish, S.D., Eide, C.R., Steffenhagen, A., Hirsch, B. and Auerbach, A.D. (2001) Somatic mosaicism in Fanconi anemia: evidence of genotypic reversion in lymphohematopoietic stem cells. *Proc Natl Acad Sci U S A*, **98**, 2532-2537.
21. Gross, M., Hanenberg, H., Lobitz, S., Friedl, R., Herterich, S., Dietrich, R., Gruhn, B., Schindler, D. and Hoehn, H. (2002) Reverse mosaicism in Fanconi anemia: natural gene therapy via molecular self-correction. *Cytogenet Genome Res*, **98**, 126-135.
22. Lo Ten Foe, J.R., Kwee, M.L., Rooimans, M.A., Oostra, A.B., Veerman, A.J., van Weel, M., Pauli, R.M., Shahidi, N.T., Dokal, I., Roberts, I. *et al.* (1997) Somatic mosaicism in Fanconi anemia: molecular basis and clinical significance. *Eur J Hum Genet*, **5**, 137-148.
23. Soulier, J., Leblanc, T., Larghero, J., Dastot, H., Shimamura, A., Guardiola, P., Esperou, H., Ferry, C., Jubert, C., Feugeas, J.P. *et al.* (2005) Detection of somatic mosaicism and classification of Fanconi anemia patients by analysis of the FA/BRCA pathway. *Blood*, **105**, 1329-1336.
24. Waisfisz, Q., Morgan, N.V., Savino, M., de Winter, J.P., van Berkel, C.G., Hoatlin, M.E., Ianzano, L., Gibson, R.A., Arwert, F., Savoia, A. *et al.* (1999) Spontaneous functional correction of homozygous fanconi anaemia alleles reveals novel mechanistic basis for reverse mosaicism. *Nat Genet*, **22**, 379-383.
25. Mankad, A., Taniguchi, T., Cox, B., Akkari, Y., Rathbun, R.K., Lucas, L., Bagby, G., Olson, S., D'Andrea, A. and Grompe, M. (2006) Natural gene therapy in monozygotic twins with Fanconi anemia. *Blood*, **107**, 3084-3090.
26. Dufour, C. (2017) How I manage patients with Fanconi anaemia. *Br J Haematol*, **178**, 32-47.
27. Guohui, S., Lijiao, Z. and Rugang, Z. (2015) The Induction and Repair of DNA Interstrand Crosslinks and Implications in Cancer Chemotherapy. *Anticancer Agents Med Chem*, **16**, 221-246.

28. Admiraal, S.J. and O'Brien, P.J. (2015) Base excision repair enzymes protect abasic sites in duplex DNA from interstrand cross-links. *Biochemistry*, **54**, 1849-1857.
29. Dutta, S., Chowdhury, G. and Gates, K.S. (2007) Interstrand cross-links generated by abasic sites in duplex DNA. *J Am Chem Soc*, **129**, 1852-1853.
30. Price, N.E., Johnson, K.M., Wang, J., Fekry, M.I., Wang, Y. and Gates, K.S. (2014) Interstrand DNA-DNA cross-link formation between adenine residues and abasic sites in duplex DNA. *J Am Chem Soc*, **136**, 3483-3490.
31. Kottemann, M.C. and Smogorzewska, A. (2013) Fanconi anaemia and the repair of Watson and Crick DNA crosslinks. *Nature*, **493**, 356-363.
32. Zhang, J., Dewar, J.M., Budzowska, M., Motnenko, A., Cohn, M.A. and Walter, J.C. (2015) DNA interstrand cross-link repair requires replication-fork convergence. *Nat Struct Mol Biol*, **22**, 242-247.
33. Räschle, M., Knipscheer, P., Knipsheer, P., Enoiu, M., Angelov, T., Sun, J., Griffith, J.D., Ellenberger, T.E., Schärer, O.D. and Walter, J.C. (2008) Mechanism of replication-coupled DNA interstrand crosslink repair. *Cell*, **134**, 969-980.
34. Schwab, R.A., Blackford, A.N. and Niedzwiedz, W. (2010) ATR activation and replication fork restart are defective in FANCM-deficient cells. *EMBO J*, **29**, 806-818.
35. Singh, T.R., Ali, A.M., Paramasivam, M., Pradhan, A., Wahengbam, K., Seidman, M.M. and Meetei, A.R. (2013) ATR-dependent phosphorylation of FANCM at serine 1045 is essential for FANCM functions. *Cancer Res*, **73**, 4300-4310.
36. Hira, A., Yoshida, K., Sato, K., Okuno, Y., Shiraishi, Y., Chiba, K., Tanaka, H., Miyano, S., Shimamoto, A., Tahara, H. *et al.* (2015) Mutations in the gene encoding the E2 conjugating enzyme UBE2T cause Fanconi anemia. *Am J Hum Genet*, **96**, 1001-1007.
37. Longerich, S., Kwon, Y., Tsai, M.S., Hlaing, A.S., Kupfer, G.M. and Sung, P. (2014) Regulation of FANCD2 and FANCI monoubiquitination by their interaction and by DNA. *Nucleic Acids Res*, **42**, 5657-5670.
38. Boisvert, R.A. and Howlett, N.G. (2014) The Fanconi anemia ID2 complex: dueling saxes at the crossroads. *Cell Cycle*, **13**, 2999-3015.
39. Joo, W., Xu, G., Persky, N.S., Smogorzewska, A., Rudge, D.G., Buzovetsky, O., Elledge, S.J. and Pavletich, N.P. (2011) Structure of the FANCI-FANCD2 complex: insights into the Fanconi anemia DNA repair pathway. *Science*, **333**, 312-316.
40. Ishiai, M., Sato, K., Tomida, J., Kitao, H., Kurumizaka, H. and Takata, M. (2017) Activation of the FA pathway mediated by phosphorylation and ubiquitination. *Mutat Res*.
41. Klein Douwel, D., Boonen, R.A., Long, D.T., Szypowska, A.A., Räschle, M., Walter, J.C. and Knipscheer, P. (2014) XPF-ERCC1 acts in Unhooking DNA interstrand crosslinks in cooperation with FANCD2 and FANCP/SLX4. *Mol Cell*, **54**, 460-471.

42. Yeo, J.E., Lee, E.H., Hendrickson, E.A. and Sobeck, A. (2014) CtIP mediates replication fork recovery in a FANCD2-regulated manner. *Hum Mol Genet*, **23**, 3695-3705.
43. Stoepker, C., Hain, K., Schuster, B., Hilhorst-Hofstee, Y., Rooimans, M.A., Steltenpool, J., Oostra, A.B., Eirich, K., Korthof, E.T., Nieuwint, A.W. *et al.* (2011) SLX4, a coordinator of structure-specific endonucleases, is mutated in a new Fanconi anemia subtype. *Nat Genet*, **43**, 138-141.
44. Yamamoto, K.N., Kobayashi, S., Tsuda, M., Kurumizaka, H., Takata, M., Kono, K., Jiricny, J., Takeda, S. and Hirota, K. (2011) Involvement of SLX4 in interstrand cross-link repair is regulated by the Fanconi anemia pathway. *Proc Natl Acad Sci U S A*, **108**, 6492-6496.
45. Kim, Y., Lach, F.P., Desetty, R., Hanenberg, H., Auerbach, A.D. and Smogorzewska, A. (2011) Mutations of the SLX4 gene in Fanconi anemia. *Nat Genet*, **43**, 142-146.
46. Bhagwat, N., Olsen, A.L., Wang, A.T., Hanada, K., Stuckert, P., Kanaar, R., D'Andrea, A., Niedernhofer, L.J. and McHugh, P.J. (2009) XPF-ERCC1 participates in the Fanconi anemia pathway of cross-link repair. *Mol Cell Biol*, **29**, 6427-6437.
47. Hashimoto, K., Wada, K., Matsumoto, K. and Moriya, M. (2015) Physical interaction between SLX4 (FANCP) and XPF (FANCQ) proteins and biological consequences of interaction-defective missense mutations. *DNA Repair (Amst)*, **35**, 48-54.
48. Bluteau, D., Masliah-Planchon, J., Clairmont, C., Rousseau, A., Ceccaldi, R., d'Enghien, C.D., Bluteau, O., Cuccuini, W., Gachet, S., de Latour, R.P. *et al.* (2017) Biallelic inactivation of REV7 is associated with Fanconi anemia. *J Clin Invest*, **127**, 1117.
49. Tomida, J., Takata, K., Lange, S.S., Schibler, A.C., Yousefzadeh, M.J., Bhetawal, S., Dent, S.Y. and Wood, R.D. (2015) REV7 is essential for DNA damage tolerance via two REV3L binding sites in mammalian DNA polymerase ζ. *Nucleic Acids Res*, **43**, 1000-1011.
50. Michl, J., Zimmer, J. and Tarsounas, M. (2016) Interplay between Fanconi anemia and homologous recombination pathways in genome integrity. *EMBO J*, **35**, 909-923.
51. Inano, S., Sato, K., Katsuki, Y., Kobayashi, W., Tanaka, H., Nakajima, K., Nakada, S., Miyoshi, H., Knies, K., Takaori-Kondo, A. *et al.* (2017) RFWD3-Mediated Ubiquitination Promotes Timely Removal of Both RPA and RAD51 from DNA Damage Sites to Facilitate Homologous Recombination. *Mol Cell*, **66**, 622-634.e628.
52. Kim, J.M., Parmar, K., Huang, M., Weinstock, D.M., Ruit, C.A., Kutok, J.L. and D'Andrea, A.D. (2009) Inactivation of murine Usp1 results in genomic instability and a Fanconi anemia phenotype. *Dev Cell*, **16**, 314-320.
53. Oestergaard, V.H., Langevin, F., Kuiken, H.J., Pace, P., Niedzwiedz, W., Simpson, L.J., Ohzeki, M., Takata, M., Sale, J.E. and Patel, K.J. (2007) Deubiquitination of FANCD2 is required for DNA crosslink repair. *Mol Cell*, **28**, 798-809.

54. Chang, E.Y. and Stirling, P.C. (2017) Replication Fork Protection Factors Controlling R-Loop Bypass and Suppression. *Genes (Basel)*, **8**.
55. Longerich, S., Li, J., Xiong, Y., Sung, P. and Kupfer, G.M. (2014) Stress and DNA repair biology of the Fanconi anemia pathway. *Blood*, **124**, 2812-2819.
56. Zhu, W. and Dutta, A. (2006) An ATR- and BRCA1-mediated Fanconi anemia pathway is required for activating the G2/M checkpoint and DNA damage repair upon rereplication. *Mol Cell Biol*, **26**, 4601-4611.
57. Bester, A.C., Roniger, M., Oren, Y.S., Im, M.M., Sarni, D., Chaoat, M., Bensimon, A., Zamir, G., Shewach, D.S. and Kerem, B. (2011) Nucleotide deficiency promotes genomic instability in early stages of cancer development. *Cell*, **145**, 435-446.
58. Bartkova, J., Rezaei, N., Liontos, M., Karakaidos, P., Kletsas, D., Issaeva, N., Vassiliou, L.V., Kolettas, E., Niforou, K., Zoumpourlis, V.C. *et al.* (2006) Oncogene-induced senescence is part of the tumorigenesis barrier imposed by DNA damage checkpoints. *Nature*, **444**, 633-637.
59. Anand, R.P., Shah, K.A., Niu, H., Sung, P., Mirkin, S.M. and Freudenreich, C.H. (2012) Overcoming natural replication barriers: differential helicase requirements. *Nucleic Acids Res*, **40**, 1091-1105.
60. Maizels, N. (2006) Dynamic roles for G4 DNA in the biology of eukaryotic cells. *Nat Struct Mol Biol*, **13**, 1055-1059.
61. Mirkin, S.M. (2007) Expandable DNA repeats and human disease. *Nature*, **447**, 932-940.
62. Fouché, N., Ozgür, S., Roy, D. and Griffith, J.D. (2006) Replication fork regression in repetitive DNAs. *Nucleic Acids Res*, **34**, 6044-6050.
63. Cimprich, K.A. (2003) Fragile sites: breaking up over a slowdown. *Curr Biol*, **13**, R231-233.
64. Ma, K., Qiu, L., Mrasek, K., Zhang, J., Liehr, T., Quintana, L.G. and Li, Z. (2012) Common fragile sites: genomic hotspots of DNA damage and carcinogenesis. *Int J Mol Sci*, **13**, 11974-11999.
65. Vesela, E., Chroma, K., Turi, Z. and Mistrik, M. (2017) Common Chemical Inductors of Replication Stress: Focus on Cell-Based Studies. *Biomolecules*, **7**.
66. Howlett, N.G., Taniguchi, T., Durkin, S.G., D'Andrea, A.D. and Glover, T.W. (2005) The Fanconi anemia pathway is required for the DNA replication stress response and for the regulation of common fragile site stability. *Hum Mol Genet*, **14**, 693-701.
67. Schlacher, K., Christ, N., Siaud, N., Egashira, A., Wu, H. and Jasin, M. (2011) Double-strand break repair-independent role for BRCA2 in blocking stalled replication fork degradation by MRE11. *Cell*, **145**, 529-542.
68. Schlacher, K., Wu, H. and Jasin, M. (2012) A Distinct Replication Fork Protection Pathway Connects Fanconi Anemia Tumor Suppressors to RAD51-BRCA1/2. *Cancer Cell*, **22**, 106-116.
69. Chaudhury, I., Sareen, A., Raghunandan, M. and Sobeck, A. (2013) FANCD2 regulates BLM complex functions independently of FANCI to promote replication fork recovery. *Nucleic Acids Res*, **41**, 6444-6459.

70. Chaudhury, I., Stroik, D.R. and Sobeck, A. (2014) FANCD2-controlled chromatin access of the Fanconi-associated nuclease FAN1 is crucial for the recovery of stalled replication forks. *Mol Cell Biol*, **34**, 3939-3954.
71. Ruiz, J.F., Gómez-González, B. and Aguilera, A. (2011) AID induces double-strand breaks at immunoglobulin switch regions and c-MYC causing chromosomal translocations in yeast THO mutants. *PLoS Genet*, **7**, e1002009.
72. Sollier, J., Stork, C.T., García-Rubio, M.L., Paulsen, R.D., Aguilera, A. and Cimprich, K.A. (2014) Transcription-coupled nucleotide excision repair factors promote R-loop-induced genome instability. *Mol Cell*, **56**, 777-785.
73. Bhatia, V., Herrera-Moyano, E., Aguilera, A. and Gómez-González, B. (2017) The Role of Replication-Associated Repair Factors on R-Loops. *Genes (Basel)*, **8**.
74. García-Rubio, M.L., Pérez-Calero, C., Barroso, S.I., Tumini, E., Herrera-Moyano, E., Rosado, I.V. and Aguilera, A. (2015) The Fanconi Anemia Pathway Protects Genome Integrity from R-loops. *PLoS Genet*, **11**, e1005674.
75. Madireddy, A., Kosiyatrakul, S.T., Boisvert, R.A., Herrera-Moyano, E., García-Rubio, M.L., Gerhardt, J., Vuono, E.A., Owen, N., Yan, Z., Olson, S. *et al.* (2016) FANCD2 Facilitates Replication through Common Fragile Sites. *Mol Cell*, **64**, 388-404.
76. Sollier, J. and Cimprich, K.A. (2015) Breaking bad: R-loops and genome integrity. *Trends Cell Biol*, **25**, 514-522.
77. Schwab, R.A., Nieminuszczy, J., Shah, F., Langton, J., Lopez Martinez, D., Liang, C.C., Cohn, M.A., Gibbons, R.J., Deans, A.J. and Niedzwiedz, W. (2015) The Fanconi Anemia Pathway Maintains Genome Stability by Coordinating Replication and Transcription. *Mol Cell*, **60**, 351-361.
78. Cimprich, K.A. and Cortez, D. (2008) ATR: an essential regulator of genome integrity. *Nat Rev Mol Cell Biol*, **9**, 616-627.
79. Matsuoka, S., Ballif, B.A., Smogorzewska, A., McDonald, E.R., Hurov, K.E., Luo, J., Bakalarski, C.E., Zhao, Z., Solimini, N., Lerenthal, Y. *et al.* (2007) ATM and ATR substrate analysis reveals extensive protein networks responsive to DNA damage. *Science*, **316**, 1160-1166.
80. Blackford, A.N. and Jackson, S.P. (2017) ATM, ATR, and DNA-PK: The Trinity at the Heart of the DNA Damage Response. *Mol Cell*, **66**, 801-817.
81. Zou, L. and Elledge, S.J. (2003) Sensing DNA damage through ATRIP recognition of RPA-ssDNA complexes. *Science*, **300**, 1542-1548.
82. Musacchio, A. and Salmon, E.D. (2007) The spindle-assembly checkpoint in space and time. *Nat Rev Mol Cell Biol*, **8**, 379-393.
83. Chen, Y.H., Jones, M.J., Yin, Y., Crist, S.B., Colnaghi, L., Sims, R.J., 3rd, Rothenberg, E., Jallepalli, P.V. and Huang, T.T. (2015) ATR-mediated phosphorylation of FANCI regulates dormant origin firing in response to replication stress. *Mol Cell*, **58**, 323-338.
84. Andreassen, P.R., D'Andrea, A.D. and Taniguchi, T. (2004) ATR couples FANCD2 monoubiquitination to the DNA-damage response. *Genes Dev*, **18**, 1958-1963.
85. Collins, N.B., Wilson, J.B., Bush, T., Thomashevski, A., Roberts, K.J., Jones, N.J. and Kupfer, G.M. (2009) ATR-dependent phosphorylation of FANCA on

serine 1449 after DNA damage is important for FA pathway function. *Blood*, **113**, 2181-2190.
86. Wang, X., Kennedy, R.D., Ray, K., Stuckert, P., Ellenberger, T. and D'Andrea, A.D. (2007) Chk1-mediated phosphorylation of FANCE is required for the Fanconi anemia/BRCA pathway. *Mol Cell Biol*, **27**, 3098-3108.
87. Ishiai, M., Kitao, H., Smogorzewska, A., Tomida, J., Kinomura, A., Uchida, E., Saberi, A., Kinoshita, E., Kinoshita-Kikuta, E., Koike, T. *et al.* (2008) FANCI phosphorylation functions as a molecular switch to turn on the Fanconi anemia pathway. *Nat Struct Mol Biol*, **15**, 1138-1146.
88. Ho, G.P., Margossian, S., Taniguchi, T. and D'Andrea, A.D. (2006) Phosphorylation of FANCD2 on two novel sites is required for mitomycin C resistance. *Mol Cell Biol*, **26**, 7005-7015.
89. Lossaint, G., Larroque, M., Ribeyre, C., Bec, N., Larroque, C., Décaillet, C., Gari, K. and Constantinou, A. (2013) FANCD2 binds MCM proteins and controls replisome function upon activation of s phase checkpoint signaling. *Mol Cell*, **51**, 678-690.
90. Pichierri, P. and Rosselli, F. (2004) Fanconi anemia proteins and the s phase checkpoint. *Cell Cycle*, **3**, 698-700.
91. Pichierri, P. and Rosselli, F. (2004) The DNA crosslink-induced S-phase checkpoint depends on ATR-CHK1 and ATR-NBS1-FANCD2 pathways. *Embo J*, **23**, 1178-1187.
92. Freie, B.W., Ciccone, S.L., Li, X., Plett, P.A., Orschell, C.M., Srour, E.F., Hanenberg, H., Schindler, D., Lee, S.H. and Clapp, D.W. (2004) A role for the Fanconi anemia C protein in maintaining the DNA damage-induced G2 checkpoint. *J Biol Chem*, **279**, 50986-50993.
93. Draga, M., Madgett, E.B., Vandenberg, C.J., du Plessis, D., Kaufmann, A., Werler, P., Chakraborty, P., Lowndes, N.F. and Hiom, K. (2015) BRCA1 Is Required for Maintenance of Phospho-Chk1 and G2/M Arrest during DNA Cross-Link Repair in DT40 Cells. *Mol Cell Biol*, **35**, 3829-3840.
94. Nalepa, G., Enzor, R., Sun, Z., Marchal, C., Park, S.J., Yang, Y., Tedeschi, L., Kelich, S., Hanenberg, H. and Clapp, D.W. (2013) Fanconi anemia signaling network regulates the spindle assembly checkpoint. *J Clin Invest*, **123**, 3839-3847.
95. Klein Douwel, D., Boonen, R.A., Long, D.T., Szypowska, A.A., Raschle, M., Walter, J.C. and Knipscheer, P. (2014) XPF-ERCC1 Acts in Unhooking DNA Interstrand Crosslinks in Cooperation with FANCD2 and FANCP/SLX4. *Mol Cell*, **54**, 460-471.
96. Hartlerode, A.J. and Scully, R. (2009) Mechanisms of double-strand break repair in somatic mammalian cells. *Biochem J*, **423**, 157-168.
97. Gottlieb, T.M. and Jackson, S.P. (1993) The DNA-dependent protein kinase: requirement for DNA ends and association with Ku antigen. *Cell*, **72**, 131-142.
98. DeFazio, L.G., Stansel, R.M., Griffith, J.D. and Chu, G. (2002) Synapsis of DNA ends by DNA-dependent protein kinase. *EMBO J*, **21**, 3192-3200.
99. Grawunder, U., Wilm, M., Wu, X., Kulesza, P., Wilson, T.E., Mann, M. and Lieber, M.R. (1997) Activity of DNA ligase IV stimulated by complex formation with XRCC4 protein in mammalian cells. *Nature*, **388**, 492-495.

100. Pace, P., Mosedale, G., Hodskinson, M.R., Rosado, I.V., Sivasubramaniam, M. and Patel, K.J. (2010) Ku70 corrupts DNA repair in the absence of the Fanconi anemia pathway. *Science*, **329**, 219-223.
101. Adamo, A., Collis, S.J., Adelman, C.A., Silva, N., Horejsi, Z., Ward, J.D., Martinez-Perez, E., Boulton, S.J. and La Volpe, A. (2010) Preventing nonhomologous end joining suppresses DNA repair defects of Fanconi anemia. *Mol Cell*, **39**, 25-35.
102. Patel, A.G., Sarkaria, J.N. and Kaufmann, S.H. (2011) Nonhomologous end joining drives poly(ADP-ribose) polymerase (PARP) inhibitor lethality in homologous recombination-deficient cells. *Proc Natl Acad Sci U S A*, **108**, 3406-3411.
103. Seol, J.H., Shim, E.Y. and Lee, S.E. (2017) Microhomology-mediated end joining: Good, bad and ugly. *Mutat Res*.
104. Bennardo, N., Cheng, A., Huang, N. and Stark, J.M. (2008) Alternative-NHEJ is a mechanistically distinct pathway of mammalian chromosome break repair. *PLoS Genet*, **4**, e1000110.
105. Lee-Theilen, M., Matthews, A.J., Kelly, D., Zheng, S. and Chaudhuri, J. (2011) CtIP promotes microhomology-mediated alternative end joining during class-switch recombination. *Nat Struct Mol Biol*, **18**, 75-79.
106. Ma, J.L., Kim, E.M., Haber, J.E. and Lee, S.E. (2003) Yeast Mre11 and Rad1 proteins define a Ku-independent mechanism to repair double-strand breaks lacking overlapping end sequences. *Mol Cell Biol*, **23**, 8820-8828.
107. Rahal, E.A., Henricksen, L.A., Li, Y., Williams, R.S., Tainer, J.A. and Dixon, K. (2010) ATM regulates Mre11-dependent DNA end-degradation and microhomology-mediated end joining. *Cell Cycle*, **9**, 2866-2877.
108. Sharma, S., Javadekar, S.M., Pandey, M., Srivastava, M., Kumari, R. and Raghavan, S.C. (2015) Homology and enzymatic requirements of microhomology-dependent alternative end joining. *Cell Death Dis*, **6**, e1697.
109. Truong, L.N., Li, Y., Shi, L.Z., Hwang, P.Y., He, J., Wang, H., Razavian, N., Berns, M.W. and Wu, X. (2013) Microhomology-mediated End Joining and Homologous Recombination share the initial end resection step to repair DNA double-strand breaks in mammalian cells. *Proc Natl Acad Sci U S A*, **110**, 7720-7725.
110. Takeda, S., Nakamura, K., Taniguchi, Y. and Paull, T.T. (2007) Ctp1/CtIP and the MRN complex collaborate in the initial steps of homologous recombination. *Mol Cell*, **28**, 351-352.
111. Ahmad, A., Robinson, A.R., Duensing, A., van Drunen, E., Beverloo, H.B., Weisberg, D.B., Hasty, P., Hoeijmakers, J.H. and Niedernhofer, L.J. (2008) ERCC1-XPF endonuclease facilitates DNA double-strand break repair. *Mol Cell Biol*, **28**, 5082-5092.
112. Kent, T., Chandramouly, G., McDevitt, S.M., Ozdemir, A.Y. and Pomerantz, R.T. (2015) Mechanism of microhomology-mediated end-joining promoted by human DNA polymerase θ. *Nat Struct Mol Biol*, **22**, 230-237.
113. Greaves, M.F. and Wiemels, J. (2003) Origins of chromosome translocations in childhood leukaemia. *Nat Rev Cancer*, **3**, 639-649.

114. Edwards, S.L., Brough, R., Lord, C.J., Natrajan, R., Vatcheva, R., Levine, D.A., Boyd, J., Reis-Filho, J.S. and Ashworth, A. (2008) Resistance to therapy caused by intragenic deletion in BRCA2. *Nature*, **451**, 1111-1115.
115. Howard, S.M., Yanez, D.A. and Stark, J.M. (2015) DNA damage response factors from diverse pathways, including DNA crosslink repair, mediate alternative end joining. *PLoS Genet*, **11**, e1004943.
116. Chen, L., Nievera, C.J., Lee, A.Y. and Wu, X. (2008) Cell cycle-dependent complex formation of BRCA1.CtIP.MRN is important for DNA double-strand break repair. *J Biol Chem*, **283**, 7713-7720.
117. Liu, J., Doty, T., Gibson, B. and Heyer, W.D. (2010) Human BRCA2 protein promotes RAD51 filament formation on RPA-covered single-stranded DNA. *Nat Struct Mol Biol*, **17**, 1260-1262.
118. Dray, E., Etchin, J., Wiese, C., Saro, D., Williams, G.J., Hammel, M., Yu, X., Galkin, V.E., Liu, D., Tsai, M.S. *et al.* (2010) Enhancement of RAD51 recombinase activity by the tumor suppressor PALB2. *Nat Struct Mol Biol*, **17**, 1255-1259.
119. Somyajit, K., Subramanya, S. and Nagaraju, G. (2010) RAD51C: a novel cancer susceptibility gene is linked to Fanconi anemia and breast cancer. *Carcinogenesis*, **31**, 2031-2038.
120. Somyajit, K., Subramanya, S. and Nagaraju, G. (2012) Distinct roles of FANCO/RAD51C protein in DNA damage signaling and repair: implications for Fanconi anemia and breast cancer susceptibility. *J Biol Chem*, **287**, 3366-3380.
121. Somyajit, K., Saxena, S., Babu, S., Mishra, A. and Nagaraju, G. (2015) Mammalian RAD51 paralogs protect nascent DNA at stalled forks and mediate replication restart. *Nucleic Acids Res*, **43**, 9835-9855.
122. Feeney, L., Muñoz, I.M., Lachaud, C., Toth, R., Appleton, P.L., Schindler, D. and Rouse, J. (2017) RPA-Mediated Recruitment of the E3 Ligase RFWD3 Is Vital for Interstrand Crosslink Repair and Human Health. *Mol Cell*, **66**, 610-621.e614.
123. Hoang, L.N. and Gilks, B.C. (2017) Hereditary Breast and Ovarian Cancer Syndrome: Moving Beyond BRCA1 and BRCA2. *Adv Anat Pathol*.
124. Kiiski, J.I., Pelttari, L.M., Khan, S., Freysteinsdottir, E.S., Reynisdottir, I., Hart, S.N., Shimelis, H., Vilske, S., Kallioniemi, A., Schleutker, J. *et al.* (2014) Exome sequencing identifies FANCM as a susceptibility gene for triple-negative breast cancer. *Proc Natl Acad Sci U S A*, **111**, 15172-15177.
125. Buys, S.S., Sandbach, J.F., Gammon, A., Patel, G., Kidd, J., Brown, K.L., Sharma, L., Saam, J., Lancaster, J. and Daly, M.B. (2017) A study of over 35,000 women with breast cancer tested with a 25-gene panel of hereditary cancer genes. *Cancer*, **123**, 1721-1730.
126. Roy, R., Chun, J. and Powell, S.N. (2011) BRCA1 and BRCA2: different roles in a common pathway of genome protection. *Nat Rev Cancer*, **12**, 68-78.
127. Armes, J.E., Trute, L., White, D., Southey, M.C., Hammet, F., Tesoriero, A., Hutchins, A.M., Dite, G.S., McCredie, M.R., Giles, G.G. *et al.* (1999) Distinct molecular pathogeneses of early-onset breast cancers in BRCA1 and BRCA2 mutation carriers: a population-based study. *Cancer Res*, **59**, 2011-2017.
128. Oliver, A.W., Swift, S., Lord, C.J., Ashworth, A. and Pearl, L.H. (2009) Structural basis for recruitment of BRCA2 by PALB2. *EMBO Rep*, **10**, 990-996.

129. Park, J.Y., Zhang, F. and Andreassen, P.R. (2014) PALB2: The hub of a network of tumor suppressors involved in DNA damage responses. *Biochim Biophys Acta*.
130. Pauty, J., Rodrigue, A., Couturier, A., Buisson, R. and Masson, J.Y. (2014) Exploring the roles of PALB2 at the crossroads of DNA repair and cancer. *Biochem J*, **460**, 331-342.
131. Zhang, F., Fan, Q., Ren, K. and Andreassen, P.R. (2009) PALB2 functionally connects the breast cancer susceptibility proteins BRCA1 and BRCA2. *Mol Cancer Res*, **7**, 1110-1118.
132. Zhang, F., Ma, J., Wu, J., Ye, L., Cai, H., Xia, B. and Yu, X. (2009) PALB2 links BRCA1 and BRCA2 in the DNA-damage response. *Curr Biol*, **19**, 524-529.
133. Zhang, J., Willers, H., Feng, Z., Ghosh, J.C., Kim, S., Weaver, D.T., Chung, J.H., Powell, S.N. and Xia, F. (2004) Chk2 phosphorylation of BRCA1 regulates DNA double-strand break repair. *Mol Cell Biol*, **24**, 708-718.
134. Xia, B., Sheng, Q., Nakanishi, K., Ohashi, A., Wu, J., Christ, N., Liu, X., Jasin, M., Couch, F.J. and Livingston, D.M. (2006) Control of BRCA2 cellular and clinical functions by a nuclear partner, PALB2. *Mol Cell*, **22**, 719-729.
135. Wesoła, M. and Jeleń, M. (2017) The risk of breast cancer due to PALB2 gene mutations. *Adv Clin Exp Med*, **26**, 339-342.
136. Antoniou, A.C., Foulkes, W.D. and Tischkowitz, M. (2014) Breast-cancer risk in families with mutations in PALB2. *N Engl J Med*, **371**, 1651-1652.
137. Antoniou, A.C., Foulkes, W.D., Tischkowitz, M. and Group, P.I. (2015) Breast cancer risk in women with PALB2 mutations in different populations. *Lancet Oncol*, **16**, e375-376.
138. Reid, S., Schindler, D., Hanenberg, H., Barker, K., Hanks, S., Kalb, R., Neveling, K., Kelly, P., Seal, S., Freund, M. *et al.* (2007) Biallelic mutations in PALB2 cause Fanconi anemia subtype FA-N and predispose to childhood cancer. *Nat Genet*, **39**, 162-164.
139. Tung, N., Battelli, C., Allen, B., Kaldate, R., Bhatnagar, S., Bowles, K., Timms, K., Garber, J.E., Herold, C., Ellisen, L. *et al.* (2015) Frequency of mutations in individuals with breast cancer referred for BRCA1 and BRCA2 testing using next-generation sequencing with a 25-gene panel. *Cancer*, **121**, 25-33.
140. Kupfer, G.M. (2013) Fanconi anemia: a signal transduction and DNA repair pathway. *Yale J Biol Med*, **86**, 491-497.
141. Naim, V. and Rosselli, F. (2009) The FANC pathway and BLM collaborate during mitosis to prevent micro-nucleation and chromosome abnormalities. *Nat Cell Biol*, **11**, 761-768.
142. Raschle, M., Knipscheer, P., Enoiu, M., Angelov, T., Sun, J., Griffith, J.D., Ellenberger, T.E., Scharer, O.D. and Walter, J.C. (2008) Mechanism of replication-coupled DNA interstrand crosslink repair. *Cell*, **134**, 969-980.
143. Knipscheer, P., Raschle, M., Smogorzewska, A., Enoiu, M., Ho, T.V., Scharer, O.D., Elledge, S.J. and Walter, J.C. (2009) The Fanconi anemia pathway promotes replication-dependent DNA interstrand cross-link repair. *Science*, **326**, 1698-1701.
144. Meetei, A.R., De Winter, J.P., Medhurst, A.L., Wallisch, M., Waisfisz, Q., Van De Vrugt, H.J., Oostra, A.B., Yan, Z., Ling, C., Bishop, C.E. *et al.* (2003) A novel ubiquitin ligase is deficient in Fanconi anemia. *Nat Genet*, **35**, 165-170.

145. Smogorzewska, A., Matsuoka, S., Vinciguerra, P., McDonald, E.R., 3rd, Hurov, K.E., Luo, J., Ballif, B.A., Gygi, S.P., Hofmann, K., D'Andrea, A.D. *et al.* (2007) Identification of the FANCI protein, a monoubiquitinated FANCD2 paralog required for DNA repair. *Cell*, **129**, 289-301.
146. Timmers, C., Taniguchi, T., Hejna, J., Reifsteck, C., Lucas, L., Bruun, D., Thayer, M., Cox, B., Olson, S., D'Andrea, A.D. *et al.* (2001) Positional cloning of a novel Fanconi anemia gene, FANCD2. *Mol Cell*, **7**, 241-248.
147. Taniguchi, T., Garcia-Higuera, I., Xu, B., Andreassen, P., Gregory, R., Kim, S., Lane, W., Kastan, M. and D'Andrea, A. (2002) Convergence of the Fanconi Anemia and Ataxia Telangiectasia Signaling Pathways. *Cell*, **109**, 459-472.
148. Crossan, G.P., van der Weyden, L., Rosado, I.V., Langevin, F., Gaillard, P.H., McIntyre, R.E., Gallagher, F., Kettunen, M.I., Lewis, D.Y., Brindle, K. *et al.* (2011) Disruption of mouse Slx4, a regulator of structure-specific nucleases, phenocopies Fanconi anemia. *Nat Genet*, **43**, 147-152.
149. Yang, Y., Liu, Z., Wang, F., Temviriyanukul, P., Ma, X., Tu, Y., Lv, L., Lin, Y.F., Huang, M., Zhang, T. *et al.* (2015) FANCD2 and REV1 cooperate in the protection of nascent DNA strands in response to replication stress. *Nucleic Acids Res*, **43**, 8325-8339.
150. Raghunandan, M., Chaudhury, I., Kelich, S.L., Hanenberg, H. and Sobeck, A. (2015) FANCD2, FANCJ and BRCA2 cooperate to promote replication fork recovery independently of the Fanconi Anemia core complex. *Cell Cycle*, **14**, 342-353.
151. Sareen, A., Chaudhury, I., Adams, N. and Sobeck, A. (2012) Fanconi anemia proteins FANCD2 and FANCI exhibit different DNA damage responses during S-phase. *Nucleic Acids Res*, **40**, 8425-8439.
152. Kohli, M., Rago, C., Lengauer, C., Kinzler, K.W. and Vogelstein, B. (2004) Facile methods for generating human somatic cell gene knockouts using recombinant adeno-associated viruses. *Nucleic Acids Res*, **32**, e3.
153. Fattah, F.J., Kweon, J., Wang, Y., Lee, E.H., Kan, Y., Lichter, N., Weisensel, N. and Hendrickson, E.A. (2014) A role for XLF in DNA repair and recombination in human somatic cells. *DNA Repair (Amst)*, **15**, 39-53.
154. Oh, S., Harvey, A., Zimbric, J., Wang, Y., Nguyen, T., Jackson, P.J. and Hendrickson, E.A. (2014) DNA ligase III and DNA ligase IV carry out genetically distinct forms of end joining in human somatic cells. *DNA Repair (Amst)*, **21**, 97-110.
155. Yuan, F., El Hokayem, J., Zhou, W. and Zhang, Y. (2009) FANCI protein binds to DNA and interacts with FANCD2 to recognize branched structures. *J Biol Chem*, **284**, 24443-24452.
156. Niraj, J., Caron, M.C., Drapeau, K., Berube, S., Guitton-Sert, L., Coulombe, Y., Couturier, A.M. and Masson, J.Y. (2017) The identification of FANCD2 DNA binding domains reveals nuclear localization sequences. *Nucleic Acids Res*, **45**, 8341-8357.
157. Ran, F.A., Hsu, P.D., Wright, J., Agarwala, V., Scott, D.A. and Zhang, F. (2013) Genome engineering using the CRISPR-Cas9 system. *Nat Protoc*, **8**, 2281-2308.
158. Latt, S.A., Kaiser, T.N., Lojewski, A., Dougherty, C., Juergens, L., Brefach, S., Sahar, E., Gustashaw, K., Schreck, R.R., Powers, M. *et al.* (1982) Cytogenetic

and flow cytometric studies of cells from patients with Fanconi's anemia. *Cytogenet. Cell Genet.*, **33**, 133-138.
159. Pierce, A.J., Johnson, R.D., Thompson, L.H. and Jasin, M. (1999) XRCC3 promotes homology-directed repair of DNA damage in mammalian cells. *Genes Dev*, **13**, 2633-2638.
160. Williams, S.A., Longerich, S., Sung, P., Vaziri, C. and Kupfer, G.M. (2011) The E3 ubiquitin ligase RAD18 regulates ubiquitylation and chromatin loading of FANCD2 and FANCI. *Blood*, **117**, 5078-5087.
161. Yu, X. and Baer, R. (2000) Nuclear localization and cell cycle-specific expression of CtIP, a protein that associates with the BRCA1 tumor suppressor. *J Biol Chem*, **275**, 18541-18549.
162. Xu, D., Guo, R., Sobeck, A., Bachrati, C.Z., Yang, J., Enomoto, T., Brown, G.W., Hoatlin, M.E., Hickson, I.D. and Wang, W. (2008) RMI, a new OB-fold complex essential for Bloom syndrome protein to maintain genome stability. *Genes Dev*, **22**, 2843-2855.
163. Davies, S.L., North, P.S. and Hickson, I.D. (2007) Role for BLM in replication-fork restart and suppression of origin firing after replicative stress. *Nat Struct Mol Biol*, **14**, 677-679.
164. Bianco, J.N., Poli, J., Saksouk, J., Bacal, J., Silva, M.J., Yoshida, K., Lin, Y.L., Tourriere, H., Lengronne, A. and Pasero, P. (2012) Analysis of DNA replication profiles in budding yeast and mammalian cells using DNA combing. *Methods*, **57**, 149-157.
165. Kalb, R., Neveling, K., Hoehn, H., Schneider, H., Linka, Y., Batish, S.D., Hunt, C., Berwick, M., Callen, E., Surralles, J. *et al.* (2007) Hypomorphic mutations in the gene encoding a key Fanconi anemia protein, FANCD2, sustain a significant group of FA-D2 patients with severe phenotype. *Am J Hum Genet*, **80**, 895-910.
166. Sims, A.E., Spiteri, E., Sims, R.J., 3rd, Arita, A.G., Lach, F.P., Landers, T., Wurm, M., Freund, M., Neveling, K., Hanenberg, H. *et al.* (2007) FANCI is a second monoubiquitinated member of the Fanconi anemia pathway. *Nat Struct Mol Biol*.
167. Colnaghi, L., Jones, M.J., Cotto-Rios, X.M., Schindler, D., Hanenberg, H. and Huang, T.T. (2011) Patient-derived C-terminal mutation of FANCI causes protein mislocalization and reveals putative EDGE motif function in DNA repair. *Blood*, **117**, 2247-2256.
168. Topaloglu, O., Hurley, P.J., Yildirim, O., Civin, C.I. and Bunz, F. (2005) Improved methods for the generation of human gene knockout and knockin cell lines. *Nucleic Acids Res*, **33**, e158.
169. Castella, M., Jacquemont, C., Thompson, E.L., Yeo, J.E., Cheung, R.S., Huang, J.W., Sobeck, A., Hendrickson, E.A. and Taniguchi, T. (2015) FANCI Regulates Recruitment of the FA Core Complex at Sites of DNA Damage Independently of FANCD2. *PLoS Genet*, **11**, e1005563.
170. Sobeck, A., Stone, S., Costanzo, V., de Graaf, B., Reuter, T., de Winter, J., Wallisch, M., Akkari, Y., Olson, S., Wang, W. *et al.* (2006) Fanconi anemia proteins are required to prevent accumulation of replication-associated DNA double-strand breaks. *Mol Cell Biol*, **26**, 425-437.

171. Boisvert, R.A., Rego, M.A., Azzinaro, P.A., Mauro, M. and Howlett, N.G. (2013) Coordinate nuclear targeting of the FANCD2 and FANCI proteins via a FANCD2 nuclear localization signal. *PLoS One*, **8**, e81387.
172. Zhang, F., Altorki, N.K., Mestre, J.R., Subbaramaiah, K. and Dannenberg, A.J. (1999) Curcumin inhibits cyclooxygenase-2 transcription in bile acid- and phorbol ester-treated human gastrointestinal epithelial cells. *Carcinogenesis*, **20**, 445-451.
173. Kee, Y. and D'Andrea, A.D. (2010) Expanded roles of the Fanconi anemia pathway in preserving genomic stability. *Genes Dev*, **24**, 1680-1694.
174. Chen, X., Bosques, L., Sung, P. and Kupfer, G.M. (2016) A novel role for non-ubiquitinated FANCD2 in response to hydroxyurea-induced DNA damage. *Oncogene*, **35**, 22-34.
175. Murina, O., von Aesch, C., Karakus, U., Ferretti, L.P., Bolck, H.A., Hanggi, K. and Sartori, A.A. (2014) FANCD2 and CtIP cooperate to repair DNA interstrand crosslinks. *Cell Rep*, **7**, 1030-1038.
176. Unno, J., Itaya, A., Taoka, M., Sato, K., Tomida, J., Sakai, W., Sugasawa, K., Ishiai, M., Ikura, T., Isobe, T. *et al.* (2014) FANCD2 binds CtIP and regulates DNA-end resection during DNA interstrand crosslink repair. *Cell Rep*, **7**, 1039-1047.
177. Ghosal, G. and Chen, J. (2013) DNA damage tolerance: a double-edged sword guarding the genome. *Transl Cancer Res*, **2**, 107-129.
178. Branzei, D. and Szakal, B. (2016) DNA damage tolerance by recombination: Molecular pathways and DNA structures. *DNA Repair (Amst)*, **44**, 68-75.
179. Brown, S., Niimi, A. and Lehmann, A.R. (2009) Ubiquitination and deubiquitination of PCNA in response to stalling of the replication fork. *Cell Cycle*, **8**, 689-692.
180. Miyagawa, K., Tsuruga, T., Kinomura, A., Usui, K., Katsura, M., Tashiro, S., Mishima, H. and Tanaka, K. (2002) A role for RAD54B in homologous recombination in human cells. *EMBO J*, **21**, 175-180.
181. Oh, S., Wang, Y., Zimbric, J. and Hendrickson, E.A. (2013) Human LIGIV is synthetically lethal with the loss of Rad54B-dependent recombination and is required for certain chromosome fusion events induced by telomere dysfunction. *Nucleic Acids Res*, **41**, 1734-1749.
182. Sato, K., Shimomuki, M., Katsuki, Y., Takahashi, D., Kobayashi, W., Ishiai, M., Miyoshi, H., Takata, M. and Kurumizaka, H. (2016) FANCI-FANCD2 stabilizes the RAD51-DNA complex by binding RAD51 and protects the 5'-DNA end. *Nucleic Acids Res*, **44**, 10758-10771.
183. Jayathilaka, K., Sheridan, S.D., Bold, T.D., Bochenska, K., Logan, H.L., Weichselbaum, R.R., Bishop, D.K. and Connell, P.P. (2008) A chemical compound that stimulates the human homologous recombination protein RAD51. *Proc Natl Acad Sci U S A*, **105**, 15848-15853.
184. Vinciguerra, P., Godinho, S.A., Parmar, K., Pellman, D. and D'Andrea, A.D. Cytokinesis failure occurs in Fanconi anemia pathway-deficient murine and human bone marrow hematopoietic cells. *J Clin Invest*, **120**, 3834-3842.
185. Liang, C.C., Li, Z., Lopez-Martinez, D., Nicholson, W.V., Venien-Bryan, C. and Cohn, M.A. (2016) The FANCD2-FANCI complex is recruited to DNA

interstrand crosslinks before monoubiquitination of FANCD2. *Nat Commun*, **7**, 12124.
186. Nakanishi, K., Yang, Y.G., Pierce, A.J., Taniguchi, T., Digweed, M., D'Andrea, A.D., Wang, Z.Q. and Jasin, M. (2005) Human Fanconi anemia monoubiquitination pathway promotes homologous DNA repair. *Proc Natl Acad Sci U S A*, **102**, 1110-1115.
187. Suzuki, S., Racine, R.R., Manalo, N.A., Cantor, S.B. and Raffel, G.D. (2016) Impairment of fetal hematopoietic stem cell function in the absence of Fancd2. *Exp Hematol*.
188. Xia, P., Sun, Y., Zheng, C., Hou, T., Kang, M. and Yang, X. (2015) p53 mediated apoptosis in osteosarcoma MG-63 cells by inhibition of FANCD2 gene expression. *Int J Clin Exp Med*, **8**, 11101-11108.
189. Joksic, I., Vujic, D., Guc-Scekic, M., Leskovac, A., Petrovic, S., Ojani, M., Trujillo, J.P., Surralles, J., Zivkovic, M., Stankovic, A. *et al.* (2012) Dysfunctional telomeres in primary cells from Fanconi anemia FANCD2 patients. *Genome Integr*, **3**, 6.
190. Petermann, E., Orta, M.L., Issaeva, N., Schultz, N. and Helleday, T. (2010) Hydroxyurea-stalled replication forks become progressively inactivated and require two different RAD51-mediated pathways for restart and repair. *Mol Cell*, **37**, 492-502.
191. Godthelp, B.C., Artwert, F., Joenje, H. and Zdzienicka, M.Z. (2002) Impaired DNA damage-induced nuclear Rad51 foci formation uniquely characterizes Fanconi anemia group D1. *Oncogene*, **21**, 5002-5005.
192. Godthelp, B.C., Wiegant, W.W., Waisfisz, Q., Medhurst, A.L., Arwert, F., Joenje, H. and Zdzienicka, M.Z. (2006) Inducibility of nuclear Rad51 foci after DNA damage distinguishes all Fanconi anemia complementation groups from D1/BRCA2. *Mutat Res*, **594**, 39-48.
193. Ohashi, A., Zdzienicka, M.Z., Chen, J. and Couch, F.J. (2005) Fanconi anemia complementation group D2 (FANCD2) functions independently of BRCA2- and RAD51-associated homologous recombination in response to DNA damage. *J Biol Chem*, **280**, 14877-14883.
194. Digweed, M., Rothe, S., Demuth, I., Scholz, R., Schindler, D., Stumm, M., Grompe, M., Jordan, A. and Sperling, K. (2002) Attenuation of the formation of DNA-repair foci containing RAD51 in Fanconi anaemia. *Carcinogenesis*, **23**, 1121-1126.
195. Wang, X., Andreassen, P.R. and D'Andrea, A.D. (2004) Functional interaction of monoubiquitinated FANCD2 and BRCA2/FANCD1 in chromatin. *Mol Cell Biol*, **24**, 5850-5862.
196. Park, J.Y., Singh, T.R., Nassar, N., Zhang, F., Freund, M., Hanenberg, H., Meetei, A.R. and Andreassen, P.R. (2014) Breast cancer-associated missense mutants of the PALB2 WD40 domain, which directly binds RAD51C, RAD51 and BRCA2, disrupt DNA repair. *Oncogene*, **33**, 4803-4812.
197. Xia, B., Dorsman, J.C., Ameziane, N., de Vries, Y., Rooimans, M.A., Sheng, Q., Pals, G., Errami, A., Gluckman, E., Llera, J. *et al.* (2007) Fanconi anemia is associated with a defect in the BRCA2 partner PALB2. *Nat Genet*, **39**, 159-161.

198. Foo, T.K., Tischkowitz, M., Simhadri, S., Boshari, T., Zayed, N., Burke, K.A., Berman, S.H., Blecua, P., Riaz, N., Huo, Y. *et al.* (2017) Compromised BRCA1-PALB2 interaction is associated with breast cancer risk. *Oncogene*, **36**, 4161-4170.
199. Ghiorzo, P., Pensotti, V., Fornarini, G., Sciallero, S., Battistuzzi, L., Belli, F., Bonelli, L., Borgonovo, G., Bruno, W., Gozza, A. *et al.* (2012) Contribution of germline mutations in the BRCA and PALB2 genes to pancreatic cancer in Italy. *Fam Cancer*, **11**, 41-47.
200. Jones, S., Hruban, R.H., Kamiyama, M., Borges, M., Zhang, X., Parsons, D.W., Lin, J.C., Palmisano, E., Brune, K., Jaffee, E.M. *et al.* (2009) Exomic sequencing identifies PALB2 as a pancreatic cancer susceptibility gene. *Science*, **324**, 217.
201. Pakkanen, S., Wahlfors, T., Siltanen, S., Patrikainen, M., Matikainen, M.P., Tammela, T.L. and Schleutker, J. (2009) PALB2 variants in hereditary and unselected Finnish prostate cancer cases. *J Negat Results Biomed*, **8**, 12.
202. Poumpouridou, N. and Kroupis, C. (2012) Hereditary breast cancer: beyond BRCA genetic analysis; PALB2 emerges. *Clin Chem Lab Med*, **50**, 423-434.
203. Rahman, N., Seal, S., Thompson, D., Kelly, P., Renwick, A., Elliott, A., Reid, S., Spanova, K., Barfoot, R., Chagtai, T. *et al.* (2007) PALB2, which encodes a BRCA2-interacting protein, is a breast cancer susceptibility gene. *Nat Genet*, **39**, 165-167.
204. Pennington, K.P. and Swisher, E.M. (2012) Hereditary ovarian cancer: beyond the usual suspects. *Gynecol Oncol*, **124**, 347-353.
205. Potapova, A., Hoffman, A.M., Godwin, A.K., Al-Saleem, T. and Cairns, P. (2008) Promoter hypermethylation of the PALB2 susceptibility gene in inherited and sporadic breast and ovarian cancer. *Cancer Res*, **68**, 998-1002.
206. Tischkowitz, M. and Xia, B. (2010) PALB2/FANCN: recombining cancer and Fanconi anemia. *Cancer Res*, **70**, 7353-7359.
207. Sy, S.M., Huen, M.S., Zhu, Y. and Chen, J. (2009) PALB2 regulates recombinational repair through chromatin association and oligomerization. *J Biol Chem*, **284**, 18302-18310.
208. Buisson, R. and Masson, J.Y. (2012) PALB2 self-interaction controls homologous recombination. *Nucleic Acids Res*, **40**, 10312-10323.
209. Jaramillo, M.C. and Zhang, D.D. (2013) The emerging role of the Nrf2-Keap1 signaling pathway in cancer. *Genes Dev*, **27**, 2179-2191.
210. Ma, J., Cai, H., Wu, T., Sobhian, B., Huo, Y., Alcivar, A., Mehta, M., Cheung, K.L., Ganesan, S., Kong, A.N. *et al.* (2012) PALB2 interacts with KEAP1 to promote NRF2 nuclear accumulation and function. *Mol Cell Biol*, **32**, 1506-1517.
211. Orthwein, A., Noordermeer, S.M., Wilson, M.D., Landry, S., Enchev, R.I., Sherker, A., Munro, M., Pinder, J., Salsman, J., Dellaire, G. *et al.* (2015) A mechanism for the suppression of homologous recombination in G1 cells. *Nature*, **528**, 422-426.
212. Bleuyard, J.Y., Fournier, M., Nakato, R., Couturier, A.M., Katou, Y., Ralf, C., Hester, S.S., Dominguez, D., Rhodes, D., Humphrey, T.C. *et al.* (2017) MRG15-mediated tethering of PALB2 to unperturbed chromatin protects active genes from genotoxic stress. *Proc Natl Acad Sci U S A*, **114**, 7671-7676.

213. Hayakawa, T., Zhang, F., Hayakawa, N., Ohtani, Y., Shinmyozu, K., Nakayama, J. and Andreassen, P.R. (2010) MRG15 binds directly to PALB2 and stimulates homology-directed repair of chromosomal breaks. *J Cell Sci*, **123**, 1124-1130.
214. Bleuyard, J.Y., Buisson, R., Masson, J.Y. and Esashi, F. (2012) ChAM, a novel motif that mediates PALB2 intrinsic chromatin binding and facilitates DNA repair. *EMBO Rep*, **13**, 135-141.
215. Buisson, R., Niraj, J., Pauty, J., Maity, R., Zhao, W., Coulombe, Y., Sung, P. and Masson, J.Y. (2014) Breast cancer proteins PALB2 and BRCA2 stimulate polymerase η in recombination-associated DNA synthesis at blocked replication forks. *Cell Rep*, **6**, 553-564.
216. Stirnimann, C.U., Petsalaki, E., Russell, R.B. and Müller, C.W. (2010) WD40 proteins propel cellular networks. *Trends Biochem Sci*, **35**, 565-574.
217. Al Abo, M., Dejsuphong, D., Hirota, K., Yonetani, Y., Yamazoe, M., Kurumizaka, H. and Takeda, S. (2014) Compensatory functions and interdependency of the DNA-binding domain of BRCA2 with the BRCA1-PALB2-BRCA2 complex. *Cancer Res*, **74**, 797-807.
218. Siaud, N., Barbera, M.A., Egashira, A., Lam, I., Christ, N., Schlacher, K., Xia, B. and Jasin, M. (2011) Plasticity of BRCA2 function in homologous recombination: genetic interactions of the PALB2 and DNA binding domains. *PLoS Genet*, **7**, e1002409.
219. Hirsch, B., Shimamura, A., Moreau, L., Baldinger, S., Hag-alshiekh, M., Bostrom, B., Sencer, S. and D'Andrea, A.D. (2004) Association of biallelic BRCA2/FANCD1 mutations with spontaneous chromosomal instability and solid tumors of childhood. *Blood*, **103**, 2554-2559.
220. Wagner, J.E., Tolar, J., Levran, O., Scholl, T., Deffenbaugh, A., Satagopan, J., Ben-Porat, L., Mah, K., Batish, S.D., Kutler, D.I. *et al.* (2004) Germline mutations in BRCA2: shared genetic susceptibility to breast cancer, early onset leukemia, and Fanconi anemia. *Blood*, **103**, 3226-3229.
221. H, E., JG, D., J, N., K, S., A, M., K, P., MC, S., K, H., A, K., AJ, V. *et al.*, Clin Cancer Res 2008;14(14) July 15, 2008, pp. 4667-4671.
222. Erkko, H., Dowty, J.G., Nikkilä, J., Syrjäkoski, K., Mannermaa, A., Pylkäs, K., Southey, M.C., Holli, K., Kallioniemi, A., Jukkola-Vuorinen, A. *et al.* (2008) Penetrance analysis of the PALB2 c.1592delT founder mutation. *Clin Cancer Res*, **14**, 4667-4671.
223. Pauty, J., Couturier, A.M., Rodrigue, A., Caron, M.C., Coulombe, Y., Dellaire, G. and Masson, J.Y. (2017) Cancer-causing mutations in the tumor suppressor PALB2 reveal a novel cancer mechanism using a hidden nuclear export signal in the WD40 repeat motif. *Nucleic Acids Res*, **45**, 2644-2657.
224. Rantakari, P., Nikkilä, J., Jokela, H., Ola, R., Pylkäs, K., Lagerbohm, H., Sainio, K., Poutanen, M. and Winqvist, R. (2010) Inactivation of Palb2 gene leads to mesoderm differentiation defect and early embryonic lethality in mice. *Hum Mol Genet*, **19**, 3021-3029.
225. Nikkilä, J., Parplys, A.C., Pylkäs, K., Bose, M., Huo, Y., Borgmann, K., Rapakko, K., Nieminen, P., Xia, B., Pospiech, H. *et al.* (2013) Heterozygous mutations in PALB2 cause DNA replication and damage response defects. *Nat Commun*, **4**, 2578.

226. Byrd, P.J., Stewart, G.S., Smith, A., Eaton, C., Taylor, A.J., Guy, C., Eringyte, I., Fooks, P., Last, J.I., Horsley, R. *et al.* (2016) A Hypomorphic PALB2 Allele Gives Rise to an Unusual Form of FA-N Associated with Lymphoid Tumour Development. *PLoS Genet*, **12**, e1005945.
227. Metzger, D., Clifford, J., Chiba, H. and Chambon, P. (1995) Conditional site-specific recombination in mammalian cells using a ligand-dependent chimeric Cre recombinase. *Proc Natl Acad Sci U S A*, **92**, 6991-6995.
228. Ameziane, N., Errami, A., Léveillé, F., Fontaine, C., de Vries, Y., van Spaendonk, R.M., de Winter, J.P., Pals, G. and Joenje, H. (2008) Genetic subtyping of Fanconi anemia by comprehensive mutation screening. *Hum Mutat*, **29**, 159-166.
229. Ran, F.A., Hsu, P.D., Wright, J., Agarwala, V., Scott, D.A. and Zhang, F. (2013) Genome engineering using the CRISPR-Cas9 system. *Nat Protoc*, **8**, 2281-2308.
230. Storchová, Z. and Kloosterman, W.P. (2016) The genomic characteristics and cellular origin of chromothripsis. *Curr Opin Cell Biol*, **40**, 106-113.
231. Terzoudi, G.I., Karakosta, M., Pantelias, A., Hatzi, V.I., Karachristou, I. and Pantelias, G. (2015) Stress induced by premature chromatin condensation triggers chromosome shattering and chromothripsis at DNA sites still replicating in micronuclei or multinucleate cells when primary nuclei enter mitosis. *Mutat Res Genet Toxicol Environ Mutagen*, **793**, 185-198.
232. Schwarz, J.M., Cooper, D.N., Schuelke, M. and Seelow, D. (2014) MutationTaster2: mutation prediction for the deep-sequencing age. *Nat Methods*, **11**, 361-362.
233. Rosen, E.M. and Pishvaian, M.J. (2014) Targeting the BRCA1/2 tumor suppressors. *Curr Drug Targets*, **15**, 17-31.
234. Buisson, R., Dion-Côté, A.M., Coulombe, Y., Launay, H., Cai, H., Stasiak, A.Z., Stasiak, A., Xia, B. and Masson, J.Y. (2010) Cooperation of breast cancer proteins PALB2 and piccolo BRCA2 in stimulating homologous recombination. *Nat Struct Mol Biol*, **17**, 1247-1254.
235. Zhang, F., Bick, G., Park, J.Y. and Andreassen, P.R. (2012) MDC1 and RNF8 function in a pathway that directs BRCA1-dependent localization of PALB2 required for homologous recombination. *J Cell Sci*, **125**, 6049-6057.
236. Sims, A.E., Spiteri, E., Sims, R.J., Arita, A.G., Lach, F.P., Landers, T., Wurm, M., Freund, M., Neveling, K., Hanenberg, H. *et al.* (2007) FANCI is a second monoubiquitinated member of the Fanconi anemia pathway. *Nat Struct Mol Biol*, **14**, 564-567.
237. Zhang, X., Lu, X., Akhter, S., Georgescu, M.M. and Legerski, R.J. (2016) FANCI is a negative regulator of Akt activation. *Cell Cycle*, **15**, 1134-1143.
238. Buisson, R., Niraj, J., Rodrigue, A., Ho, C.K., Kreuzer, J., Foo, T.K., Hardy, E.J., Dellaire, G., Haas, W., Xia, B. *et al.* (2017) Coupling of Homologous Recombination and the Checkpoint by ATR. *Mol Cell*, **65**, 336-346.